Doctoral theses at NTNU, 2024:63

Therese Frostad

Control of Magnon Condensates

Doctoral thesis

NTNU
Norwegian University of Science and Technology
Thesis for the Degree of
Philosophiae Doctor
Faculty of Natural Sciences
Department of Physics

NTNU
Norwegian University of
Science and Technology

Therese Frostad

Control of Magnon Condensates

Thesis for the Degree of Philosophiae Doctor

Trondheim, March 2024

Norwegian University of Science and Technology
Faculty of Natural Sciences
Department of Physics

NTNU
Norwegian University of
Science and Technology

NTNU
Norwegian University of Science and Technology

Thesis for the Degree of Philosophiae Doctor

Faculty of Natural Sciences
Department of Physics

ISBN 978-82-326-7726-9 (printed ver.)
ISBN 978-82-326-7725-2 (electronic ver.)
ISSN 1503-8181 (printed ver.)
ISSN 2703-8084 (online ver.)

Doctoral theses at NTNU, 2024:63

Printed by NTNU Grafisk senter

Abstract

Spintronics is a technology driven field aimed at harnessing the electron spin for novel devices [1]. This is in contrast to traditional electronics, where the electron charge is used as an information carrier. Advances in electronics has to a large extent relied on making components smaller and stacking them closer together. When the components become very small, we enter the quantum mechanical realm, where the properties of the electron are very different. And when we stack the components closer together, we generate a lot of heat. Spintronics may solve some of the challenges traditional electronics face today.

Magnons can be used as information carriers in spintronic devices. Magnons are bosons, and are allowed to share the same quantum state. When a large population of magnons thermalize down to the lowest energy state of the system, they may form what we call a *Bose-Einstein condensate* [2]. The particles in the condensate behave coherently, and they represent a macroscopic manifestation of a single quantum state. These condensates are interesting to fundamental research, and recently we realize that they may also have some exotic practical applications [3, 4, 5]. If we want to utilize the magnon condensates for practical applications, we need to be able to control their properties. This is the main motivation behind the research in the present thesis.

The research accompanying this thesis contains theoretical investigations of methods for creating and controlling magnon condensates. In Ref. [6], we present how the presence of spin-transfer-torques may be used to assist or inhibit magnon creation. In Ref. [7], we provide a theoretical explanaition of how an out-of.plane easy-axis anisotropy may assist condensate formation, as observed experimentally by Divinskiy et al. [8]. In Refs. [7, 9] we calculate the magnon interactions for condensate magnons in a thin-film ferromagnet, a uniaxial antiferromagnet, and in a biaxial antiferromagnet. In Ref. [7] we investigate how the two condensate populations in the ferromagnetic film are affected by the external field strength, film thickness and out-of-plane easy-axis anisotropy. We show how these parameters can be used to control properties such as the magnon distribution between the two populations. In Ref. [9] we show how the two condensate populations in the uniaxial film with DzyaloshinskiiMoriya interaction (DMI) are affected by parameters such as the DMI-strength and strength of the in-plane easy-axis anisotropy.

Preface

This thesis is submitted to the Norwegian University of Science and Technology (NTNU) as a partial fulfilment of the requirements for the degree of Philosophiae doctor.

The research projects were supported by the Research Council of Norway through its Centres of Excellence funding scheme, project number 262633, "QuSpin".

Trondheim, December 2023

Therese Frostad

List of Papers

Paper I :
Therese Frostad, Hans Langva Skarsvåg, Alireza Qaiumzadeh, and Arne Brataas
Spin-transfer-assisted Parametric Pumping of Magnons in Yttrium Iron Garnet
Physical Review B (2022) [6]

Paper II :
Therese Frostad, Philipp Pirro, Alexander A. Serga, Burkard Hillebrands, Arne Brataas, and Alireza Qaiumzadeh
Anisotropy-assisted Magnon Condensation in Ferromagnetic Thin Films
arXiv preprint arXiv:2309.05982 (2023) [7]

Paper III :
Anne Louise Kristoffersen, Therese Frostad, Roberto E. Troncoso, Arne Brataas and Alireza Qaiumzadeh
Phase Diagram for Magnon Condensate in Antiferromagnetic Insulators
Preprint (2023) [9]

My contribution to the papers : I performed analytical claculations and conducted micromagnetic simulations for Paper I and Paper II, and wrote the initial manuscripts. I also revised the manuscripts together with my coauthors. I performed analytical calculations together with my coauthors for Paper III, and contributed to the writing and discussion.

Motivation

We live in the age of electronics. Today, many of our devices are based on classical physics. But some of the electronic components are becoming very small. As we start to work with features below a few nanometers, we are approaching the quantum mechanical regime where everything is unfamiliar and seemingly unpredictable.

For the last fifty years, the number of transistors on a microchip as doubled every two years. This trend is known as *Moore's law* [10]. The doubling of transistors on a chip can be translated into an expectation of roughly a doubling in speed and other performance parameters per watt. Our devices are also becoming more energy efficient, and *Koomey's law* described the trend that the energy consumption decreases by a factor of two for every 2.5 years [11]. Koomey's law is strongly correlated to Moore's law. Recently, it seems like both trends are slowing down [12, 13].

Until now, our strategy for improving devices has to a large extent relied on making components smaller, and cramming them closer together. But this strategy can not continue forever. When we approach the quantum regime, the position and behaviour of the electrons differ from classical predictions. The next innovations in computation needs to rely on other strategies than shrinking components and stacking them closer. One of the exciting new solutions is to design quantum computation systems that take advantage of quantum properties such as the superposition and entanglement principle [14, 15, 16, 17, 18, 19]. These systems will likely be able to perform certain tasks such as factorizations and discrete Fourier transforms much faster than a classical computer [20], and will represent a revolution in computation. But there are many challenges, as many of the suggested architectures are difficult to scale up, and often require cold temperatures [21].

Technology can move forward in a continuous development or in a more disruptive fashion. Quantum computers are examples of novel technology that have many challenges to overcome before they are ready to be commercialized [21]. However, it turns out that we may solve some of the obstacles of charge-based electronics through quite simple spin-based ideas. Moreover, many of these ideas can be integrated with current electronics. We have already started walking down this path, which has led to a field of spin-based electronics; *Spintronics* [1].

In traditional electronics, the electron charge is the main information carrier. Electrons travelling in a material typically produce a significant amount of Joule heating. If we send a pure spin current without the accompanying charge, we may avoid the problems of Joule heating. We expect spintronic devices to offer fast computation at low energy costs [22]. while most proposed quantum

computation architectures can only operate in the milli-Kelvin range [4], many spintronic architectures are designed to operate at room temperature. Another benefit of spintronic devices is that they may be suitable for integration with traditional electronics [22]. In addition to walking hand-in-hand with developments in quantum computation, spintronics may play well with other visionary technologies. In particular, spintronic devices might be relevant as components in neuromorphic computation architectures, which is a novel field of computation aiming to mimic the way our brain and nervous system works [23, 24].

In a similar way as sound waves need a medium to propagate through, spin waves need a spin system to travel in. Magnetic materials have organized spin systems, and one can disrupt the order of the spin system to send spin waves. We often find it useful to describe the particle-like properties of the sound wave as a phonon. Similarily, we can describe the spin wave as a magnon. The phonon and magnon are both examples of *quasiparticles*. Magnons behave like particles in the sense that they have properties such as energy, momentum and spin. Magnons are *bosonic* quasiparticles, and they are alowed to share the same quantum state. They can form *Bose-Eistein condensates* at room temperature [2]. In this condensate, all the particles occupy the lowest energy state. The particles behave coherently, and represent a macroscopic manifestation of a particle population in the same quantum state.

There has been extensive experimental and theoretical work done the last years to investigate the condensate properties [25, 26, 27, 28, 29, 30, 31, 8]. The condensates are interesting research subjects for fundamental science, and we are recently investigating possible practical applications. Magnon condensates have been suggested as qubit units for quantum computation architectures [3, 32]. It has also been suggested to implement a semi-classical room temperature qubit based on the magnon condensate [4]. Any practical applications of a magnon condensate would require us to understand how they form, how we can stabilize them, and how we can control their properties. This is the central topic of the present thesis.

Organization of Thesis

This thesis investigates methods to form and control magnon condensates. In 2006, Demokritov et al. published the first experimental observation of a magnon Bose-Einstein condensate *at room temperature* in a ferromagnetic film [2]. Since then, there has been extensive research on magnon condensates [25, 26, 27, 28, 29, 30, 31, 8]. Although the condensates are valuable for fundamental research, we only recently started to chart their future in practical applications [3, 32, 4, 5]. This requires an effort to control and manipulate the properties of the magnon condensate.

Thesis introduction

In the last part of the thesis, three research papers are presented. The introductory chapters of the thesis give a quick overview of the theoretical frameworks used in the papers, and provide a context to the work in terms of the research field and technological opportunities. We try to keep the introductory chapters as general as possible, but to illustrate how to use the theoretical frameworks in Chapter 3, we include a few examples for ferromagnetic and antiferromagnetic systems. The papers contain the main findings of our research. A short summary of the results can be found in Chapter 4 of the thesis introduction.

The first chapter introduces the electron spin, and its usefulness in future technologies. We discuss the potential of spintronic devices, how spintronic concepts can solve problems with traditional electronics, and how spin technology can be coordinated with other novel fields such as quantum computation and neuromorphic computation.

The second chapter is an introduction to magnon condensates. We start with an introduction to Bose-Einstein condensates before we move on to magnon condensates. The magnon condensate is a relatively new field of research, and certain aspects of the condensation has sparked debate and even some controvercy [33]. We mention some properties we expect to find in Bose-Einstein condensates, and discuss some aspects around the nomenclature and quantum nature of the condensate.

The third chapter introduces some theoretical frameworks used to study spin waves or magnons. In the accompanying research papers, we have used two quite different approaches. The first approach is to describe spin waves in a semi-classical way, through the Landau - Lifshitz - Gilbert equation and micromagnetic simulations. The second approach is a quantum mechanical treatment, where the Holstein-Primakoff transformation is used to replace the spin operators by bosonic creation and annihilation operators. We also introduce the Dyson-Maleev transformation, and how it differs from the Holstein-Primakoff transformation. Our focus is aimed at describing the magnetization dynamics in a thin film ferromagnetic film, since this is a common system for xperimental work on magnon condensates [7, 8]. However, we have also included some demonstrations of antiferromagnetic systems.

The fourth chapter is a short summary where we present some results from the papers attached to the thesis.

Thesis research

Paper I [6] investigates the interplay of two mechanisms that can be exploited to create magnon condensates in ferromagnetic films; parallel pumping [7] and spin-transfer torques [8]. We present how a weak spin-transfer torque can ei-

ther assist or inhibit the parallel pumping. We conduct numerical simulations, and present a picture on the magnon density one could expect from the two excitation techniques, and how the density changes as a function of external field strength and excitation strength. These parameters could act as control parameters for the magnon condensate creation. We also present examples of which magnon modes we can expect to get from the two excitations techniques.

Paper II [7] is a theoretical explanation on how an out-of-plane easy-axis anisotropy assists the formation of magnon condensation in a thin ferromagnetic film. Our results are based on analytical calculations in the Holstein-Primakoff framework, in addition to micromagnetic simulations in the Landau-Lifshitz-Gilbert framework. We argue that the anisotropy makes the depth and shape of the thin film dispersion relation more pronounced, and that this is beneficial to the condensation process. We also present calculations of the magnon interactions as a function of system parameters such as the film thickness, strength of the anisotropy, and strength of the external field applied to the film. We describe the two condensate populations by their phase and number of magnons. We may the study the difference in magnon number between the two condensate populations, and the sum of their phases. The non-linear magnon interactions of the system is a function of the distribution difference and phase sum of the two magnon populations. We are particularly interested in knowing whether the two condensates are likely to have a symmetric population distribution, or if more magnons tend to gather in one of the two minima. We find that by changing the system parameters such as the external field strength, one could manipulate the distribution difference.

Paper III [9] presents theoretical investigations of magnon condensation in two antiferromagnetic systems. The first system is a uniaxial antiferromagnet, while the second system is a biaxial antiferromagnet. Similar to Paper II, we conduct analytical calculations in the Holstein-Primakoff framework. We also conduct calculations in the Dyson-Maleev framework, and highlight the similarities and differences between these two bosonization techniques. We calculate the nonlinear magnon-magnon interactions of the condensate magnons. Our results can be used to predict properties such as the magnon distribution difference and phase sum of the condensate populations.

Acknowledgements

I want to express my deepest gratitude to my supervisor, Professor Arne Brataas. You have provided the best environment a PhD candidate could have. Thank you for supporting me through the PhD, especially through the hard times. You always showed me patience and saw solutions.

I am highly grateful for the guidance I received from Senior Researcher Alireza Qaiumzadeh. Your skills in a wide range of fields in physics is inspiring, and I am happy that you have shared some of your knowledge with me. You have become a mentor to me, and I have enjoyed our discussions and work on the research projects.

I want to thank my co-supervisor, Professor Justin Wells. Thank you for introducing me to your group at the ARPES lab. I am grateful for the time I spent in the lab, and the people I met. Thank you to the ARPES goup for welcoming me and letting me tag along some of your experimental projects.

Thank you to my coauthors for our collaborations on the research projects. Thank you to the Idun infrastructure for letting me borrow your computational resources.

During the PhD, I have been in a supportive environment, surrounded by coworkers that want the best for each other. I have enjoyed the company of my office mates; Hans, Camilla, Lars, Øyvind, Martin, Haakon, Jonas and Chi. Apart from my own office, I also spent quite some time in the office of Marina, experimenting with new and exotic cappuccinos. Thank you for your loving company and support. I am especiallt grateful to Stefan and Verena for providing feedback on my thesis, and to Anne Louise and Vemund for our discussions on magnon condensates. Thank you Eirik, Jeroen, Nicolai, Ali, Vetle, Sverre, Henning, Arnau, Erlend, André, Roberto, Cecilia, Akash, Lina, Håvard, Atousa, Eirik, Even and Niklas for your advice and support. Thank you Karen Elizabeth, Bjørnulf, Matthias, Kristian, Anna Cecilie, Christian, Niels Henrik, Payel, Sol and everyone at QuSpin for the coffee breaks, conferences and discussions.

To my friends outside of physics, thank you for making my life enjoyable.

I'm lucky to come from a large family, and I had a good childhood in the company of grandparents, uncles, aunts and cousins. The family is growing, and one of the newest members is my lovely niece. To my whole family, I appreciate all of you dearly and I am always looking forward to seeing you when I come home.

Thank you to my mom, dad, sister and brother for your love and support these years.

Contents

Chapter 1

Spintronics - Harnessing the electron spin

In this chapter, we will get to know *spintronics* [1]. Spintronics is a portmanteau of *spin* and *electronics*. Spintronics is a technology-motivated field of science where the electron spin properties are being utilized. This is in contrast to traditional electronics, which mainly makes use of the electron charge.

We will start the chapter with introducing the electron spin in Section 1.1. Next, in Section 1.2 we describe the magnetic materials in which spin waves can travel. Section 1.3 is a short introduction to spin waves. Then, in Section 1.4 we are ready to discuss how recent discoveries in spintronics may be used to address the challenges traditional spintronics face today. We highlight one of the true strengths of spintronics; its prospects for integration with other novel fields of technology, such as quantum computation and neuromorphic computation [34, 35, 36, 23].

1.1 Spin

The electron is a tiny elementary particle with a negative charge. We can use the charge to sustain a range of useful devices. In our daily lives, we use electric charge currents as an energy source for our cars and household appliances, and we use the charge as an information carrier in countless electronic gadgets.

Like all elementary particles, the electron has a feature known as *spin*. Spin is a quantum mechanical property. We can measure the spin of a particle [37].

Yet, it is difficult to provide an intuitive picture of what spin really is. Some like to think of the spin as an *intrinsic* quantum mechanical property. It differs from the angular momentum associated with the electrons orbital motion. In the next section, we will find out how we can use the electron spin to advance electronics.

1.2 Magnetic materials

We have known about magnetic materials for thousands of years. I northern Greece, close to a location known as *Magnesia*, people found stones that could attract iron [38]. We have records of people playing with magnetic materials in the ancient civilizations of Greexe, China, and Egypt [39]. We can assume that these civilizations also made observations of static electricity. The invisible magnetic and electric forces acting between objects at a distance was must have been fascinating to play with, and it is likely that very early on, people had an intuition that there is a strong relationship between magnetism and electricity. This relationship was studied by Ørsted in 1820 [40]. The following years were filled with a series of groundbreaking experiments by well-known names such as Ampere, Biot, Savart, Gauss, Tesla, Edison and Faraday. Maxwell demonstrated how electric charges and fields related to magnetic fields in his well known Maxwell's equations [41]. Einstein expanded on these laws in his work on special relativity [42]. His work made it possible to study the relationship between electricity and magnetism in different reference frames, accompanied by solutions of how to transform the Maxwell equations accordingly.

If an electric current flows in a circular coil, it produces a magnetic field, which can be calculated using the Biot-Savart law [43]. Although it is not a correct picture, we can imagine that the electrons in an atom travel in a circular motion around the nucleus, and that this orbital motion produces an orbital magnetic moment. The orbital magnetic moment, together with the electron intrinsic spin magnetic moment, makes up the magnetic properties of the material. The origin of magnetism can not be fully understood within the framework of classical physics. When analyzing magnetism in materials within statistical mechanics and classical physics, it is found that the thermal average of the magnetization cancels out. This statement is known as the *Bohr-Van Leeuwen theorem* [44, 45, 38]. Magnetic materials must be understood from a quantum physics viewpoint, considering the electron spin and the Pauli exclusion principle.

In most materials, the magnetic moments of the individual atomic sites are randomly oriented. In this case, the material does not have a macroscopic magnetic field, and no ordered spin system. However, in some materials, the moments align spontaneously, as long as the temperature is below some critical threshold. In this thesis, we are interested in the magnetization dynamics of

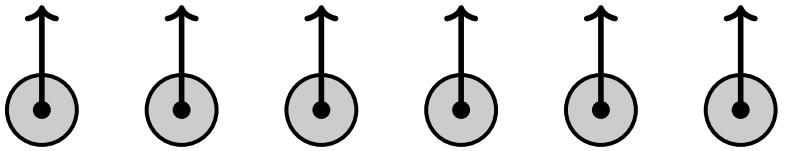

Figure 1.1: A ferromagnetic chain. Here, each site has a magnetic moment aligned parallel to each other.

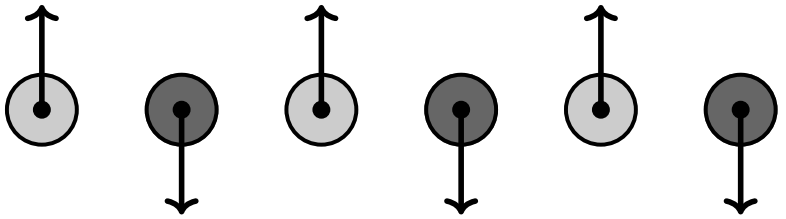

Figure 1.2: An antiferromagnetic chain with two sublattices. The magnetic moments of the two sublattices point in opposite directions. Since the magnetic moments on the two sublattices are equal in strength, the net magnetization of the antiferromagnet vanishes.

ferro/ferrimagnets and antiferromagnets. The critical temperature limit of the ferromagnet and antiferromagnet is referred to as Curie temperature and Néel temperature, respectively.

In Chapter 3, we will investigate some of the ways the magnetic moments in a material interact with each other and their surroundings. In particular, the exchange interaction between the moments will describe the tendency of the moments to align in parallel or antiparallel to each other. If we assume an isotropic homogeneous coupling, we can model the exchange interaction between neighbouring spins as [46, 47],

$$\mathcal{H}_{\text{ex}} = -\frac{1}{2} J_{\text{ex}} \sum_{i,j} \boldsymbol{S}_i \cdot \boldsymbol{S}_j \,. \tag{1}$$

The sign of the exchange constant J_{ex} can be both positive and negative. If $J_{\text{ex}} > 0$, then the spins will tend to align themselves parallel to each other, favouring ferromagnetism. If $J_{\text{ex}} < 0$, an antiferromagnetic arrangements is favoured. Fig. 1.1 illustrates a ferromagnetic spin system, while Fig. 1.2 illustrates an antiferromagnetic spin system.

In *ferromagnets*, the magnetic moments align to points in the same direction.

The ferromagnet has a non-zero macroscopic total magnetic moment. In practice, a slab of ferromagnetic material may have several domains [48], where the orientation of the moments differ from domain to domain. In this case, the resulting magnetic field of the entire slab may amount to zero.

In *ferrimagnets*, there are two or more sublattices, where the magnetic moments are collinear. One of the sublattices could be antiparallel, but have weaker magnetic moments than the other sublattice. In this case, there is a non-zero macroscopic total magnetic moment. Since both ferrimagnets and ferromagnets have a macroscopic total moment, we sometimes neglect distinguishing the ferrimagnetic character. For instance, it is common to refer to yttrium iron garnet (YIG) as a ferromagnet, although it has a ferrimagnetic structure [48]. YIG can be considered as a ferromagnet only in the low-energy limit [49].

In *antiferromagnets*, there are two or more sublattices with a total macroscopic moment that cancels out to zero. In the most simple case, the antiferromagnet has two antiparallel sublattices [48], so that the magnetic moments are equal in size, but have opposite direction.

There are several other possibilities of ordered spin systems, some of which can not be described by simple models of sublattices [48]. And often, a material might have local variations or several domains, where the spins have different direction.

In the present thesis, we are particularly interested in the ferrimagnetic insulator *yttrium iron garnet* (YIG, $Y_3Fe_2(FeO_4)_3$) [49]. The garnet has a high Curie temperature $T_c = 560\,\mathrm{K}$, and a complicated unit cell containing 80 atoms [48]. In the low-energy limit, YIG can be considered a ferromagnet [49]. YIG is a material of high interest to spintronic applications [50]. Some of the reasons for the popularity of YIG lies in the low spin wave damping of the material, which makes it possible to transfer pure spin waves over long distances. One can obtain thin YIG films with very low Gilbert damping parameter (see Eq. (1)), in the range of $\alpha \sim 10^{-5}$ or $\sim 10^{-4}$ [51, 52]. The low damping makes YIG an excellent candidate for investigating spin wave propagation, magnon lifetimes, and thermalization properties [52].

1.3 Spin waves

Magnetic materials are examples of ordered spin systems. Such ordered spin systems might have one or several ground states with respect to the direction of the magnetic moments. In the early 1930s, Bloch considered the excitations in spin systems, and introduced the concept of spin waves [53, 54]. Bloch's ideas were later extended by Heller and Kramers [55], and developed into a semi-

classical description by Landau and Lifschitz [56], which we will return to in Chapter 3.

In Figs. 1.1 and 1.2, we visualized the ferromagnetic and antiferromagnetic spin systems as a chain of magnetic moments pointing in a certain direction. The magnetic moments couple to each other through e.g. the exchange interaction of Eq. (1) and other coupling mechanisms we will introduce in Chapter 3. If we consider a spin system in its ground state, we can create excitations in the system by for example flipping a spin. We could also create some other disturbances from the ground state, for example by creating a torque that causes the magnetic moment to rotate. Since the magnetic moments interact with each other, the disturbance may propagate through the system, and generate a collective excitation of the spin system. Such an excitation can often be described as a *spin wave* which carries energy and momentum, and we can identify them by their wave length, frequency and amplitude. When describing the propagating spin wave we often introduce the concept of *magnons*. The magnon is a quasiparticle describing the quantized spin wave. Magnons behave like particles in the sense that they have energy, momentum and spin. They can be created and annihilated, and they interact with each other. The magnon is bosonic in nature, and has spin-1. Five years after Landau and Lifshitz developed their semi-classical spin wave approach [56], Holstein and Primakoff developed a quantum bosonization approach, focusing on the particle-like properties of the magnon [57]. We will return to both the semi-classical approach and quantum mechanical bosonization treatment in Chapter 3.

1.4 Spintronics

Spintronics is the field of science and technology where the electron spin properties are being utilized [1]. In some spintronic devices, the spin plays a passive role, while in others, spin plays an active role, using spin waves as the main information carrier. The branch of spintronics that focuses on magnon dynamics in magnetic structures is often referred to as *magnonics* [50, 58, 59, 60]. In general, information transfer through spin currents can take place with or without any accompanying charge transfer. The field where information is transferred only through pure spin currents is promising for developing technology with low power consumption. By transferring spin currents only, one avoids the Joule heating associated with an electric charge travelling through a material. Most spintronic devices still rely on travelling electrons as the main information carrier [22]. The field of spintronics that focuses exclusively on utilizing high-fidelity pure spin currents is magnetic insulators is referred to as *insulatronics* [22].

Both antiferromagnets and ferromagnets are of interest to spintronic applications. Ferromagnets usually have precession frequencies in the GHz range, while

antiferromagnets have precession frequencies in the THz range [22]. Working in the GHz regime is more convenient for experimental work and applications, and allows for a more smooth integration with other electronic devices that also operate in the GHz regime. Although the THz regime of antiferromagnets can be challenging to work with, there has been an increased interest in investigating the ultrafast dynamics [61]. The THz regime is in the range of far infrared light frequencies, and one might gain advantages from coupling to optical properties [61]. Moreover, antiferromagnets do not produce stray fields. This means they are resistant to disturbances by external magnetic noise. However, for the same reasons, they are also harder to manipulate and detect than their ferromagnetic counterparts [62].

The first steps toward spin-based electronics were taken in the 80s, when magnetic nanostructures were beginning to gain popular interest [63]. Two ferromagnetic layers, separated by a thin non-magnetic layer, may interact with each other, mainly through an indirect exchange interaction. The groups of Albert Fert and Peter Grünberg found that a parallel or antiparallel alignment of the magnetization of the two ferromagnetic layers would lead to the device possessing a low of high electrical resistance, respectively [64, 65]. Even a small difference in the magnetization direction of two ferromagnetic layers can give a large change in the measured electrical resistance, and the effect got to be known as the *giant magneto resistance* (GMR). The discovery proved itself to be very useful, as it was later used for magnetic sensors, and subsequently for reading data in hard disk drives. Fert and Grünberg received the 2007 Nobel Price in physics for their independent discoveries [66]. The read heads in magnetic hard drives was one of the big commercial successes following the research on the GMR [67]. Another important commercialization includes the *magnetic random access memory* (MRAM) [68], which is a non-volatile memory where data is stored in magnetic domains. Other interesting suggestions for spintronic memories include the racetrack memories [69, 70]. Today, many electronic devices are based on *von Neumann architectures* [71], where the working memory and CPU are separated, and must communicate with each other through a single shared bus, which can only access one of the two components at a time. The number of information units the bus can handle is often lower than what is suitable for a high-performance CPU, which means that the CPU may spend a fair amount of time waiting. This is what we refer to as the *von Neumann bottleneck* [71]. In general, embedded systems such as the MRAM can be solutions to the challenges of the the von Neumann bottleneck.

The successes of the magnetic hard drive read heads and the MRAM are partly responsible for the attention the spintronics field gets from the commercial market. The spintronics field is wide, and includes applications based on magnetic and magneto-resistive effects [37], and developments of devices such as the spin valve sensors used in MRAMs [72], logic devices based on tunnel junctions [73], and sensors for rotational speed control [74] or spin-valve based current sensors [75].

Another reason spintronics is a successful field, is that the field makes use of synergies with other research fields, such as nanotechnology and microelectronics [76]. Spintronic developments are well suited to be integrated with conventional electronics [22]. However, the spintronics field may also bring more novel computational devices based on Ising machines [77, 78], reservoir computing [79] and spin wave computing components [80, 35, 81]. In particular, spintronic platforms may be suitable for analog devices. Analog devices might be the perfect platforms for one of the fastest expanding fields today; *machine learning* [82]. Analog architectures may utilize the evolution of a continuous physical system to perform calculations [82, 83, 84, 85]. Analog systems can be designed to perform a specialized task, and may do so at high speeds compared to digital multipurpose devices. In particular, the interest in neuromorphic computation is partly motivated by the inefficiency of digital systems such as CPUs and GPUs to perform inherently analog tasks [36]. It is possible to use a general physical wave system with trainable parameters to implement analog components for machine learning [82]. A ferromagnetic film can be a suitable medium. One can train a magnetic medium by e.g. scatterers or magnetic arrays to produce the desired output signal based on one of several input signals [36]. The process of specifying the desired outcome first, and then changing the device design through feedback-based algorithms is known as *inverse-design* [86]. The concept of inverse-design is well known from photonics [87], and recently, we have started to take steps towards inverse-design magnonics [86, 88]. Such systems may play very well together with the developments in neuromorphic computation.

We will proceed to present a few cherry-picked ideas of how spintronics can be used in quantum computation and neuromorphic computation.

1.4.1 Spintronics and quantum computation

One of the most exciting prospects for the future of computation is the quantum computer [14, 34]. One of the basic units of the quantum computer is the quantum bit, or *qubit*. A qubit could be a quantum two-level system, where the system finds itself to be in one of two states, or a superposition between the two. One would need some way to prepare the qubit in the desired state, and to read out the state. One would also need to implement single- and two-qubit gates to manipulate the qubit state. Furthermore, the decoherence times of the qubits must be longer than the gate operation times, and the system must be scalable [34].

There are many suggestions on how to realize a qubit system [15, 16, 17, 18, 19]. One of the more explored applications of spin technology in quantum computation is the use of spin qubits [34]. One could use the spin state of an electron as a two-level system. We could imagine that spin qubits can be manipulated by spin-dependent transport, spin-orbit interactions and magnetic fields, which

are all central aspects in the development of spintronic devices. Furthermore, advances in novel spintronic materials could help spin qubits become more resistant to decoherence. And perhaps most important, the techniques researched in spintronics could be used to prepare and read out spin states. Spintronics could facilitate the potentially difficult integration of quantum and classical computation. The field where magnonic systems are integrated with quantum platforms has been referred to as *quantum magnonics* [89].

There has also been suggestions for different ways to utilize magnon condensates for qubits and semi-classical qubits [3, 32, 4]. There are several advantages of using magnon condensates. Magnon condensates can have quite long decoherence times, and magnons are not sensitive to electric noise [3].

1.4.2 Spintronics and neuromorphic computation

In neuromorphic computation, we want to mimic the way the brain works, both in the way we write software, and also in the way we engineer the hardware. This could be done by engineering specialized components, consisting of neuron models, synaptic models, memristors, circuits and sensors, and try to apply parallel processing and learning algorithms that are similar to how the neurons in our brain operate and communicate to each other. We could expect that neuromorphic computers will perform well in pattern recognition and predictions [90]. Another advantage of designing a whole new memory structure, is that we may avoid the issues of the von Neumann bottleneck [71].

Spintronic analogies to synapses and neurons are already being developed [90]. Components such as the magnetic tunnel junction can be used as building blocks in neuromorphic architectures [91]. One could also design small specialized systems where spintronic nano-oscillators act as the basic unit in the neural network [92]. In particular, weighted spin torque nano oscillators could be promising units in multilayer architectures. Other devices of interest include suggestions for analog magnon adders [93] and domain-wall based leaky integrate-and-fire neurons [94].

Chapter 2

Magnon condensates

In this chapter we discuss the main research subjects of this thesis; magnon condensates.

The research on Bose-Einstein condensates (BECs) started roughly a century ago, initiated by theoretical predictions by Satyendra Nath Bose and Albert Einstein [95, 96]. The work on bosons, Bose-Einstein statistics and the Bose-Einstein condensate has been important, and the 2001 Nobel Price in physics went to Cornell, Wieman and Ketterle for *"the achievement of Bose-Einstein condensation in dilute gases of alkali atoms, and for early fundamental studies of the properties of the condensates"* [97].

We discuss general Bose-Einstein condensates in Section 2.1. We proceed to discuss the magnon condensate and Bose-Einstein statistics in Section 2.2. In Section 2.3, we highlight some features we expect Bose-Einstein condensates to possess, and try to discuss whether the magnon condensate fulfils thesis criteria. In Section 2.4, we list a few proposed applications for BECs.

2.1 Bose-Einstein condensation

Subatomic particles can be classified based on their spin quantum number. Bosons have integer spin quantum number, while fermions have odd half-integer spin number. The Pauli exclusion principle states that fermions, such as the electron cannot occupy the same quantum mechanical state. Bosons, however, do not obey these rules. Any number of bosons are allowed to occupy the same quantum state. This means that it is possible for a large number of bosons to

all occupy the same state. Condensation can happen when the bosons share the lowest accessible ground state. The population becomes a macroscopic representation of a quantum mechanical state. This macroscopic occupation of a single quantum state is a phase transition we today know as Bose-Einstein condensation [98].

In 1924, Einstein published some of his work on the *quantum theory of the monoatomic ideal gas* [96, 99]. He had been reading through works by Bose [95], and was inspired to continue the research on boson gases. Einstein realized that the gas could transition into a phase where all the bosons occupied the lowest quantum state, and he expected that this new type of phase would have exotic properties. The theoretical predictions were solid, but there was a doubt whether it would be possible to find a physical realization of the boson condensate. If one would consider atomic gases, one would need a very high density to reach the BEC phase. More than a decade later, Fritz London suggested that there was some link between superfluidity in helium-4 and macroscopic wavefunctions such as the ones predicted in the theories on Bose-Einstein condensation [100, 101]. These claims were controversial at the time. A few years after Londons theories, Landau studied Bose liquids, and found that at low enough temperatures, there exists conditions where the liquid may show superfluid behaviour [102]. These ideas were further investigated by Bogoliubov, who developed models for a weakly interacting Bose-gas [103, 104].

The experimental verifications of the theories by Bose and Einstein turned out to become a long and confusing journey [105]. Now that we look back, we can say that the first experimental demonstration of a condensed Bose-gas might have been the work on liquid helium-4 by Kapitza [106] and Allen and Misener [107] in 1938. At that time, many scientists believed that liquid helium-4 could be an example of a BEC. But this was not straight forward to establish, as there were also some scientists that shared strong arguments for the opposing view [105]. It turned out to be very difficult to obtain any experimental evidence on the existence for any other type of bosonic condensate at the time.

By the time the 1990s arrived, scientists were still debating whether the liquid helium-4 systems were true BECs [105]. But the obstacles soon loosened up and in 1995, three different groups from the US reported observations of BEC behaviour in ultracold atomic gases [108, 109, 110]. After further investigations, Cornell, Ketterle and Wieman shared the 2001 Nobel Price in physics for their initial discoveries and subsequent work on the properties of the condensates [97]. The 2000s brought further observations of BEC in a range of systems, including quasiparticle condensates. For a comparison of some different BECs and their properties, one may refer to Ref. [105].

2.2 Magnon condensates and Bose-Einstein statistics

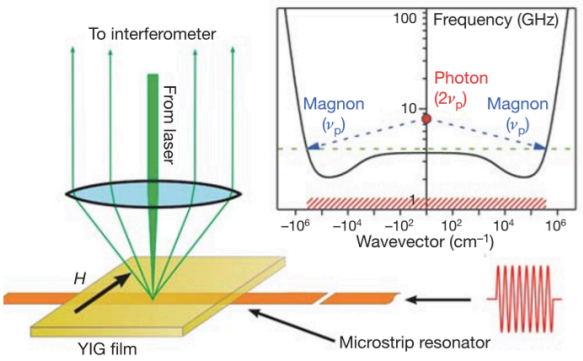

Figure 2.1: Figure from Ref. [2] illustrating the experimental setup used by Demokritov et al. when studying a magnon condensate in a thin YIG film. Magnons are excited by parametric pumping, and the resulting magnetization dynamics is studied by Brillouin light scattering. Spin waves travelling in the same direction as the external field have the lowest energy. This branch of the spin wave spectra has a double minima at finite wavevector number, where two condensate populations can form. During pumping, magnons are excited at opposite wavevectors at half of the pumping frequency, as illustrated by the blue dashed arrows. The magnons thermalize down to the minima. The red marking beneath the dispersion relation indicates the wave vector range accessible by Brillouin light scattering.

In 2006, Demokritov et al. reported their observations of a magnon BEC at room temperature in a thin ferromagnetic film [2]. This type of condensates are the main topic of this thesis. Quickly after the initial publication in 2006, several additional experiments were performed to investigate some central aspects of the condensate, such as the thermalization process and the resulting coherence[25, 26, 27, 28, 29, 30, 31]. In most of these early experiments on room temperature magnon BECs, the condensate is created by microwave pumping in a YIG film. Usually, a static field is orienting the magnetization to point along a chosen in-plane direction, and the pumping field in applied in parallel to the static field. Fig. 2.1, taken from Ref. [2], illustrates the experimental setup used by Demokritov et al. Magnons are excited in by parallel pumping, and the dynamics of the system is investigated by Brillouin light scattering (BLS). The parallel pumping technique and spin wave spectra of the thin ferromagnetic film will be discussed in Chapter 3. For now, it is sufficient to mention that because of the effects of the dipolar and exchange interaction, the dispersion for spin

waves travelling along the direction of the external fields will typically have a double minima at some finite wavevector number. Normally, BECs in other systems are described by a single spatially uniform wave function, while the ferromagnetic double condensate can be described by a linear combination of two non-uniform wave-functions [30]. In 2012, experiments by Nowik-Boltyk et al. showed that the double degenerate condensate results in the formation of a non-uniform ground state, where the condensate shows a standing wave pattern in real space [30].The observation is interpreted as a direct evidence that the double condensate shows spatial coherence. Recently, it was found that one can move magnon condensates spatially [111]. One can study the interactions between the two condensate populations theoretically using bosonization techniques. We will return to this topic in Chapter 3.

2.2.1 Bose-Einstein statistics

Magnons are bosonic quasiparticles, and follow Bose-Einstein statistics. According to Bose-Einstein statistics, the average number of bosons $\bar{n}_k$ in a particular state with energy $\hbar\omega_k$ in thermal equilibrium is given by the Bose-Einstein distribution function [112],

$$\bar{n}_k = [e^{\frac{\hbar\omega_k}{k_B T}} - 1]^{-1} \tag{1}$$

Here, k_B is the Boltzmann constant and T is the temperature. In thermal equilibrium, the corresponding probability $\rho_{th}(n_k)$ of finding n_k magnons at a certain energy $\hbar\omega_k$ is found by [112, 113],

$$\rho_{th}(n_k) = \frac{(\bar{n}_k)^{n_k}}{(1+\bar{n}_k)^{n_k+1}}. \tag{2}$$

In contrast, the probability $\rho_{coh}(n_k)$ to find n_k magnons in a coherent state $|\alpha_k\rangle$ such as the expected condensate state is given by a Poisson distribution [112, 113],

$$\rho_{coh}(n_k) = \frac{|\alpha_k\rangle^{2n_k}}{n_k!} e^{-|\alpha_k|^2}. \tag{3}$$

Note that the coherent probability distribution $\rho_{coh}(n_k)$ describes a peak centered at $\langle n_k\rangle = |\alpha_k|^2$, while the thermal distribution $\rho_{th}(n_k)$ resembles an exponential decay $\propto e^{-\bar{n}_k}$ for high number of magnons [112].

In the experiments on magnon BECs, a microwave field oscillating at frequency ω_p pumps magnons into the system and these magnons will have energies at $\omega_p/2$. The number of pumped magnons is large conpared to the themal magnon population. The magnons may scatter and redistribute over a broad range of frequencies and wavevectors, before thermalizing down to the dispersion minima at ω_{min}. In YIG, we expect that the spin-lattice relaxation time is low compared to the inter-magnon decay time [112]. The injected magnon gas then has a long life time over which its magnon number does not change drastically, and we can think of this population as being decoupled from the surrounding system. We now restate the Bose-einstein distribution for this population as,

$$\bar{n}_{\mathrm{BEC}} = [e^{\frac{\hbar\omega - mu}{k_B T}} - 1]^{-1} \tag{4}$$

Here, μ is the chemical potential. A spin system in thermal equilibrium has a chemical potential of zero [101]. At high temperatures ($k_B T \gg \mu$), the distribution is similar to the classical Maxwell-Boltzmann distribution, and the bosons behave similarly to classical particles. At low temperatures ($k_B T \ll \mu$), the number of bosons in the lowest energy state can become macroscopically large. As the chemical potential approaches the ground state energu, the boson gas may undergo a phase transition into a BEC.

For systems with constant number of particles, we usually use Eq. (4) and not Eq. (1), provided that the system is in equilibrium and there is no interaction between the bosons of the populations [112]. As a crude model with two temperatures, we could view the system of microwave pumped BEC to be consisting of two subsystems [112]. The first is the thermal equilibrium populations for magnons at energies higher than $\omega_p/2$. The second subsystem is the population described by Eq. (4) for magnons at energies between ω_{min} and $\omega_p/2$. The second subsystem can be said to have its own effective temperature, which is high compared to the first subsystem.

2.3 Bose-Einstein condensate properties

Although Bose-Einstein condensation manifests in a different way in the wide range of bosonic systems, there are some common characteristics we expect the BEC to possess. There is wide agreement that magnons form coherent populations at the lowest energy state, and today, this phenomena is usually referred to as a Bose-Einstein condensate. In the case of a ferromagnetic double magnon condensate at positive and negative wave vector number, there has been experimental observations of spatial interference between the two condensate populations, which suggests that the condensate is indeed coherent [30, 101]. In addition to this absolute requirement, we should also address another canonical

property of Bose-Einstein condensation; the *spontaneous* emergence of the coherent state [33]. When we demand that the magnon condensate should appear spontaneously, this means that we should not inject magnons straight into the lowest energy state, keep driving the system in this state, and then refer to it as a magnon BEC. One should observe that magnons that occupy one or several other energy states thermalize down to the lowest energy state. The BEC terminology is usually associated with quantum behaviour, such as superfluidity and Josephson oscillations [114, 5, 115, 116, 117, 118, 119, 120, 117]. However, certain aspects of the magnon condensation can be explained by semi-classical physics [121]. Ref. [33] suggests that we could adopt a more general terminology, and describe the magnon condensate simply as a *spontaneous emergence of coherence*.

Therese has been as discussion whether the concept of Bose-Einstein condensation truly should apply to magnons [33]. One of the first questions to consider is whether there really can be anything such as a quasiparticle BEC. Quasiparticles have finite lifetimes. However, if the lifetime of the particle is long compared to their scattering times, one should be able to say that condensation is possible [33]. In the case of magnons, their lifetime is strongly dependent on factors such as material parameters. For ferromagnets with low damping, the ratio of the magnon lifetime to the thermalization time can be as large as 500 [2].

2.4 Bose-Einstein condensate application

BECs are interesting subjects in fundamental research, since they represent a macroscopic quantum state. The condensates may also have some relevant practical applications. The coherent nature of the condensates could perhaps be useful for precision measurements, e.g. in the form of sensors. For example, one could use BECs for highly accurate atomic clocks [122] or sensors for detecting gravitational waves [123].

As we discussed in Section 1.1, the magnon BECs may be useful for potential quantum computation platforms [3, 32], even if we do not take advantage of all quantum properties of the condensate [4]. The room temperature magnon BEC would be convenient to work with for future applications. Fig. 2.2 from Ref. [4] illustrates a semi-classical magnon qubit. The double condensate system is characterized by the relative phases of the condensates, and the number of magnons in the condensate populations. In this way, the condensate can be in a variety of states. There are examples of problems one can solve using quit calculus that is not dependent on entanglement [35], including the quantum Fourier transform [125, 126, 35]. The coupling between the magnon BEC qubits could be implemented through magnon supercurrents and Josephson os-

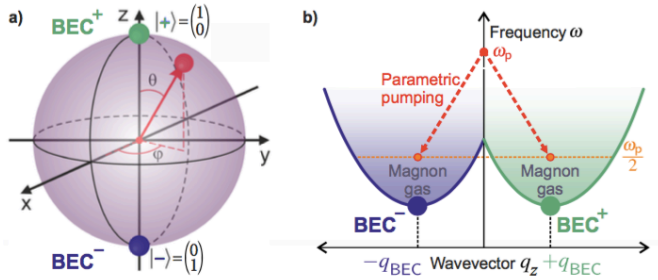

Figure 2.2: Figure from Ref. [4] illustrating how the magnon Bose-Einstein condensate can be used as a semi-classical qubit for a quantum computation platform. The Bloch sphere [124] in (a) shows the pure states $|+\rangle$ (green) and $|-\rangle$ (blue), representing populations in the two energy minima of the dispersion relation. The condensate can also be found in a mixed state (red). By controlling the number of magnons in each of the condensates and the relative phase of the condensate, one may reach any position on the Bloch sphere. Figure (b) shows the well known dispersion relation of the ferromagnetic film. The two pure states are indicated by the green and blue part of the symmetric dispersion.

cillations [35, 4, 120, 119]. The semi-classical magnon BEC qubit might help bridge the gap between traditional computation and quantum computation. The Josephson oscillations of magnon BECs [127] may become interesting also for other applications, in light of suggestions that magnon BECs may be used to generate and control spin-wave currents in ferromagnetic insulators [5].

Today, Bose.Einstein condensation represents a large interdisciplinary field of research. The advances and setbacks of creating and observing different BECs constitute a chaotic storyline. One can consult the book Universal Themes of Bose-Einstein Condensation [98] for a valuable and entertaining summary.

Chapter 3

Theoretical frameworks

In this chapter, we introduce some theoretical frameworks that are useful when studying magnetic systems.

We focus on two main strategies; a *semi-classical* approach and a *quantum* approach. We will demonstrate how these two different methods can be applied to study a magnetic system, and which information we can gain about the system by the two approaches. Our main interest is to use the frameworks to study magnon creation, magnon interactions, and subsequently the magnon condensates. Since the experimental work on magnon condensates often is performed for thin ferromagnetic films, we will start by focusing on ferromagnetic spin dynamics.

Section 3.1 is a short introduction to some different ways to study magnetic systems. Section 3.2 will introduce how to set up micromagnetic simulations utilizing the Landau-Lifshitz-Gilbert (LLG) equation, which allows us to calculate the dynamics of magnetic moments due to some effective field describing the surroundings. We discuss the spin wave spectra of a thin ferromagnetic film. We also discuss two ways to create magnons in the thin-film ferromagnet; parallel pumping and spin-transfer torques. The section is intended to explain the frameworks used in Ref. [6]. Section 3.3 introduces a quantum approach where the Holstein-Primakoff transformation allows us to express the spin system in terms of bosonic creation and annihilation operators. This approach is familiar from quantum mechanics, and is more directed towards the particle-like properties of the magnon. We discuss how one can use the expressions for the magnon interactions to gain knowledge about the properties of the two magnon populations in a thin ferromagnetic film. The section is meant to explain the frameworks we used in our work in [7]. In Section 3.4 we present some examples on how to apply the bosonization techniques from Section 3.3 to antiferromag-

netic systems. In addition, we take a quick look at an alternative bosonization approach; the Dyson-Maleev transformation. Since we are already familiar with the bosonization approach from Section 3.3, we use the opportunity to present the uniaxial and biaxial antiferromagnetic systems of our research in Ref. [9].

3.1 Studying magnetic systems

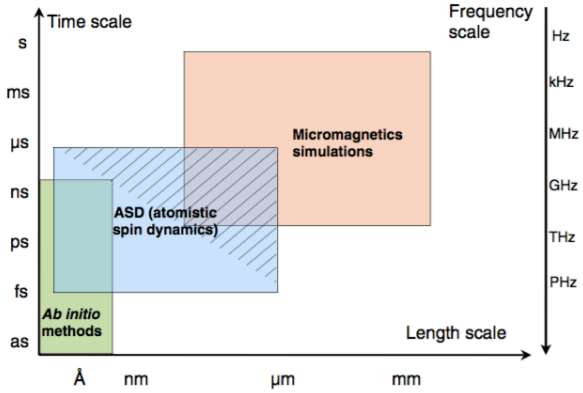

Figure 3.1: Figure from Ref. [128]. Ab initio methods are generally useful for small systems with fast spin dynamics. Micromagnetic simulations can be used for larger systems. Atomistic spin-dynamics (ASD) can bridge the gap between the two modelling tactics [128].

The most accurate quantum mechanical picture of a magnetic system would require modelling every spin as a separate unit, and then solving the n-body problem. Only the most simple systems would be possible to solve analytically without approximations [129].

There are several methods based on *ab-initio* approaches that produce useful predictions of macroscopic material properties. For instance, density functional theory (DFT) calculations [130] allows us to study band formation and spin pairing of materials. This can provide us information on the expected magnetic properties of a material, and the expected distribution of magnetization density in a lattice [38]. Nevertheless, one can not expect to be able to explain all features of a magnetic material starting from first-principle calculations.

In practice, most ab initio approaches are usually restricted to length scales below a few nanometers. In general, micromagnetics are suitable for studying spin wave dynamics of systems that are in the range of a few nanometers to a

few micrometers, or even millimetres [129, 128]. Approaches such as atomistic spin dynamics can bridge the gap between ab initio methods and micromagnetics [131, 128]. There are more factors to consider than the size of the system. In the micromagnetic approach we normally consider some average magnetization for the whole lattice unit, and we lose lattice structure information. The micromagnetic approach does not account for atomic-size defects [131].

In general, the time and length scales for our system strongly influences which theoretical model we use to describe the systems [131, 128]. Fig. 3.1 from Ref. [128] summarizes the typical length and time scales where micromagnetic simulations are useful.

3.2 The *semi-classical* approach : micromagnetics

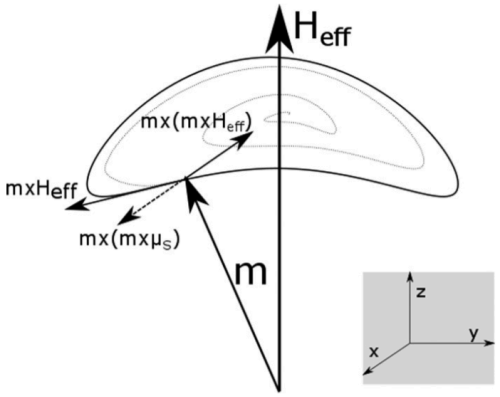

Figure 3.2: The magnetization $\boldsymbol{m}$ precesses around the effective field $\boldsymbol{H}_{\text{eff}}$ due to the field-like-torque $-\boldsymbol{m} \times \boldsymbol{H}_{\text{eff}}$. The damping $-\boldsymbol{m} \times (\boldsymbol{m} \times \boldsymbol{H}_{\text{eff}})$ tends to align the magnetization along the ground state determined by the effective field. The damping can be manipulated by applying spin-transfer-torques via the spin accumulation μ_S as in Eq. (1.7). The figure is from Ref. [6].

Magnetic materials usually have one or several ground states, determined by the magnetic free energy of the system. If the individual magnetic moments are not aligned according to the ground state of the spin system, the moments will experience a torque. This torque will induce a precession of the magnetic moments. In addition to the free energy terms that we combine into the concept of an *effective field*, the system also has processes we associate with energy loss, or spin

wave damping. There are several mechanisms that may lead to spin wave damping. In actual experimental systems, spin waves couple to their environment, and the spin-lattice interactions lead to a loss of energy that is often realized as phonons. But one can also have damping due to spin-spin interactions. An example is the intrinsic spin-spin relaxation due to magnon scattering processes involving three or more magnons [59, 132]. One can quantify the damping of a material experimentally by conducting ferromagnetic resonance linewidth measurements [132]. Altogether, the magnetic moment will pursuit to align itself along the ground state, so that the energy is minimized. The resulting motion is therefore a precession with damping towards the ground state.

In 1035, Landau and Lifshitz presented a dynamical equation predicting the time development of a magnetic moment due to their surroundings magnetic free energy [56]. The equation was later extended by Gilbert to include a damping term, describing the dissipation of energy, or magnon annihilation [133]. The resulting Landau-Lifshitz-Gilbert equation gives us the dynamics of the magnetization,

$$\dot{\boldsymbol{m}} = -\gamma(\boldsymbol{m} \times \boldsymbol{H}_{\text{eff}}) + \alpha(\boldsymbol{m} \times \dot{\boldsymbol{m}})\,. \tag{1}$$

Here, $\boldsymbol{m}$ is the reduced magnetization of unit length, α is the dimensionless Gilbert damping constant, and $\gamma = 1.7595 \times 10^{11}\,\mathrm{rad\,T^{-1}\,s^{-1}}$ is the gyromagnetic ratio. The effective field $\boldsymbol{H}_{\text{eff}} = -\frac{1}{\mu_0 M_S}\frac{\partial U}{\partial \boldsymbol{m}}$ is the variational derivative of the magnetic free energy U with respect to the magnetization [129]. M_S is the saturation magnetization. The effective field includes the chosen contributions of magnetic free energies in the system, such as externally applied fields, the exchange interaction, dipolar interactions, magneto-crystalline anisotropies, and the Dzyaloshinskii-Moriya interaction [134]. We will encounter these energies in Section 3.2.3.

Fig. 3.2 illustrates the temporal dynamics of the magnetization as described by the LLG-equation. The first term of Eq. (1) represents the precession of the magnetization around the effective magnetic field. The term is sometimes referred to as the field-like torque. The second term represents the damping. If allowed enough time, a system will tend to align itself to the ground state along the effective field.

The LLG equation was initially derived phenomenologically [56, 133], meaning that it was not entirely derived from first principles, but partly based on experimental observations. We highlight three properties of the LLG equation [135]. The first point to mention, is that the LLG equation preserves the length of the normalized magnetization. Secondly, the equation is said to have a *Lyapunov structure* [135, 129] given that the applied field is constant and we do not include anti-damping-like terms such as the spin-transfer-torques of Eq. (17).

This means that the free energy will never increase as a function of time. At any point, the system will approach a state of lower energy, though this might not necessarily be the global energy minima. Thirdly, if we ignore the damping-like terms, the LLG equation has a Hamiltonian structure [136, 129].

The LLG equation is derived within the continuum model that assumes that the magnetic properties of the system is continuous and smooth, instead of discrete. For the continuum model to be valid, one assumes that the relevant length scales of the system are *large enough* so that we can substitute the individual spins with a continuous magnetization function. In general, such a classical continuum description requires that the magnetization is nearly homogeneous over a length scale greater than the lattice constant of the material. On the other end, the relevant length scales should be *small enough* to resolve any important features such as domain walls and vortices [137]. In this sense, one expects that the spin direction does not change dramatically between the neighbouring sites. In the case of a ferromagnet, the magnetic moments are near perfectly aligned, given that the temperature is below the Curie temperature. In this case, the magnetization can be expressed in terms of the homogeneous saturation magnetization strength M_S.

We will proceed to show how the LLG equation can be used in numerical simulations.

3.2.1 Micromagnetics

The LLG equation is nonlinear. There are few situations where one can work analytically with the LLG equation, even when applying linearization techniques. However, micromagnetic simulations based on the LLG equation have become popular [138].

When using micromagnetic simulations to analyze a device or material, one would start off be defining a suitable geometry and material properties. The geometry is then discretized into cells, each defined by a magnetization unit vector $\boldsymbol{m}_i$ at position $\boldsymbol{r}_i$. The positions can be arranged using finite difference methods, where the geometry is divided into predetermined sites, usually with a fixed distance between each point. This is convenient when working with geometries that are easily discretized into straight arrays of cuboids. For some geometries and parameter choices, a primitive cuboid discretization may add up to non-negligible errors, especially when calculating the dipolar interactions. If one needs more flexibility in the chosen geometry one could choose an approach based on finite element methods instead. The improved error estimates will generally be accompanied by an increase in the computational costs.

Given some initial magnetization state, one can calculate the magnetic free

energy, and solve the LLG equation for each successive time step. This approach gives the user a complete description of how the magnetization behaves at each point as time advances. From this, one can analyze which spin waves are present, and resolve them in momentum and frequency through discrete Fourier transforms, such as in Eq. (4).

Micromagnetic simulations allow us to model the magnetization dynamics for the magnetic moment in each cell, and one can obtain full information of which magnons are present in the system. The simulations also allow us freedom to investigate exciting geometries. This means that one can study and create theoretical prototypes for devices [139, 59, 140, 86].

Working with micromagnetic simulations can be challenging. In some ways, conducting simulations may feel a bit similar to running an experiment one does not know the outcome of. The LLG equation in nonlinear, and even in a simple system, one encounters hysteretic behaviour, critical thresholds for magnon creation, critical thresholds for condensate formations, and so on.

Even though the simulations give us full information on the spin waves, it is difficult to analyze concepts we think of as particle-like, such as the interaction between magnons. Another challenge with the simulations is the computational cost. Usually, the dipole-dipole energies will be the most computationally expensive term, since it needs to take into account the long range interactions between each magnetic moment.

Micromagnetic simulations are getting popular, and there exist several options for prewritten micromagnetic software. Many frameworks are open-source. Some of the more popular choices of micromagnetic software includes OOMMF [141], MicroMagnum [142], MuMax3 [134], Nmag [143], FastMag [144] and Boris [145]. In Refs. [6] and [7] we used MuMax3m which utilizes GPU computations. MuMax3 is based on finite-difference discretization which is sufficient for our square film system. The software has low memory requirementsm and allows us to model a range of phenomena, including the presence of time-dependent external magnetic fields and spin-transfer torques [134].

3.2.2 Thin film simulations

Let us consider a thin film ferromagnet in the $\hat{\mathbf{y}}$,$\hat{\mathbf{z}}$-plane. The film has lateral lengths $L_y = L_z$ which are much larger than the film thickness L_x. We choose to model the film as a 2D-system, where the magnetization in the thickness direction is uniform. The film is discretized into $N_y \times N_z$ cells, each containing a magnetization unit vector $\boldsymbol{m}(\boldsymbol{r}_i, t)$.

There are several considerations to make when choosing system parameters for

performing micromagnetic simulations. As a general rule, one should try to keep the cell size small enough, e.g. $\Delta y, \Delta z \leq l_{\text{ex}}$, where l_{ex} is the exchange length of Eq. (7). We would also like the cell sizes $\Delta x, \Delta y, \Delta z$ to be within two orders of magnitude of each other [134].

After considering the resolution in real space, one should also plan for the resolution one needs in momentum and frequency space [146]. We may analyze the spin wave frequency and wavevectors by performing discrete Fourier transforms such as in Eq. (9). The resolved waves then have a wavevector and frequency discretization Δk and Δf, while the highest wavevector and frequency we can resolve is $k^{\max}$ and $f^{\max}$.

$$\begin{aligned} \Delta k_z &= \frac{1}{N_z \Delta z} = \frac{1}{L_z} & \qquad \Delta f &= \frac{1}{N_t \Delta t} \\ k_z^{\max} &= \frac{1}{2\Delta z} & \qquad f^{\max} &= \frac{1}{2\Delta t} \end{aligned} \tag{2}$$

Here, N_t and Δt is the number of time steps and length of each time step for the time window $t_F = N_t \Delta t$ we do the Fourier transform over. A good wavevector and frequency resolution (low Δk_z and Δf) requires a large film size $N_z \Delta z$ and time window $\mathrm{N}_t \Delta t$. As a general requirement, we should choose a low enough $\Delta y, \Delta z, \Delta t$ to represent the spin waves, e.g. by choosing discretizations that satisfy the Nyquist-Shannon sampling theorem [147, 148].

When choosing time discretization, one should think about which magnetization dynamics one expects to appear in the system. Typically, ferromagnets have frequencies in the GHz range. In the case of the thin ferromagnetic film, the dispersion relation is well known, and we have some idea about the frequencies and wavevector numbers of the expected spin waves in the system. If we want to analyze high-energy magnons we must make sure that the numerical $f^{\max}$ of Eq. (2) is high enough, which means we need small time steps. Furthermore, if we study a thin ferromagnetic film with a very flat dispersion relation minima, we may want to have a high resolution in frequency space. This requires us to do the Fourier transformation over a large time window, and we may risk that our condensate properties will have changed during that time window. For this reason, one may prefer to study semi-stable states where properties such as the magnon density does not change drastically during the relevant time window.

When running simulations, one gets information on the magnetization at each timestep. The magnon density in the film is proportional to the average deviation from the ground state. If this is along the external field in the z-direction, then the magnon density η is determined by the longitudinal component of the

average magnetization,

$$\eta = 1 - \langle m_z \rangle = 1 - \frac{1}{N} \sum_{i}^{N} m_z(y_i, z_i)\,. \tag{3}$$

The frequencies and wavevectors of the magnons in our simulation are analyzed by performing a discrete Fourier transform over the transversal magnetization components as a function over both the spatial and temporal dimensions, i-e- our plane directions and time. This gives us the magnon distribution $\xi(k_y, k_z, \omega)$ [6],

$$\xi(k_y, k_z, \omega) = |\mathcal{F}[\boldsymbol{m}_x(x, y, t)]|^2 + |\mathcal{F}[\boldsymbol{m}_y(x, y, t)]|^2\,. \tag{4}$$

We will now introduce the magnetic free energies that are commonly included in the effective field H_{eff} of Eq. (1).

3.2.3 Magnetic free energies

The magnetic free energy of a ferromagnetic film typically contains terms such as the exchange energy, dipolar energy, magneto-crystalline anisotropies and external fields. These energy terms can be linearly combined into the effective field H_{eff} of Eq. (1).

Zeeman field

We can orient the magnetization of a spin system along a desired direction by applying a sufficiently strong static field of strength H_0. Id we choose to apply the static field in the $\hat{\mathbf{z}}$-direction, the resulting Zeeman energy reads [6],

$$\boldsymbol{H}_{\text{ext}} = H_0 \hat{\mathbf{z}}\,. \tag{5}$$

When modelling magnon excitation by parametric pumping, one may also choose to include additional dynamic fields to this external field term, such as in Ref. [6].

Exchange field

The exchange field originated from the quantum mechanical Heisenberg exchange interaction. the exchange interaction is short-range, and usually only computed for spins at the nearest neighbour sites. For a ferromagnet, the exchange field promotes a homogeneous magnetization. In the micromagnetic formulation for a ferromagnet, the exchange field can be expressed as [134],

$$\boldsymbol{H}_{\text{exch}} = 2\frac{A_{\text{ex}}}{M_S}\nabla^2\boldsymbol{m}\,. \tag{6}$$

Here, A_{ex} is the exchange stiffness [149], and M_S is the saturation magnetization. We define the exchange length as,

$$l_{\text{ex}} = \sqrt{2A_{\text{ex}}/(\mu_0 M_S^2)}\,. \tag{7}$$

The exchange length [137] may act as a measure for the relative importance of the exchange energy compared to the demagnetization energy.

Dipole field

The dipole field consists of two-parts; the static demagnetization field and the dynamic terms due to the long-range magnon-magnon interactions. In general, the dipole field at position $\boldsymbol{r}$ can be expressed in terms of contributions from the magnetization $\boldsymbol{m}(\boldsymbol{r'})$ at distance $\boldsymbol{d} = \boldsymbol{r} - \boldsymbol{r'}$, integrated over the film volume V [150],

$$\boldsymbol{H}_{\text{d-d}}(\boldsymbol{r}) = \frac{\mu_0}{4\pi}M_S\int_V \mathrm{d}\boldsymbol{r'}\frac{3(\boldsymbol{m}(\boldsymbol{r'})\cdot\boldsymbol{d})\boldsymbol{d}}{|\boldsymbol{d}|^5} - \frac{\boldsymbol{m}(\boldsymbol{r'})}{|\boldsymbol{d}|^3}\,. \tag{8}$$

Here, μ_0 is the permeability of free space. The dipole field can be rewritten in terms of a 3×3 tensor $\hat{G}(\boldsymbol{r},\boldsymbol{r'})$,

$$\boldsymbol{H}_{\text{d-d}}(\boldsymbol{r}) = \mu_0 M_S\int_V \mathrm{d}\boldsymbol{r'}\hat{G}(\boldsymbol{r},\boldsymbol{r'})\cdot\boldsymbol{m}(\boldsymbol{r'})\,. \tag{9}$$

Here, the tensor elements of $\hat{G}(\boldsymbol{r},\boldsymbol{r'})$ are $G_{\alpha,\beta} = -\frac{1}{4\pi}\frac{\partial}{\partial\alpha}\frac{\partial}{\partial\beta}\frac{1}{|\boldsymbol{d}|}$, for coordinates $\alpha,\beta = x,y,z$.

Anisotropy field

The magnetic anisotropy describes the tendency of the magnetic moments to prefer a certain direction within the lattice. These preferred directions are often referred to as easy-axes. The magnetic anisotropy energy accounts for the deviation from these directions. One may also have hard-axes, which describes directions the magnetic moments prefer not to align to.

A material might have one or several preferred axes to align to. Often, the source of the anisotropy can come from spin-orbit interactions in the material, or from some shape anisotropy from the dipolar interaction. One can to some extent manipulate the anisotropy by doping the material [151]. In particular, one can introduce anisotropy by doping the material with a heavy metal with large spin-orbit interaction [8]. One may also introduce stress or strain to the material [152]. Stress and strain may break the symmetry so that one can increase the materials spin-orbit interaction which in turn affects the anisotropy.

A simple easy-axis uniaxial anisotropy along a direction $\hat{\mathbf{n}}$ can be modelled as [134],

$$\boldsymbol{H}_{anis} = \frac{2K_{\text{an}}}{\mu_0 M_S}(\hat{\mathbf{n}} \cdot \boldsymbol{m})\hat{\mathbf{n}}\,. \tag{10}$$

Here, $K_{\text{an}} > 0$ is the anisotropy constant [134]. One can change the sign of the anisotropy constant so that Eq. (10) describes a hard-axis instead. A hard-axis anisotropy in e.g. the $\hat{\mathbf{x}}$-direction would correspond to an easy-plane in the $\hat{\mathbf{y}}, \hat{\mathbf{z}}$-directions.

Spin wave spectra for the thin film ferromagnet

Spin waves in ferromagnets have been extensively studied for more than half a century [153, 154, 155, 156, 157, 158, 159, 160, 112, 121].

For a YIG film where the magnetization is oriented by an external field, it is customary to include the Zeeman, exchange, and dipole interaction terms. We follow the procedure in Ref. [6], where we employ a thin-film approximation by assuming that there is no variation in the magnetization in the film thickness direction, which we will call the $\hat{\mathbf{x}}$-direction in our chosen geometry. We express the Hamiltonian of the thin film in terms of the in-plane coordinate $\boldsymbol{\rho} = y\hat{\mathbf{y}} + z\hat{\mathbf{z}}$,

$$\boldsymbol{H}_{\text{eff}}(\boldsymbol{\rho},t) = H_0\hat{\mathbf{z}} + 2\frac{A_{\text{ex}}}{M_S}\nabla^2_{\boldsymbol{\rho}}\boldsymbol{m}(\boldsymbol{\rho},t) + \mu_0 M_S \int_S \hat{G}(\boldsymbol{\rho},\boldsymbol{\rho'})\boldsymbol{m}(\boldsymbol{\rho'},t)\mathrm{d}\boldsymbol{\rho}\,. \tag{11}$$

Since the system is effectively 2-dimensional, we can integrate the dipolar expression over the thickness direction. We assume that the lateral lengths of the film are much larger than the thickness. When calculating the dipole terms, we may then do the integration over infinite lateral lengths [150]. Furthermore, we consider a linear response regime, with magnetization vector $\boldsymbol{m}(y,z,t) = \hat{\mathbf{z}} + \boldsymbol{\delta}_m(y,z,t)$. Here, the small deviation $\boldsymbol{\delta}_m(y,z,t)$ from the ground state lies in the ($\hat{\mathbf{x}}$,$\hat{\mathbf{y}}$)-plane. We retain only first-order terms in the deviation, and we assume that the magnetization precesses with frequency ω, so that $\boldsymbol{\delta}_m(y,z,t) = \boldsymbol{\delta}_m(y,z)e^{i\omega t}$. Then, we can express the LLG equation as an eigen value problem, where the eigenvalues are the precession frequencies ω.

We define the angle θ_k as the angle between the spin wave propagation direction and the ground state direction $\hat{\mathbf{z}}$. the magnon wavevector is then $\boldsymbol{k} = |k|(\cos(\theta_k)\hat{\mathbf{y}} + \sin(\theta_k)\hat{\mathbf{z}})$.

We proceed to define the Fourier transform pair,

$$\boldsymbol{m}(\boldsymbol{k}) = \mathcal{F}[\boldsymbol{m}(\boldsymbol{\rho})] = \frac{1}{2\pi}\int \boldsymbol{m}(\boldsymbol{\rho})e^{-i\boldsymbol{k}\cdot\boldsymbol{\rho}}\mathrm{d}\boldsymbol{\rho}\,. \tag{12}$$

$$\boldsymbol{m}(\boldsymbol{\rho}) = \int \boldsymbol{m}(\boldsymbol{k})e^{-i\boldsymbol{k}\cdot\boldsymbol{\rho}}\mathrm{d}\boldsymbol{k}\,. \tag{13}$$

This allows us to express the magnon energies in terms of the wavevector, and we may obtain the dispersion relation [156, 160, 121, 6],

$$\omega(k,\theta_k) = \sqrt{\omega_H + \omega_M l_{\text{ex}}^2 k^2 + \omega_M(1-f_k)\sin^2(\theta_k)} \times \sqrt{\omega_H + \omega_M l_{\text{ex}}^2 k^2 + \omega_M f_k}\,. \tag{14}$$

Here, $\omega_M = \gamma\mu_0 M_S$, $\omega_H = \gamma H_0$ and l_{ex} is the exchange length from Eq. (7). The form factor f_k arising form the dipole interaction account for the film thickness,

$$f_k = \frac{1 - e^{-|k|L_x}}{|k|L_x} \tag{15}$$

Fig. 3.3 shows the spin-wave dispersion of Eq. (1.4). Spin waves travelling in the direction of the external field ($\theta_k = 0$) have the lowest energy. We note that the dispersion relation is symmetric in k, and has a double minima at finite wavevector number $k = \pm Q$. At high wavevectors, $k \gg l_{\text{ex}}^{-1}$, the exchange interaction dominates, and the precession is circular. At small wavevectors, $k < L_x^{-1}$, the dipole interaction dominates and the precession is more elliptical. In the case of spatially uniform precession ($k = 0$), the system is said to be in ferromagnetic resonance (FMR). The spin wave spectra also gives the information on the group velocity, which is proportional to the derivative $d\omega/dk$.

The different spin waves of a ferromagnetic system has been characterized by Damon and Eshbach [153]. There are three types of magnetostatic spin waves that are particularly relevant to the thin-film ferromagnet [59, 161].

Backward-volume magnetostatic spin waves (BVMSWs) are spin waves ravelling in parallel to the in-plane external magnetic field (see the solid branch of Fig. 3.3). These spin waves have low energy. The magnon condensates we discuss in this thesis are usually formed for these low energy magnons. At low wavevector number, they have negative group velocity.

Magnetostatic surface-spin waves (MSSWs) are spin waves travelling perpendicular to the external in-plane field (see the dotted branch of Fig. 3.3). They are sometimes referred to as Damon-Eshbach modes [162], and have positive group velocity.

Forward-volume magnetostatic spin waves (FVMSWs) are spin waves that travel in the film plane, in a system where the external field is directed out of the film plane. This means that the spin waves travel perpendicular to the field.

3.2.4 Magnon excitation

Now that we have derived the spin wave spectra for the thin film ferromagnet in Eq. (1.4), we may discuss how to excite magnons in the system. Magnon creation can happen through a range of mechanisms. At finite temperatures, the spin system will experience random fluctuations. This means that a spin system at non-zero temperature will have a population of incoherent thermal magnons at low energies. Furthermore, magnons can be created by an external magnetic field. In a ferromagnet, the spins in the material will align with the direction of the magnetic field if the field is strong enough, and one can use the field to create oscillations (or spin flips) in the material.

We will focus on two common techniques for magnon creation in ferromagnetic thin films; parallel parametric pumping by a microwave field, and spin-transfer torques. Both parametric pumping [2] and spin-transfer torques [8] have been

utilized to create magnon BECs in thin ferromagnetic films.

Parametric pumping

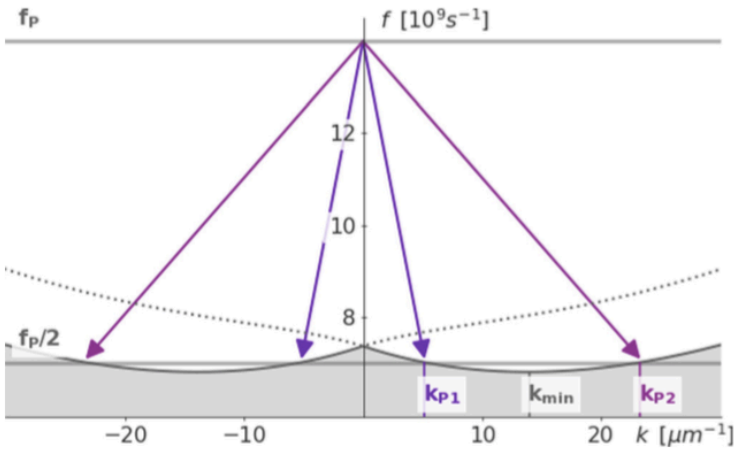

Figure 3.3: Figure from Ref. [6]. The dispersion relation for a thin ferormagnetic film. We show the lowest energy branch, which corresponds to spin waves that travel in the plane in the same direction as the applied magnetic field. Spin waves traveling perpendicularly to the field have higher energies, as indicated by the dashed line. During parametric pumping, two magnons are created at wavevectors of opposite signs. These magnons both have half of the frequency of the pumping field f_p. In the k_z branch, these magnons are found at $\pm k_{p1}$ or $\pm k_{p2}$. In turn, they thermalize and eventually occupy the dispersion minimum at $k_{\min}$.

Parametric pumping is a non-linear excitation technique where an external microwave field creates magnons in the spin system [163]. In this way, we could think of the pumping as a process where photons are converted into magnons. The technique was introduced in the 1950s [164, 165, 166]. The parametric pumping ha become quite common, and was utilized to generate the first magnon Bose-Einstein condensate in a room temperature ferromagnetic film in 2006 [2]. The relevance to the BEC has motivated further studies on magnon creation by pumping, thermalization processes of the created magnons, and the coherence of the emerging condensate [167, 168, 169, 170, 171]. The parametric pumping technique has also been investigated as a tool to amplify spin waves [172, 173, 163].

We will focus on the parallel pumping geometry. We consider a ferromagnetic

film where the external static magnetic field orients the magnetizationalong the in-plane direction $\hat{\mathbf{z}}$. A microwave AC pumping field is applied in parallel to the static external field. The pumping field of frequency ω_p will couple to the longitudinal component $\boldsymbol{m}_z$ of the ferromagnets magnetic moments. If the pumping field is strong enough, the coupling will subsequently induce oscillations in the transversal magnetization components $\boldsymbol{m}_x$ and $\boldsymbol{m}_y$. The transversal components will oscillate at half of the frequency of the longitudinal component.

Fig. 3.3 shows the familiar dispersion relation for the ferromagnetic film. The solid line is the branch for magnons travelling along the direction of the magnetic field $H_0\hat{\mathbf{z}}$. During parallel pumping, two magnons will be created at opposite momenta, at half the pumping frequency. The excitation by parallel pumping is most effective for elliptical modes. Circular modes have less oscillation in the longitudinal magnetization component, which mean that they couple weaker to the pumping field. The dipole-dominated modes at low wavevectors are elliptical, while the exchange-dominated modes at high wavevector precess more circularly. We therefore expect that magnons are pumped in the k_z-branch at $k_z = k_{p1}$, rather than at $k_z = k_{p2}$, illustrated in Fig. 3.3. Moreover, we expect that the most efficient pumping occurs when $k_{p1} = k_{p2} = 0$, at ferromagnetic resonance conditions, since the ellipticity is highest in that situation.

I the micromagnetic simulations, we may include the effects of the pumping field in the Zeeman term of Eq. (5). The effective field H_{eff} of the LLG equation in Eq. (1) then gets the following contribution,

$$H_{\text{ext}} = (H_0 + h_p \cos(\omega_p t))\hat{\mathbf{z}}\,. \tag{16}$$

Here, H_0 is the strength of the external static field, while h_p is the strength of the pumping field. The strength of the pumping field must overcome some critical threshold strength before any spin wave is excited. This threshold is likely to show some hysteretic behaviour, since it is easier to drive spin waves that are already present in the system, than to excite spin waves in a homogeneous "stiff" spin system.

The parallel pumping allows us to excite magnons at a specific energy. This means we have a high control of the types of magnons we create.

Spin-transfer torques

The spin-transfer torques (STTs) are a more recent approach to generate magnons in thin films [63, 174]. It has been found that the STT can be used as a control mechanism for the formation properties of the magnon BEC [175].

In the early 1970s, Dyakonov and Perel investgated the coupling mechanisms between charge and spin currents [176, 177, 132]. Almost 30 years later, Hirsch realized that this coupling mechanism could be very useful, and referred to the effect as the *spin-Hall effect* (SHE). In metals with strong spin-orbit interactions, the spin-Hall effect can convert a charge current into a transverse spin current [22].

The research on STTs can be said to begin in the late 70s with Bergers work on domain wall motion [178, 179, 63]. The torques did not gain a lot of attention at the time. The film dimensions were in the millimetre regime, and one needed very high currents to achieve a significant response in the system [63]. However, as the research on interactions between the magnetic layers of the GMR nanostructures began to gain traction in the late eighties, there were some very productive years with much work on interlayer exchange coupling [63].

n the late nineties, Slonczewski and Berger independently published works on multilayer structures similar to the nanostructures used when studying the GMR effect [180, 181]. They saw that the STT in their systems was strong enough to control the magnetization in a ferromagnetic layer. This could be used to switch the direction of the magnetization, or to create spin waves in the ferromagnet.

The SHE also has a reciprocal mechanism where the spin current can cause a charge current. This effect is known as the *inverse spin-Hall effect* (ISHE) [22]. When the ferromagnet is layered next to the normal metal, the dynamics of the ferromagnet may exert a torque on the spins of electrons in vicinity of the ferromagnet [182, 183, 184]. In this way, a spin current in a ferromagnetic system may transfer spin angular momentum to an adjacent normal metal [185]. This effect is known as *spin pumping*, and makes it possible to inject a pure spin current into the metal, without the accompanying charge current [132]. The spin-Hall and inverse spin-Hall effect allow us to create a connection between charge-based and spin-based signals [174]. This makes spin-transfer torques and spin pumping useful for bridging spintronic devices with electronic devices.

A typical experimental setup for exciting magnons by STT is to layer a normal metal on top of the ferromagnet. Often platinum is chosen, as this metal has a high spin-orbit coupling. A charge current is applied in the metal layer, which produces a spin accumulation.

The LLG equation can be extended to account for the effects of the STTs. We consider a thin film in the $\hat{\mathbf{y}}, \hat{\mathbf{z}}$-plane, where an external magnetic field is applied so that the magnetization mainly points along the $\hat{\mathbf{z}}$-direction. We may model a spin accumulation polarized along the $\hat{\mathbf{z}}$-axis. The resulting torque on the ferromagnetic film interface is expressed in terms of the spin-mixing conductance per area $g_\perp \sim [1/\Omega \mathrm{m}^2]$ and spin accumulation density $\boldsymbol{\mu}_S = \mu_S uvecz$ [134],

$$\dot{\boldsymbol{m}} = -\gamma(\boldsymbol{m} \times \boldsymbol{H}_{\text{eff}}) + \alpha(\boldsymbol{m} \times \dot{\boldsymbol{m}}) - \frac{\gamma\hbar}{2e^2 L_x M_S} g_\perp \boldsymbol{m} \times (\boldsymbol{m} \times \boldsymbol{\mu}_S)\,. \tag{17}$$

Here, e is the elementary charge, and $\hbar$ is the reduced Planck constant. L_x is the film thickness. We see that the torque term is similar to the damping term of Eq. (1). In our geometry, a positive (negative) spin accumulation results in a damping-like (anti-damping-like) STT. In this way, the STT can be used as a tool to control the damping, as illustrated in Fig. 3.2. Depending on the sign of the the spin accumulation, the STT may be used to create magnons, or to increase the damping and subsequently inhibit magnon creation [185, 186].

The STT is a surface technique, which usually requires strong spin currents. This also means that the ferromagnetic film must be quite thin, often below 100 nanometers. It has been difficult to obtain magnon BECs in such thin films, but recently STT was used to create a magnon BEC in a thin-film BiYIG [8].

3.3 The *quantum* approach : boson operators

In this section, we w will study the magnons in terms of quantum mechanical creation and annihilation operators. There are several variations on bosonization techniques. This section will focus on the Holstein-Primakoff transformation. We will also introduce the alternative Dyson-Maleev transformation.

In 1940, five years after Landau and Lifshitz presented their classical equations [56], Holstein and Primakoff published their quantum mechanical treatment of the spin wave [57, 54]. They developed a representation of the spin system where spin operators were expressed in terms of bosonic creation and annihilation operators. The approach facilitated a quantum mechanical view, focused on the magnon as a particle, instead of the spin waves through a lattice of spins.

The bosonization approach stared with considering the Heisenberg exchange interaction [187]. Later, the approach was expanded to include a wide range of magnetic interactions, including the dipole-dipole interactions. For a spin system with some noise or temperature, there will always be some small deviations from its ground state. Holstein and Primakoff were able to show that these deviations would lead to propagating spin waves. They could also show that magnons behave like weakly interacting bosons.

3.3.1 The Holstein-Primakoff transformation

Let us consider a system where the ground state and quantization axis lies in the $\hat{\mathbf{z}}$-direction. The spin components S^x and S^y can be expressed in terms of the spin-raising and lowering operators S^+ and S^-,

$$S^x = \frac{1}{2}(S^+ + S^-) \tag{18}$$

$$S^y = \frac{1}{2i}(S^+ - S^-) \tag{19}$$

The Holstein-Primakoff spin-boson transformation [57] allows us to express the spin operators in terms of magnon creation and annihilation operators $\hat{a}^\dagger$ and $\hat{a}$.

$$S^+ = \hbar\sqrt{2S}(\sqrt{1-\hat{a}^\dagger\hat{a}/(2S)})\hat{a} \tag{20}$$

$$S^- = \hbar\sqrt{2S}\hat{a}^\dagger(\sqrt{1-\hat{a}^\dagger\hat{a}/(2S)}) \tag{21}$$

$$S^z = \hbar(S-\hat{a}^\dagger\hat{a}) \tag{22}$$

In the case for YIG, $S \approx 14.2$ [188, 189, 190] is large, and we may apply the binomial approximation,

$$S^+ \approx \hbar\sqrt{2S}(\hat{a}-\hat{a}^\dagger\hat{a}\hat{a}/(4S)) \tag{23}$$

$$S^- \approx \hbar\sqrt{2S}(\hat{a}^\dagger-\hat{a}^\dagger\hat{a}^\dagger\hat{a}/(4S)) \tag{24}$$

We proceed to introduce the magnetic free energies in terms of the spin operators.

3.3.2 Magnetic free energies

We have already encountered the magnetic free energies expressed in context of the continuum model. Here, we will quickly list the corresponding energies in terms of spin operators. We include the DzyaloshinskiiMoriya interaction, which is not usually included in the YIG systems we have focused on bit is relevant to our work in [9].

Zeeman field

The Zeeman energy due to an in-plane external magnetic field of strength H_0 along the $\hat{\mathbf{z}}$-direction reads [46, 47],

$$\mathcal{H}_\mathrm{Z} = -g\mu_B H_0 \sum_i \boldsymbol{S}_i^z \,. \tag{25}$$

Here, μ_B is the Bohr magneton and g is the effective Landé g-factor.

Exchange field

The exchange energy between the nearest neighbouring spins for an istropic homogeneous coupling reads [46, 47],

$$\mathcal{H}_{\rm ex} = -\frac{1}{2} J_{\rm ex} \sum_{i,j} \boldsymbol{S}_i \cdot \boldsymbol{S}_j \,. \tag{26}$$

Here, $J_{\rm ex} > 0$ (or $J_{\rm ex} < 0$) is the ferromagnetic (or antiferromagnetic) exchange constant.

Dipole field

The dipolar field can be expresssed as [160],

$$\mathcal{H}_{dip} = -\frac{1}{2} \sum_{i,j} \sum_{\alpha,\beta} D_{i,j}^{\alpha,\beta} S_i^{\alpha} S_j^{\beta}, \tag{27a}$$

$$D_{i,j}^{\alpha,\beta} = (g\mu_B)^2 (1-\delta_{i,j}) \frac{\partial^2}{\partial r_{ij}^{\alpha} \partial r_{ij}^{\beta}} \frac{1}{|\boldsymbol{r}_{ij}|} \,. \tag{27b}$$

Here, $\boldsymbol{r}_{ij}$ is the distance vector between the spin sites i and j. α, β denote the spatial components x, y, z.

Magneto-crystalline anisotropy field

A simple model for a magneto-crystalline anisotropy along the $\hat{\mathbf{n}}$-direction is given by,

$$\mathcal{H}_{\rm an} = -K_{an} \sum_{i} (\boldsymbol{S}_i \cdot \hat{\mathbf{n}})^2 \,. \tag{28}$$

Here, $K_{an} > 0$ (or $K_{an} < 0$) is the easy-axis (or hard-axis) anisotropy constant [191].

DzyaloshinskiiMoriya interaction (DMI)

Thin films with out-of-plane symmetry breaking may have an induced DzyaloshinskiiMoriya interaction [192, 134]. In our chosen geometry, it is expressed as the z-component of the cross product between two spin sites.

$$\mathcal{H}_{\text{DMI}} = K_{DMI} \sum_{i,j} v_{ij} [\boldsymbol{S}_i \cdot \boldsymbol{S}_j]_z \,. \tag{29}$$

Here,K_{DMI} is the strength of the interaction, and the sign parameter v_{ij} accounts for the ferromagnetic or antiferromagnetic symmetry, see Ref. [193]. The DMI interaction is calculated for nearest neighbouring spins. While the Heisenberg exchange interaction promotes a parallel aligment in ferromagnets, the DMI interaction promotes a perpendicular alignment. When these two interactions combine, it may facilitate the stability of exotic magnetic structures with winded symmetries, such as skyrmions [194].

3.3.3 Thin-film ferromagnet

We now return to the thin film ferromagnet. An external field directs the magnetization along the in-plane axis $\hat{\mathbf{z}}$. We will consider an easy-axis anisotropy in the our-of-plane direction $\hat{\mathbf{x}}$, since this is relevant to our work in Ref. [7],

$$\mathcal{H}_{\text{an}} = -K_{an} \sum_{i} (\boldsymbol{S}_i \cdot \hat{\mathbf{x}})^2 \,. \tag{30}$$

The Hamilton operator for our system contains the Zeeman energy, exchange energy, dipolar energy and anisotropy,

$$\mathcal{H} = \mathcal{H}_{\text{Z}} + \mathcal{H}_{\text{ex}} + \mathcal{H}_{\text{dip}} + \mathcal{H}_{\text{an}} \tag{31}$$

The expressions for $\mathcal{H}_{\text{Z}}$, $\mathcal{H}_{\text{ex}}$ and $\mathcal{H}_{\text{dip}}$ are listed in Section 3.3.2. The magnetic free energy terms are usually first- or second-order in the spin-operators. From the Holstein-Primakoff transformation in Eq. (24) we may then expect that our Hamiltonian operator will contain terms up to 6th-order in magnon operators. Since S is large, the high-order terms are small, and we may choose to only collect terms up to 4th-order. The dipolar interaction could ave given us third-order terms in magnon operators. However, if we consider a thin film ferromagnet with lateral lengths that are much larger than the film thickness,

we can view the system as being quasi-2D. It can then be shown that the off-diagonal terms ($\alpha \neq \beta$) of Eq. (276) vanishes. [195, 160]- For this reason, our Hamiltonian operator can then be divided into a two-magnon part $\mathcal{H}_2$ and a four-magnon part $\mathcal{H}_4$

$$\mathcal{H} = \mathcal{H}_2 + \mathcal{H}_4 \,. \tag{32}$$

We note that when swapping operators we may end up with renormalization terms. However, we will not collect any 2-magnon renormalization terms, as they are an order $1/S$ smaller in magnitude.

The two magnon Hamiltonian gives us the magnon energies, while the four-magnon Hamiltonian gives us the magnon interactions. We will discuss them separately in the following sections.

Spin wave spectra

We express the bosonic operators through their Fourier transform,

$$\hat{a}_j = \frac{1}{N} \sum_k e^{-ikr_j} \hat{a}_k, \tag{33}$$

$$\hat{a}_j^\dagger = \frac{1}{N} \sum_k e^{ikr_j} \hat{a}_k^\dagger. \tag{34}$$

When evaluating sums over multiple Fourier terms, the following relation is useful,

$$\sum_k e^{ik(r_j + r_{j'})} = N\delta_{j,j'} \tag{35}$$

Here, $\delta_{j,j'}$ is the Kronecker delta function, and N is the number of sites we sum over.

The general two-magnon Hamiltonian can be expressed as,

$$\mathcal{H}_2 = \sum_k A_k \hat{a}_k^\dagger \hat{a}_k + \frac{1}{2} B_k \hat{a}_k \hat{a}_{-k} + \frac{1}{2} B_k^* \hat{a}_k^\dagger \hat{a}_{-k}^\dagger. \tag{36}$$

Here, the expressions for A_k and B_k will contain contributions from the magnetic free energies of the system. The two-magnon Hamiltonian can be diagonalized

by utilizing the Bogoliubov transformation,

$$\hat{a}_k = u_k \hat{c}_k + v_k \hat{c}^\dagger_{-k} \tag{37}$$

$$\hat{a}^\dagger_k = u_k \hat{c}^\dagger_k + v_k \hat{c}_{-k} \tag{38}$$

Here, u_k and v_k are the Bogoliubov constants, which we express as [188],

$$u_k = \sqrt{\frac{A_k + \hbar\omega_k}{2\hbar\omega_k}} \tag{39}$$

$$v_k = sgn(B_k)\sqrt{\frac{A_k - \hbar\omega_k}{2\hbar\omega_k}} \tag{40}$$

Here, $sgn()$ is the sign-function. After diagonalizing the system, the magnon dispersion in the Bogoliubov operator basis gives us the spin wave spectra,

$$\mathcal{H}_2 = \sum_k \hbar\omega_k \hat{c}^\dagger \hat{c} = \sqrt{A_k - |B_k|^2}. \tag{41}$$

Here, $\hat{c}^\dagger$ ($\hat{c}$) are the creation (annihilation) operators in the new Bogoliubov basis.

In Ref. [7] we derive the spin wave spectra of a ferromagnetic film with out-plane anisotropy using the Holstein-Primakoff transformation, and express the lower branch of the magnon dispersion as,

$$A_k = D_{ex}k^2 + \gamma(H_0 + 2\pi M_S f_k) - K_{\text{an}}S, \tag{42}$$

$$B_k = 2\pi\gamma M_S f_k - K_{\text{an}}S. \tag{43}$$

Here, D_{ex} is the exchange stiffness (see Ref. [7]) and f_k is the formfactor[196, 197] from Eq. (15).

Magnon interactions

The thin film Hamiltonian operator of Eq. (31) will produce terms that are fourth order in magnon operators. Each of these terms will produce 16 four-operator terms in the new Bogoliubov basis after we apply Eq. (38). These

terms are evaluated in the two minima $k = \pm Q$. Due to conservation laws, there are only a few possible combinations of four-magnon operator terms that appear in the final interaction Hamiltonian. For our thin-film ferromagnet, the general expression of the nonlinear four-magnon interactions consists of intra- and inter-band contributions,

$$\mathcal{H}_4 = \mathcal{H}_{\text{intra}} + \mathcal{H}_{\text{inter}} \tag{44}$$

$$\mathcal{H}_{\text{intra}} = A(\hat{c}^\dagger_Q \hat{c}^\dagger_Q \hat{c}_Q \hat{c}_Q + \hat{c}^\dagger_{-Q} \hat{c}^\dagger_{-Q} \hat{c}_{-Q} \hat{c}_{-Q}) \tag{45}$$

$$\begin{aligned}\mathcal{H}_{\text{inter}} &= 2B(\hat{c}^\dagger_Q \hat{c}^\dagger_{-Q} \hat{c}_Q \hat{c}_{-Q}) \\ &+ C(\hat{c}^\dagger_Q \hat{c}_Q \hat{c}_Q \hat{c}_{-Q} + \hat{c}^\dagger_{-Q} \hat{c}_{-Q} \hat{c}_{-Q} \hat{c}_Q + \text{h.c.}) \\ &+ D(\hat{c}^\dagger_Q \hat{c}^\dagger_Q \hat{c}^\dagger_{-Q} \hat{c}^\dagger_{-Q} + \text{h.c.})\end{aligned} \tag{46}$$

Here, A, B, C, D are 4-magnon interaction amplitudes, see Ref. [7] for details. The 4-magnon interactions have been studied earlier in Refs. [198, 195, 188, 47] for ferromagnetic systems without anisotropy. Ref. [7] lists the calculated amplitudes we found for A, B, C, D for a ferromagnetic film with out-of-plane anisotropy.

We now proceed to perform the Madelungs transform to describe the two magnon condensation populations with a coherent phase $\phi_{\pm Q}$ and a population number $N_{\pm Q}$ [188, 47],

$$\hat{c}_{\pm Q} = \sqrt{N_{\pm Q}} e^{i\phi_{\pm Q}} \, . \tag{47}$$

The total number of condensed magnons is $N_c = N_Q + N_{-Q}$ while the distribution difference is $\delta = N_Q - N_{-Q}$. We also define the total phase as $\Phi = \phi_Q + \phi_{-Q}$. The four-magnon Hamiltonian is then expressed as,

$$\begin{aligned}\mathcal{H}_4(\delta, \Phi) = \frac{N_c^2}{2}\Big(A + B + D\cos(2\Phi) + 2C\cos(\Phi)\sqrt{1 - \frac{\delta^2}{N_c^2}} \\ - (B - A + D\cos(2\Phi))(\frac{\delta^2}{N_c^2})\Big)\end{aligned} \tag{48}$$

We want to know which values of δ and Φ we are likely to find our condensates in. We should then find the minima of $\mathcal{H}_4$. We find five critical points that may be candidates for being valid minima [47],

$$\delta_1 = 0, \Phi_1 = 0; \tag{49a}$$
$$\delta_2 = 0, \Phi_2 = \pi; \tag{49b}$$
$$\delta_3 = 0, \Phi_3 = \cos^{-1}(-\frac{C}{2D}); \tag{49c}$$
$$\delta_4 = N_c\big(1 - (\frac{C}{B - A + D})^2\big)^{\frac{1}{2}}, \Phi_4 = 0; \tag{49d}$$
$$\delta_5 = \delta_4, \Phi_4 = \pi. \tag{49e}$$

The second derivative discriminant $\mathcal{D}$ of the function determines whether any of the critical points are a minima,

$$\mathcal{D} = \Big[(\frac{\partial^2 \mathcal{H}_4}{\partial \delta^2})(\frac{\partial^2 \mathcal{H}_4}{\partial \Phi^2}) - (\frac{\partial^2 \mathcal{H}_4}{\partial \delta \partial \Phi})^2\Big] \tag{50}$$

The discriminant should be positive for the critical point to be a maxima or minima. To find the minima, we require $(\frac{\partial^2 \mathcal{H}_4}{\partial \delta^2}) > 0$ and $(\frac{\partial^2 \mathcal{H}_4}{\partial \Phi^2}) > 0$.

Whether the critical points listed in Eq. (49) may be minimas, depends on the numerical values of the prefactors A, B, C, D. The prefactors are functions of material and system parameters such as the external field strength, film thickness, and strength of the anisotropy. In Ref. [7] we find that the anisotropy can affect whether we are likely to find a symmetric or asymmetric magnon population distribution between the two magnon populations.

3.4 Antiferromagnetic systems

In this section, we will apply the Holstein-Primakoff bosonization technique to two antiferromagnetic systems. We will also include a short demonstration of the alternative Dyson-Maleev approach.

We model our antiferromagnetic system as a chain of magnetic moments that alternate between pointing in the positive or negative $\hat{\mathbf{z}}$-direction, as illustrated in Fig. 1.2. We will refer to these as sublattice A and B. In antiferromagnets, the net magnetization cancels out, and the dipolar interactions are very weak. For this reason, an antiferromagnetic model usually does not include the dipolar interactions.

We present a general Hamiltonian that contains contributions for an external magnetic field in the $\hat{\mathbf{z}}$-direction, the exchange interaction, the DMI interaction,

and two anisotropy terms. The first anisotropy is an easy axis in the in-plane direction $\hat{\mathbf{z}}$, while the second term is a hard axis in the out-of-plane direction $\hat{\mathbf{x}}$,

$$\begin{aligned} H = &- g\mu_B H_0 \sum_j \boldsymbol{S}_j^z + J_{\text{ex}} \sum_{i,j} \boldsymbol{S}_i \cdot \boldsymbol{S}_j + K_{\text{DMI}} \sum_{i,j} v_{ij} [\boldsymbol{S}_i \cdot \boldsymbol{S}_j]_z \\ &- K_{\text{Az}} \sum_j (\boldsymbol{S}_j \cdot \hat{z})^2 + K_{\text{Ax}} \sum_j (\boldsymbol{S}_j \cdot \hat{x})^2 \end{aligned} \tag{51}$$

Here, $J_{\text{ex}} > 0$ is the antiferromagnetic exchnge constant, $K_{\text{Az}} > 0$ and $K_{\text{Ax}} > 0$ are the easy-axis and hard-axis anisotropy strengths, and K_{DMI} is the DMI-constant. Se Ref. [9] for details. the sign parameter $v_{ij} = -v_{ji}$ accounts for the DMI symmetry, since we model the DMI vector as $K_{DMI} = v_{ij}\hat{\mathbf{z}}$ with opposite sign for the sublattices [193].

3.4.1 The Holstein-Primakoff transformation

The spin operators at sublattice A are,

$$S_i^+ \approx \hbar\sqrt{2S}(\hat{a}_i - \hat{a}_i^\dagger \hat{a}_i \hat{a}_i/(4S)) \tag{52}$$
$$S_i^- \approx \hbar\sqrt{2S}(\hat{a}_i^\dagger - \hat{a}_i^\dagger \hat{a}_i^\dagger \hat{a}_i/(4S)) \tag{53}$$
$$S_i^z = \hbar(S - \hat{a}_i^\dagger \hat{a}_i) \tag{54}$$

The spin operators at sublattice B are,

$$S_j^+ \approx \hbar\sqrt{2S}(\hat{b}_j^\dagger - \hat{b}_j^\dagger \hat{b}_j^\dagger \hat{b}_j/(4S)) \tag{55}$$
$$S_j^- \approx \hbar\sqrt{2S}(\hat{b}_j - \hat{b}_j^\dagger \hat{b}_j \hat{b}_j/(4S)) \tag{56}$$
$$S_j^z = -\hbar(S - \hat{b}^\dagger \hat{b}) \tag{57}$$

3.4.2 The Dyson-Maleev transformation

We proceed to present the spin operators in the Dyson-Maleev bosonization [199].

The spin operators at sublattice A are,

$$S_i^+ \approx \hbar\sqrt{2S}(\hat{a}_i - \hat{a}_i^\dagger \hat{a}_i \hat{a}_i/(2S)) \tag{58}$$
$$S_i^- \approx \hbar\sqrt{2S}(\hat{a}_i^\dagger) \tag{59}$$
$$S_i^z = \hbar(S - \hat{a}_i^\dagger \hat{a}_i) \tag{60}$$

The spin operators at sublattice B are,

$$S_j^+ \approx \hbar\sqrt{2S}(\hat{b}_j^\dagger - \hat{b}_j^\dagger \hat{b}_j^\dagger \hat{b}_j/(2S)) \tag{61}$$
$$S_j^- \approx \hbar\sqrt{2S}(\hat{b}_j) \tag{62}$$
$$S_j^z = -\hbar(S - \hat{b}^\dagger \hat{b}) \tag{63}$$

This transformation differs in the sense that we do not need to apply any approximation like we did from Eq. (22) to Eq. (24). However, we see that S^+ and S^- no longer commute. Furthermore, we see that some combinations, e.g. $S_i^- S_j^-$, no longer produce any 4-magnon or 6-magnon operator terms. the question then arises whether one can expect to get similar results using the Holstein-Primakoff transformation and Dyson-Maleev transformation[199]. In [9] we address this issue for a uniaxial antiferromagnetic system, and demonstrate that the Dyson-Maleev approach might give non-Hermitian terms in the four-magnon interactions. We will return to this topic in Section 3.5.

3.4.3 Spin wave spectra

The approach to analyze the spin wave spectra is similar to the approach discussed in Section 3.3. We may apply a Fourier transform to the magnon operators and their complex conjugates,

$$\hat{a}_i = \frac{1}{N/2} \sum_k e^{-ikr_j} \hat{a}_k, \tag{64}$$
$$\hat{b}_j = \frac{1}{N/2} \sum_k e^{-ikr_j} \hat{b}_k. \tag{65}$$

We define the following energies,

$$\omega_E = 2SJ_{\text{ex}} \tag{66}$$
$$\omega_D = 2SK_{\text{DMI}} \tag{67}$$
$$\omega_{Ax} = SK_{\text{Ax}} \tag{68}$$
$$\omega_{Az} = SK_{\text{Az}} \tag{69}$$
$$\omega_H = \frac{1}{2}\mu H_0. \tag{70}$$

We proceed by presenting two systems that are relevant to the work in Ref. [9]; an uniaxial antiferromagnet with DMI-interaction, and a biaxial antiferromagnet without DMI-interaction.

3.5 Uniaxial antiferromagnet with DMI

We consider the Hamiltonian of in the case where $K_{\text{x}} = 0$. In the presence of the DMI-interaction, the spin wave spectra of the antiferromagnet may have minimas at finite wavevector $k = \pm Q$ [200]. We follow the approach in Ref. [193] to derive the spin wave spectra. The two-magnon Hamiltonian can be diagonalized using a Bogoliubov transform,

$$\hat{a}_k = u_k\hat{\alpha}_k - v_k\hat{\beta}^\dagger_{-k}, \tag{71}$$
$$\hat{b}_{-k} = -v_k\hat{\alpha}_k + u_k\hat{\beta}^\dagger_{-k}. \tag{72}$$

Here, $\hat{\alpha}$ and $\hat{\beta}$ are the magnon operators in the new Bogoliubov basis. u_k and v_k are given by [193],

$$u_k^2 = \sqrt{\frac{(\omega_E + \omega_{Az})^2}{(\omega_E + \omega_{Az})^2 - (\omega_E\cos(k) + \omega_D\sin(k))^2}} + 1 \tag{73}$$
$$v_k^2 = \sqrt{\frac{(\omega_E + \omega_{Az})^2}{(\omega_E + \omega_{Az})^2 - (\omega_E\cos(k) + \omega_D\sin(k))^2}} - 1 \tag{74}$$

In Ref. [9] we find that the spin wave spectra of the two magnon populations are,

$$\omega_\alpha = \sqrt{(\omega_E + \omega_{Az})^2 - (\omega_E \cos(k) + \omega_D \sin(k))^2} + \omega_H, \tag{75}$$

$$\omega_\alpha = \sqrt{(\omega_E + \omega_{Az})^2 - (\omega_E \cos(k) + \omega_D \sin(k))^2} - \omega_H. \tag{76}$$

Figure 3.4: Figure from Ref. [9]. The dispersion relation for the uniaxial antiferromagnet of Eq. (76) is plotted as a function of wavevector k. In the presence of the easy axis anisotropy, the external field breaks the degeneracy of the dispersion relation for the magnon populations α and β of right handed (clockwise) and left handed (counterclockwise) magnetization precession (see Ref. [193]). The DMI interaction shifts the two bands horizontally, so that the minimas appear at finite wavevector numbers. The strengths of the DMI-interaction, anisotropy and external field compared to the exchange energy are $K_{DMI}/J_{\text{ex}} = 0.03$, $K_{\text{Az}}/J_{\text{ex}} = 0.05$ and $H_0/J_{\text{ex}} = 0.01$.

We plot the dispersion relation of Eq. (76) in Fig. 3.4. We find that the external field will create a band splitting, while the DMI interaction shifts the dispersions horizontally so that we get a double minima at finite wavevector number $k = \pm Q$. We are interested in the populations that form in the two minima, and proceed to investigate the four-magnon terms that are combinations of $\hat{\alpha}_{-Q}$, $\hat{\beta}_Q$, and their hermitian conjugates. The expression for the magnon interactions becomes,

$$\begin{aligned}
\mathcal{H}_4 =& A_{1,2}[\hat{\alpha}_{-Q}\hat{\beta}^\dagger_Q\hat{\beta}_Q\hat{\beta}_Q + \hat{\beta}^\dagger_Q\hat{\alpha}_{-Q}\hat{\alpha}^\dagger_{-Q}\hat{\alpha}^\dagger_{-Q}] \\
&+A_{3,4}[\hat{\alpha}_{-Q}\hat{\alpha}_{-Q}\hat{\beta}_Q\hat{\alpha}^\dagger_{-Q} + \hat{\beta}^\dagger_Q\hat{\beta}^\dagger_Q\hat{\beta}_Q\hat{\alpha}^\dagger_{-Q}] \\
&+B[\hat{\alpha}_{-Q}\hat{\alpha}_{-Q}\hat{\beta}_Q\hat{\beta}_Q + \text{h.c.}] \\
&+C[\hat{\alpha}_{-Q}\hat{\alpha}_{-Q}\hat{\alpha}^\dagger_{-Q}\hat{\alpha}^\dagger_{-Q} + \hat{\beta}_Q\hat{\beta}_Q\hat{\beta}^\dagger_Q\hat{\beta}^\dagger_Q] \\
&+D[\hat{\alpha}_{-Q}\hat{\alpha}^\dagger_{-Q}\hat{\beta}_Q\hat{\beta}^\dagger_Q]
\end{aligned} \tag{77}$$

Ref. [9] lists the calculated amplitudes $A_{1,2}, A_{3,4}, B, C, D$ we found. We perform the Madelung transformation,

$$\langle \alpha_{-Q} \rangle \to \sqrt{N_\alpha} e^{i\phi_\alpha}, \tag{78}$$

$$\langle \beta_Q \rangle \to \sqrt{N_\beta} e^{i\phi_\beta}. \tag{79}$$

Here, N_α and N_β are the number of magnons in the two condensate populations,

while ϕ_α and ϕ_β are their phases. We proceed to define

$$A = \frac{1}{2}(A_{1,2} + A_{3,4}), \tag{80}$$

$$\Delta_A = \frac{1}{2}(A_{1,2} - A_{3,4}), \tag{81}$$

$$N_c = N_\alpha + N_\beta, \tag{82}$$

$$\delta = N_\alpha - N_\beta, \tag{83}$$

$$\Phi = \phi_\alpha + \phi_\beta. \tag{84}$$

We then arrive at the following expression for the four-magnon Hamiltonian,

$$\mathcal{H}_4 = \frac{N_c^2}{2}\Big[(\frac{1}{2}D + B\cos(2\Phi))(1 - (\frac{\delta}{N_c})^2) + C(1 + (\frac{\delta}{N_c})^2) \tag{85}$$

$$+ \sqrt{1 - (\frac{\delta}{N_c})^2}(2A\cos(\Phi) + 2i\frac{\delta}{N_c}\sin(\Phi)\Delta_A)\Big] \tag{86}$$

In the Holstein-Primakoff transformation, we find that $\Delta_A = 0$. However, in Ref. [9] we find $\Delta_A \neq 0$ using the Dyson-Maleev approach, and the interaction generally has a non-Hermitian term. However, we find that the real part of Eq. (86) is minimized for $\Phi = 0$ or $\Phi = \pi$. In these critical point, the imaginary term of Eq. (86) vanishes. In this sense, the Holstein-Primakoff transformation and Dyson-Maleev transformation results in the same predictions for which distribution difference δ and phase sum Φ will minimize Eq. (86).

3.6 Biaxial antiferromagnet without DMI

We consider the Hamiltonian of Section 3.5 in the case where $K_{DMI} = 0$. This system is similar to the one studied in Ref. [201]. For materials such as NiO we would assume that $J_{\rm ex} > K_{\rm Ax} > K_{\rm Az}$ [201, 191]. We present calculations in the Holstein-Primakoff transformation only.

The spin wave spectra has a minima at $k = 0$ [201], and the magnon energies in the minima are given by,

$$\omega_{\alpha,\beta}^2 = \frac{1}{4}(\omega_E + \omega_{Ax} + 2\omega_{Az})^2 + \omega_H - \frac{1}{4}(\omega_{Ax}^2 + \omega_E^2)$$

$$\pm \frac{1}{2}\sqrt{4\omega_H((\omega_E + \omega_{Ax} + 2\omega_{Az})^2 - \omega_E^2) + \omega_E^2\omega_{Ax}^2} \tag{87}$$

Here, β-magnons have the lowest energy. We see that the degeneracy of is broken even if $H_0 = 0$, due to the presence of the out-of-plane hard-axis anisotropy. To diagonalize the Hamiltonian, we apply the following Bogoliubov transformation for $k = 0$,

$$\hat{a} = u_\alpha \hat{\alpha} - v_\beta \hat{\beta}^\dagger \tag{88}$$

$$\hat{b}^\dagger = -v_\alpha \hat{\alpha} + u_\beta \hat{\beta}^\dagger. \tag{89}$$

We use the approximated Bogoliubov parameters evaluated at $k = 0$ from Ref. [201],

$$u_{\alpha,\beta} = \sqrt{\frac{(\omega_E + \omega_{Ax} + 2\omega_{Az})^2 + \omega_{\alpha,\beta}}{2\omega_{\alpha,\beta}(H_0 = 0)}} \tag{90}$$

$$v_{\alpha,\beta} = \sqrt{\frac{(\omega_E + \omega_{Ax} + 2\omega_{Az})^2 - \omega_{\alpha,\beta}}{2\omega_{\alpha,\beta}(H_0 = 0)}} \tag{91}$$

We are interested in analyzing the interactions of the magnon population of lowest energy. We will only collect four-magnon operator terms that are combinations of $\hat{\beta}$ and $\hat{\beta}^\dagger$,

$$\mathcal{H}_4 = C_2(\hat{\beta}\hat{\beta}\hat{\beta}^\dagger\hat{\beta}^\dagger) + G_{5,8}(\hat{\beta}\hat{\beta}\hat{\beta}\hat{\beta} + \text{h.c.}) + G_{6,7}(\hat{\beta}\hat{\beta}\hat{\beta}\hat{\beta}^\dagger + \text{h.c.}) \tag{92}$$

We present the interaction amplitudes C_2, $G_{5,8}$, $G_{6,7}$ in Ref. [9]. We proceed to perform the Madelung transformation,

$$\langle\beta\rangle \to \sqrt{N_\beta} e^{i\phi_\beta}. \tag{93}$$

Here, N_β and ϕ_β are the magnon number and phase of the condensate population. We arrive at the following expression for the magnon interactions,

$$\mathcal{H}_4/(N_\beta^2) = C_2 + 2G_{6,7}\cos(2\phi_\beta) + 2G_{5,8}\cos(4\phi_\beta) \tag{94}$$

In Ref. [9] we find that $G_{5,8} = 0$. The possible critical points for Eq. (94) is

then,

$$\phi_1^\beta = \frac{1}{2}\cos^{-1}(-\frac{C_2}{2G_{6,7}}), \tag{95a}$$

$$\phi_2^\beta = n\pi - \frac{1}{2}\cos^{-1}(-\frac{C_2}{2G_{6,7}}). \tag{95b}$$

In Ref. [9] we find that $|\frac{C_2}{2G_{6,7}}| > 1$, so there are no valid critical points with respect to the phase ϕ_β.

Chapter 4

Summary : controlling magnon condensates

This final chapter gives some thoughts on which information on magnon BECs we gained using the theoretical frameworks presented in Chapter 3.

4.1 Magnon creation

The parallel pumping and STT techniques have both been used to create magnon condensates in thin ferromagnetic films [2, 8]. In Ref. [6], we investigated magnon excitation by the two techniques, and a combination of them. We performed micromagnetic simulations based on the LLG equation. We presented a picture on how the density of magnons varied as a function of the external field strength H_0 and pumping strength h_p. We showed how this pictures changed as we applied a weak damping-like or anti-damping like STT. Fig. 4.1 from [6] shows how the presence of the torques affect the expected magnon densities. The simulations confirm that the torque can be used to assist or inhibit magnon creation. We expect that the STT can be used to assist and inhibit the formation of the magnon condensate. The possibility of using the STT as a control of the magnon condensate has also been investigated experimentally in Ref. [175]. In Ref. [6] we also performed simulations of magnon creation by STT only. We investigated which magnons were excited by the two methods, and confirmed our expectations that the parallel pumping produces dipole dominated spin waves along the direction of the external field, while STTs produce magnons at a wide range of different energies and wavevectors.

4.2 Magnon energy spectra

If the ferromagnetic film is very thin, the minima in the spin wave spectra of Eq. (14) is very flat. This is perceived as challenging got the condensation process, since magnons at roughly the same energy can have a wide variety in wavevector number. In Ref. [7], we found that the presence of an out-of-plane easy-axis anisotropy makes the minima deeper and increases the curvature. We argue that both effects are beneficial for the condensation process. Our findings support experimental work by Divinskiy et al. [8]. Fig. 4.2 shows the magnon density from micromagnetic simulations, comparing a system with and without anisotropy. The simulations support the analytical arguments that the presence of the anisotropy is beneficial for the condensation process. The condensate population in the film with anisotropy is clearer, and has less variation in energy and wavevector number.

In Ref. [9] we studied the spin wave spectra of a uniaxial antiferromagnet. If the system is only influenced by the exchange interaction and in-plane easy-axis anisotropy, then the spin wave spectra has a minima at $k = 0$. If we add an external magnetic field, we can create a band splitting. If we further add the presence of the DMI interaction, then this induces a horizontal shift in the spectra, so that we will have two non-degenerate minima at finite wavevector number. We also studied a biaxial antiferromagnetic system without the DMI interaction, similar to Refs. [201, 191]. In addition to the easy in-plane axis, the system now was an out-of-plane hard-axis. The spectra has minima at $k = 0$, and due to the hard-axis, the minima is non-degenerate, even in the absence of the external magnetic field. Our interest is then to investigate the magnon interactions in the condensate populations.

4.3 Magnon interactions

In Ref. [7] we calculated the magnon interactions between the two condensate populations in a ferromagnetic film with out-of-plane easy axis anisotropy. The magnon interactions depend on parameters such as the strength of the external field, the film thickness, and the anisotropy strength. The magnon interactions also depends on condensate parameters such as the difference in magnon number and the phase sum of the two populations. By minimizing the magnon interaction expression, we may predict whether the system may have a symmetrical or asymmetrical distribution of magnons between the two condensate populations. The anisotropy and film thickness are usually fixed parameters for a system, but the external field strength may be used to control the energy levels and magnon interactions, which in turn controls the properties of the condensate.

In Ref. [9], we calculated the magnon interactions between the two condensate populations in a uniaxial antiferromagnetic system. We also calculated the magnon interactions for the lowest condensate population in a biaxial antiferromagnetic system. In the uniaxial case, we presented the criteria to predict the phase sum of the two condensate populations, and predictions on the magnon distribution between the two condensates. We also compared the Holstein-Primakoff bosonization and the Dyson-Maleev bosonization technique. We found that although the Dyson-Maleev approach gives the same spin wave spectra, we may get non-Hermitian terms in the expression for the magnon interactions. In the case of the uniaxial antiferromagnetic system, we found that this would not affect the predictions on the condensates phase sum and distribution difference.

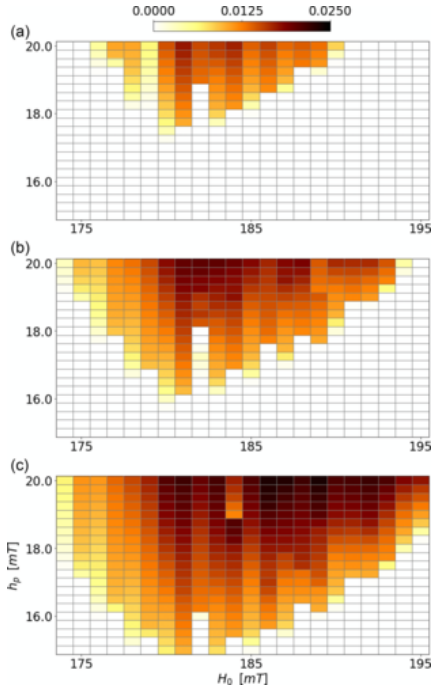

Figure 4.1: Figure from Ref. [6]. the relative magnon density found by micromagnetic simulations during parallel parametric pumping of a thin (100nm) YIG film. H_0 and h_p are the strengths of the static external field and pumping field. In a) and c) an STT due to a weak spin accumulation μ_S is applied.
a) Damping-like STT, $\mu_S g_\perp / e = -1 \times 10^{10}\,\mathrm{A\,m^{-2}}$
a) No STT, $mu_S = 0$
c) Anti-damping-like STT, $\mu_S g_\perp / e = 1 \times 10^{10}\,\mathrm{A\,m^{-2}}$
The simulation series for each fixed H_0 represent one column of he figures, where each pixel represents the relative magnon density from Eq. (3). See Ref. [6] for parameters and details.

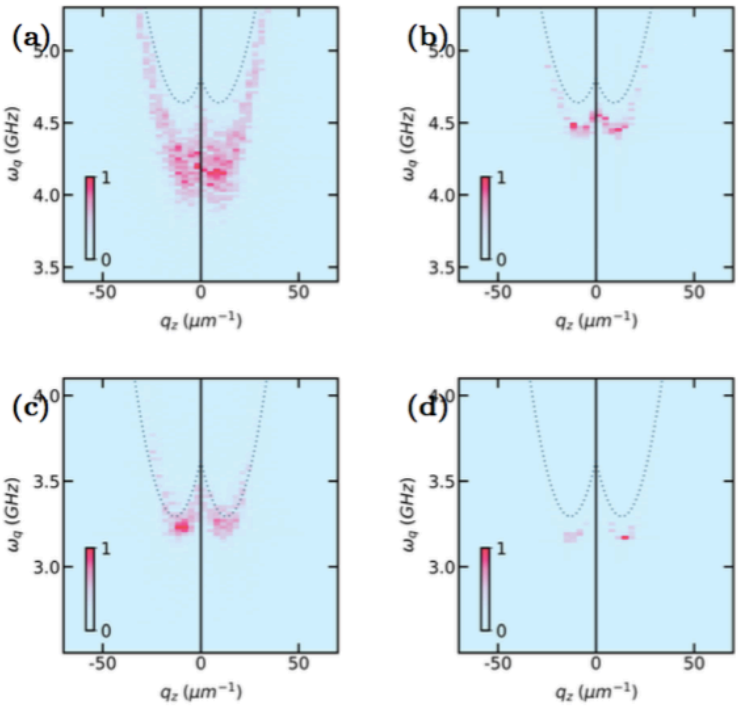

Figure 4.2: Figure from Ref. [7]. Magnon distribution from micromagnetic simulations of a 50nm thick ferromagnetic film. Magnons are created by STT. In a) and b), there is no anisotropy in the system. I c) and d) there is an easy-axis out-of-pane anisotropy. We show the early stages of magnon excitation i a) and c). After some time, the system reaches a quasi-equilibrium steady state, and we see that the magnons have condensed. The dashed line is the analytical spin wave spectra. Due to the nonlinear magnon interactions, we may observe a spectrum shift in the simulated magnon dispersion compared to the noninteracting analytical results. See Ref. [7] for parameters and details.

Chapter 5

Bibliography

[1] Yongbing Xu, David D Awschalom, and Junsaku Nitta. *Handbook of spintronics*. Springer Publishing Company, Incorporated, 2016.

[2] Sergej O Demokritov, Vladislav E Demidov, Oleksandr Dzyapko, Gennadii A Melkov, Alexandar A Serga, Burkard Hillebrands, and Andrei N Slavin. Bose–einstein condensation of quasi-equilibrium magnons at room temperature under pumping. *Nature*, 443(7110):430–433, 2006.

[3] SN Andrianov and SA Moiseev. Magnon qubit and quantum computing on magnon bose-einstein condensates. *Physical Review A*, 90(4):042303, 2014.

[4] Morteza Mohseni, Vitaliy I Vasyuchka, Victor S Lvov, Alexander A Serga, and Burkard Hillebrands. Classical analog of qubit logic based on a magnon bose–einstein condensate. *Communications physics*, 5(1):196, 2022.

[5] Kouki Nakata, Kevin A van Hoogdalem, Pascal Simon, and Daniel Loss. Josephson and persistent spin currents in bose-einstein condensates of magnons. *Physical Review B*, 90(14):144419, 2014.

[6] Therese Frostad, Hans L Skarsvåg, Alireza Qaiumzadeh, and Arne Brataas. Spin-transfer-assisted parametric pumping of magnons in yttrium iron garnet. *Physical Review B*, 106(2):024423, 2022.

[7] Therese Frostad, Philipp Pirro, Alexander A Serga, Burkard Hillebrands, Arne Brataas, and Alireza Qaiumzadeh. Anisotropy-assisted magnon condensation in ferromagnetic thin films. *arXiv preprint arXiv:2309.05982*, 2023.

[8] B Divinskiy, H Merbouche, VE Demidov, KO Nikolaev, L Soumah, D Gouéré, R Lebrun, V Cros, Jamal Ben Youssef, P Bortolotti, et al. Evidence for spin current driven bose-einstein condensation of magnons. *Nature communications*, 12(1):6541, 2021.

[9] Anne-Louise Kristoffersen, Therese Frostad, Roberto E. Troncoso, Arne Brataas, and Alireza Qaiumzadeh. Phase diagram for magnon condensates in antiferromagnetic insulators. *Preprint*, 2023.

[10] Gordon E Moore. Cramming more components onto integrated circuits. *Proceedings of the IEEE*, 86(1):82–85, 1998.

[11] Jonathan Koomey, Stephen Berard, Marla Sanchez, and Henry Wong. Implications of historical trends in the electrical efficiency of computing. *IEEE Annals of the History of Computing*, 33(3):46–54, 2010.

[12] John Shalf. The future of computing beyond moores law. *Philosophical Transactions of the Royal Society A*, 378(2166):20190061, 2020.

[13] Jonathan Koomey. Our latest on energy efficiency of computing over time, now out in electronic design. *URL: https://www. koomey. com/post/153838038643*, 2016.

[14] Michael A Nielsen and Isaac L Chuang. Quantum computation and quantum information. *Phys. Today*, 54(2):60, 2001.

[15] David Kielpinski, Chris Monroe, and David J Wineland. Architecture for a large-scale ion-trap quantum computer. *Nature*, 417(6890):709–711, 2002.

[16] Pieter Kok, William J Munro, Kae Nemoto, Timothy C Ralph, Jonathan P Dowling, and Gerard J Milburn. Linear optical quantum computing with photonic qubits. *Reviews of modern physics*, 79(1):135, 2007.

[17] Silas Hoffman, Constantin Schrade, Jelena Klinovaja, and Daniel Loss. Universal quantum computation with hybrid spin-majorana qubits. *Physical Review B*, 94(4):045316, 2016.

[18] Morten Kjaergaard, Mollie E Schwartz, Jochen Braumüller, Philip Krantz, Joel I-J Wang, Simon Gustavsson, and William D Oliver. Superconducting qubits: Current state of play. *Annual Review of Condensed Matter Physics*, 11:369–395, 2020.

[19] Anasua Chatterjee, Paul Stevenson, Silvano De Franceschi, Andrea Morello, Nathalie P de Leon, and Ferdinand Kuemmeth. Semiconductor qubits in practice. *Nature Reviews Physics*, 3(3):157–177, 2021.

[20] Michael A Nielsen and Isaac L Chuang. Quantum computation and quantum information. chapter 5. *Phys. Today*, 54(2):60, 2001.

[21] Nathalie P De Leon, Kohei M Itoh, Dohun Kim, Karan K Mehta, Tracy E Northup, Hanhee Paik, BS Palmer, Nitin Samarth, Sorawis Sangtawesin, and David W Steuerman. Materials challenges and opportunities for quantum computing hardware. *Science*, 372(6539):eabb2823, 2021.

[22] Arne Brataas, Bart van Wees, Olivier Klein, Grégoire de Loubens, and Michel Viret. Spin insulatronics. *Physics Reports*, 885:1–27, 2020.

[23] Julie Grollier, Damien Querlioz, KY Camsari, Karin Everschor-Sitte, Shunsuke Fukami, and Mark D Stiles. Neuromorphic spintronics. *Nature electronics*, 3(7):360–370, 2020.

[24] Aleksandr Kurenkov, Shunsuke Fukami, and Hideo Ohno. Neuromorphic computing with antiferromagnetic spintronics. *Journal of Applied Physics*, 128(1), 2020.

[25] VE Demidov, O Dzyapko, SO Demokritov, GA Melkov, and AN Slavin. Thermalization of a parametrically driven magnon gas leading to bose-einstein condensation. *Physical review letters*, 99(3):037205, 2007.

[26] O Dzyapko, VE Demidov, SO Demokritov, GA Melkov, and AN Slavin. Direct observation of bose–einstein condensation in a parametrically driven gas of magnons. *New Journal of Physics*, 9(3):64, 2007.

[27] VE Demidov, O Dzyapko, SO Demokritov, GA Melkov, and AN Slavin. Observation of spontaneous coherence in bose-einstein condensate of magnons. *Physical review letters*, 100(4):047205, 2008.

[28] VE Demidov, O Dzyapko, M Buchmeier, T Stockhoff, G Schmitz, GA Melkov, and SO Demokritov. Magnon kinetics and bose-einstein condensation studied in phase space. *Physical review letters*, 101(25):257201, 2008.

[29] O Dzyapko, VE Demidov, SO Demokritov, GA Melkov, and VL Safonov. Monochromatic microwave radiation from the system of strongly excited magnons. *Applied Physics Letters*, 92(16), 2008.

[30] P Nowik-Boltyk, O Dzyapko, VE Demidov, NG Berloff, and SO Demokritov. Spatially non-uniform ground state and quantized vortices in a two-component bose-einstein condensate of magnons. *Scientific reports*, 2(1):482, 2012.

[31] Alexander A Serga, Vasil S Tiberkevich, Christian W Sandweg, Vitaliy I Vasyuchka, Dmytro A Bozhko, Andrii V Chumak, Timo Neumann, Björn Obry, Gennadii A Melkov, Andrei N Slavin, et al. Bose–einstein condensation in an ultra-hot gas of pumped magnons. *Nature communications*, 5(1):3452, 2014.

[32] Yu M Bunkov, AN Kuzmichev, TR Safin, PM Vetoshko, VI Belotelov, and MS Tagirov. Quantum paradigm of the foldover magnetic resonance. *Scientific Reports*, 11(1):7673, 2021.

[33] David Snoke. Coherent questions. *Nature*, 443(7110):403–404, 2006.

[34] Yongbing Xu, David D Awschalom, and Junsaku Nitta. *Handbook of spintronics, Chapter 2*. Springer Publishing Company, Incorporated, 2016.

[35] Andrii V Chumak, Pavel Kabos, Mingzhong Wu, Claas Abert, Christoph Adelmann, AO Adeyeye, J Åkerman, Farkhad G Aliev, Abdelmadjid Anane, A Awad, et al. Advances in magnetics roadmap on spin-wave computing. *IEEE Transactions on Magnetics*, 58(6):1–72, 2022.

[36] Ádám Papp, Wolfgang Porod, and Gyorgy Csaba. Nanoscale neural network using non-linear spin-wave interference. *Nature communications*, 12(1):6422, 2021.

[37] Supriyo Bandyopadhyay and Marc Cahay. *Introduction to spintronics*. CRC press, 2008.

[38] Attila Szilva, Yaroslav Kvashnin, Evgeny A Stepanov, Lars Nordström, Olle Eriksson, Alexander I Lichtenstein, and Mikhail I Katsnelson. Quantitative theory of magnetic interactions in solids. *Reviews of Modern Physics*, 95(3):035004, 2023.

[39] Etienne Du Trémolet de Lacheisserie, Damien Gignoux, and Michel Schlenker. *Magnetism*, volume 1. Springer Science & Business Media, 2005.

[40] Hans Christian Oersted. Experiments on the effect of a current of electricity on the magnetic needle. *Annals of Philosophy*, 16(1820):273–276, 1820.

[41] Mikhail L'vovich Levin and Mikhail Adol'fovich Miller. Maxwell's" treatise on electricity and magnetism". *Soviet Physics Uspekhi*, 24(11):904, 1981.

[42] Albert Einstein et al. On the electrodynamics of moving bodies. *Annalen der physik*, 17(10):891–921, 1905.

[43] Yongbing Xu, David D Awschalom, and Junsaku Nitta. *Handbook of spintronics, Chapter 1*. Springer Publishing Company, Incorporated, 2016.

[44] Niels Bohr. *Studier over metallernes elektrontheori*. Thaning et Appel in Komm., 1911.

[45] H-J Van Leeuwen. Problemes de la théorie électronique du magnétisme. *J. phys. radium*, 2(12):361–377, 1921.

[46] Ralph Skomski. *Simple models of magnetism*. Oxford university press, 2008.

[47] Hayder Salman, Natalia G Berloff, and Sergej O Demokritov. Microscopic theory of bose–einstein condensation of magnons at room temperature. 2017.

[48] Victor S L'vov. *Wave turbulence under parametric excitation: applications to magnets. Chapter 2*. Springer Science & Business Media, 2012.

[49] Vladimir Cherepanov, Igor Kolokolov, and Victor L'vov. The saga of yig: Spectra, thermodynamics, interaction and relaxation of magnons in a complex magnet. *Physics reports*, 229(3):81–144, 1993.

[50] AA Serga, AV Chumak, and B Hillebrands. Yig magnonics. *Journal of Physics D: Applied Physics*, 43(26):264002, 2010.

[51] Houchen Chang, Peng Li, Wei Zhang, Tao Liu, Axel Hoffmann, Longjiang Deng, and Mingzhong Wu. Nanometer-thick yttrium iron garnet films with extremely low damping. *IEEE Magnetics Letters*, 5:1–4, 2014.

[52] Robert L Stamps and Helmut Schultheiss. Recent advances in topological ferroics and their dynamics preface. chapter 3, 2019.

[53] Felix Bloch. Zur theorie des ferromagnetismus. *Zeitschrift für Physik*, 61(3-4):206–219, 1930.

[54] Sergej O Demokritov and Andrei N Slavin. *Magnonics: From fundamentals to applications. Chapter 4*, volume 125. Springer Science & Business Media, 2012.

[55] G Heller, HA Kramers, and K Akad. Amsterdam proc. *Amsterdam Proc*, 37(7):378–385, 1934.

[56] E Lifshitz and LD Landau. On the theory of the dispersion of magnetic permeability in ferromagnetic bodies. *Phys. Z. Sowjetunion*, 8(135), 1935.

[57] T Holstein and Hl Primakoff. Field dependence of the intrinsic domain magnetization of a ferromagnet. *Physical Review*, 58(12):1098, 1940.

[58] Sergio M Rezende. *Fundamentals of magnonics*, volume 969. Springer, 2020.

[59] Philipp Pirro, Vitaliy I Vasyuchka, Alexander A Serga, and Burkard Hillebrands. Advances in coherent magnonics. *Nature Reviews Materials*, 6(12):1114–1135, 2021.

[60] Sergej O Demokritov and Andrei N Slavin. *Magnonics: From fundamentals to applications*, volume 125. Springer Science & Business Media, 2012.

[61] Vincent Baltz, Aurelien Manchon, M Tsoi, Takahiro Moriyama, T Ono, and Y Tserkovnyak. Antiferromagnetic spintronics. *Reviews of Modern Physics*, 90(1):015005, 2018.

[62] Tomas Jungwirth, X Marti, P Wadley, and J Wunderlich. Antiferromagnetic spintronics. *Nature nanotechnology*, 11(3):231–241, 2016.

[63] Daniel C Ralph and Mark D Stiles. Spin transfer torques. *Journal of Magnetism and Magnetic Materials*, 320(7):1190–1216, 2008.

[64] Mario Norberto Baibich, Jean Marc Broto, Albert Fert, F Nguyen Van Dau, Frédéric Petroff, P Etienne, G Creuzet, A Friederich, and J Chazelas. Giant magnetoresistance of (001) fe/(001) cr magnetic superlattices. *Physical review letters*, 61(21):2472, 1988.

[65] Grünberg Binasch, Peter Grünberg, F Saurenbach, and W Zinn. Enhanced magnetoresistance in layered magnetic structures with antiferromagnetic interlayer exchange. *Physical review B*, 39(7):4828, 1989.

[66] Albert Fert and Peter Grnberg. The nobel prize in physics 2007. *URL http://www. nobelprize. org*, 2007.

[67] Yongbing Xu, David D Awschalom, and Junsaku Nitta. *Handbook of spintronics, Chapter 25*. Springer Publishing Company, Incorporated, 2016.

[68] Yongbing Xu, David D Awschalom, and Junsaku Nitta. *Handbook of spintronics, Chapter 26*. Springer Publishing Company, Incorporated, 2016.

[69] Stuart SP Parkin, Masamitsu Hayashi, and Luc Thomas. Magnetic domain-wall racetrack memory. *Science*, 320(5873):190–194, 2008.

[70] Riccardo Tomasello, E Martinez, Roberto Zivieri, Luis Torres, Mario Carpentieri, and Giovanni Finocchio. A strategy for the design of skyrmion racetrack memories. *Scientific reports*, 4(1):1–7, 2014.

[71] John Von Neumann. First draft of a report on the edvac. *IEEE Annals of the History of Computing*, 15(4):27–75, 1993.

[72] PP Freitas, F Silva, NJ Oliveira, LV Melo, L Costa, and N Almeida. Spin valve sensors. *Sensors and Actuators A: Physical*, 81(1-3):2–8, 2000.

[73] Jianguo Wang, Hao Meng, and Jian-Ping Wang. Programmable spintronics logic device based on a magnetic tunnel junction element. *Journal of applied physics*, 97(10), 2005.

[74] PP Freitas, JL Costa, N Almeida, LV Melo, F Silva, J Bernardo, and C Santos. Giant magnetoresistive sensors for rotational speed control. *Journal of applied physics*, 85(8):5459–5461, 1999.

[75] C Reig, D Ramırez, F Silva, J Bernardo, and P Freitas. Design, fabrication, and analysis of a spin-valve based current sensor. *Sensors and Actuators A: Physical*, 115(2-3):259–266, 2004.

[76] Bernard Dieny, Ioan Lucian Prejbeanu, Kevin Garello, Pietro Gambardella, Paulo Freitas, Ronald Lehndorff, Wolfgang Raberg, Ursula Ebels, Sergej O Demokritov, Johan Akerman, et al. Opportunities and challenges for spintronics in the microelectronics industry. *Nature Electronics*, 3(8):446–459, 2020.

[77] Artem Litvinenko, Roman Khymyn, Victor H González, Roman Ovcharov, Ahmad A Awad, Vasyl Tyberkevych, Andrei Slavin, and Johan Åkerman. A spinwave ising machine. *Communications Physics*, 6(1):227, 2023.

[78] Giovanni Finocchio, Supriyo Bandyopadhyay, Peng Lin, Gang Pan, J Joshua Yang, Riccardo Tomasello, Christos Panagopoulos, Mario Carpentieri, Vito Puliafito, Johan Åkerman, et al. Roadmap for unconventional computing with nanotechnology. chapter 8. *arXiv preprint arXiv:2301.06727*, 2023.

[79] Ryosho Nakane, Gouhei Tanaka, and Akira Hirose. Reservoir computing with spin waves excited in a garnet film. *IEEE access*, 6:4462–4469, 2018.

[80] Giovanni Finocchio, Supriyo Bandyopadhyay, Peng Lin, Gang Pan, J Joshua Yang, Riccardo Tomasello, Christos Panagopoulos, Mario Carpentieri, Vito Puliafito, Johan Åkerman, et al. Roadmap for unconventional computing with nanotechnology. chapter 3. *arXiv preprint arXiv:2301.06727*, 2023.

[81] Andrii V Chumak, Alexander A Serga, and Burkard Hillebrands. Magnon transistor for all-magnon data processing. *Nature communications*, 5(1):4700, 2014.

[82] Tyler W Hughes, Ian AD Williamson, Momchil Minkov, and Shanhui Fan. Wave physics as an analog recurrent neural network. *Science advances*, 5(12):eaay6946, 2019.

[83] Jacob Biamonte, Peter Wittek, Nicola Pancotti, Patrick Rebentrost, Nathan Wiebe, and Seth Lloyd. Quantum machine learning. *Nature*, 549(7671):195–202, 2017.

[84] Yichen Shen, Nicholas C Harris, Scott Skirlo, Mihika Prabhu, Tom Baehr-Jones, Michael Hochberg, Xin Sun, Shijie Zhao, Hugo Larochelle, Dirk Englund, et al. Deep learning with coherent nanophotonic circuits. *Nature photonics*, 11(7):441–446, 2017.

[85] Xing Lin, Yair Rivenson, Nezih T Yardimci, Muhammed Veli, Yi Luo, Mona Jarrahi, and Aydogan Ozcan. All-optical machine learning using diffractive deep neural networks. *Science*, 361(6406):1004–1008, 2018.

[86] Qi Wang, Andrii V Chumak, and Philipp Pirro. Inverse-design magnonic devices. *Nature communications*, 12(1):2636, 2021.

[87] Sean Molesky, Zin Lin, Alexander Y Piggott, Weiliang Jin, Jelena Vuckovi ́c, and Alejandro W Rodriguez. Inverse design in nanophotonics. *Nature Photonics*, 12(11):659–670, 2018.

[88] Elena Yu Vedmedenko, Roland Kenji Kawakami, Denis D Sheka, Pietro Gambardella, Andrei Kirilyuk, Atsufumi Hirohata, Christian Binek, Oksana Chubykalo-Fesenko, Stefano Sanvito, Brian J Kirby, et al. The 2020 magnetism roadmap : Section 9. *Journal of Physics D: Applied Physics*, 53(45):453001, 2020.

[89] HY Yuan, Yunshan Cao, Akashdeep Kamra, Rembert A Duine, and Peng Yan. Quantum magnonics: When magnon spintronics meets quantum information science. *Physics Reports*, 965:1–74, 2022.

[90] Elena Yu Vedmedenko, Roland Kenji Kawakami, Denis D Sheka, Pietro Gambardella, Andrei Kirilyuk, Atsufumi Hirohata, Christian Binek, Oksana Chubykalo-Fesenko, Stefano Sanvito, Brian J Kirby, et al. The 2020 magnetism roadmap : Section 11. *Journal of Physics D: Applied Physics*, 53(45):453001, 2020.

[91] Giovanni Finocchio, Supriyo Bandyopadhyay, Peng Lin, Gang Pan, J Joshua Yang, Riccardo Tomasello, Christos Panagopoulos, Mario Carpentieri, Vito Puliafito, Johan Åkerman, et al. Roadmap for unconventional computing with nanotechnology. chapter 2. *arXiv preprint arXiv:2301.06727*, 2023.

[92] Akash Kumar, Himanshu Fulara, Roman Khymyn, Artem Litvinenko, Mohammad Zahedinejad, Mona Rajabali, Xiaotian Zhao, Nilamani Behera, Afshin Houshang, Ahmad A Awad, et al. Robust mutual synchronization in long spin hall nano-oscillator chains. *Nano Letters*, 23(14):6720–6726, 2023.

[93] Thomas Brächer and Philipp Pirro. An analog magnon adder for all-magnonic neurons. *Journal of Applied Physics*, 124(15), 2018.

[94] Verena Brehm, Johannes W Austefjord, Serban Lepadatu, and Alireza Qaiumzadeh. A proposal for leaky integrate-and-fire neurons by domain walls in antiferromagnetic insulators. *Scientific Reports*, 13(1):13404, 2023.

[95] Satyendra Nath Bose. Plancks law and the hypothesis of light quanta. *Z. Phys*, 26(178):1–5, 1924.

[96] Albert Einstein. Quantentheorie des einatomigen idealen gases, sitzungsberichte kgl. *Preuss. Akad. Wiss*, 261, 1924.

[97] Eric A Cornell, Wolfgang Ketterle, and Carl E Wieman. The nobel prize in physics 2001. *URL http://www. nobelprize. org*, 2001.

[98] Nick P Proukakis, David W Snoke, and Peter B Littlewood. *Universal themes of Bose-Einstein condensation*. Cambridge university press, 2017.

[99] Nick P Proukakis, David W Snoke, and Peter B Littlewood. *Universal themes of Bose-Einstein condensation, Chapter 1*. Cambridge university press, 2017.

[100] Fritz London. On the bose-einstein condensation. *Physical Review*, 54(11):947, 1938.

[101] Yury Bunkov. Magnon bec versus atomic bec. *Journal of Low Temperature Physics*, 185:399–408, 2016.

[102] L Landau. The theory of suprafluidity of helium ii j. phys. ussr 5, 71 (1941). *JETP*, 11:592, 1941.

[103] N Bogoliubov. On the theory of superfluidity. *J. Phys*, 11(1):23, 1947.

[104] NN Bogoliubov. Energy levels of the imperfect bose-einstein gas. *Bull. Moscow State Univ*, 7:43–56, 1947.

[105] Nick P Proukakis, David W Snoke, and Peter B Littlewood. *Universal themes of Bose-Einstein condensation, Chapter 1*. Cambridge university press, 2017.

[106] Pyotr Kapitza. Viscosity of liquid helium below the λ-point. *Nature*, 141(3558):74–74, 1938.

[107] John F Allen and AD Misener. Flow of liquid helium ii. *Nature*, 141(3558):75–75, 1938.

[108] Mike H Anderson, Jason R Ensher, Michael R Matthews, Carl E Wieman, and Eric A Cornell. Observation of bose-einstein condensation in a dilute atomic vapor. *science*, 269(5221):198–201, 1995.

[109] Cl C Bradley, CA Sackett, JJ Tollett, and Randall G Hulet. Evidence of bose-einstein condensation in an atomic gas with attractive interactions. *Physical review letters*, 75(9):1687, 1995.

[110] Kendall B Davis, M-O Mewes, Michael R Andrews, Nicolaas J van Druten, Dallin S Durfee, DM Kurn, and Wolfgang Ketterle. Bose-einstein condensation in a gas of sodium atoms. *Physical review letters*, 75(22):3969, 1995.

[111] Igor V Borisenko, VE Demidov, VL Pokrovsky, and SO Demokritov. Spatial separation of degenerate components of magnon bose–einstein condensate by using a local acceleration potential. *Scientific Reports*, 10(1):14881, 2020.

[112] Sergio M Rezende. Theory of coherence in bose-einstein condensation phenomena in a microwave-driven interacting magnon gas. *Physical Review B*, 79(17):174411, 2009.

[113] Roy J Glauber. Coherent and incoherent states of the radiation field. *Physical Review*, 131(6):2766, 1963.

[114] Yuriy M Bunkov. Spin superfluidity and magnons bose–einstein condensation. *Physics-Uspekhi*, 53(8):848, 2010.

[115] Dmytro A Bozhko, Alexander A Serga, Peter Clausen, Vitaliy I Vasyuchka, Frank Heussner, Gennadii A Melkov, Anna Pomyalov, Victor S Lvov, and Burkard Hillebrands. Supercurrent in a room-temperature bose–einstein magnon condensate. *Nature Physics*, 12(11):1057–1062, 2016.

[116] Dmytro A Bozhko, Alexander A Serga, Peter Clausen, Vitaliy I Vasyuchka, Gennadii A Melkov, Victor S L'vov, and Burkard Hillebrands. On supercurrents in bose-einstein magnon condensates in yig ferrimagnet. *arXiv preprint arXiv:1608.01813*, 2016.

[117] Chen Sun, Thomas Nattermann, and Valery L Pokrovsky. Bose–einstein condensation and superfluidity of magnons in yttrium iron garnet films. *Journal of Physics D: Applied Physics*, 50(14):143002, 2017.

[118] Yury M Bunkov and Vladimir L Safonov. Magnon condensation and spin superfluidity. *Journal of Magnetism and Magnetic Materials*, 452:30–34, 2018.

[119] Alexander JE Kreil, Anna Pomyalov, Victor S Lvov, Halyna Yu Musiienko-Shmarova, Gennadii A Melkov, Alexander A Serga, and Burkard Hillebrands. Josephson oscillations in a room-temperature bose–einstein magnon condensate. *arXiv preprint arXiv:1911.07802*, 2019.

[120] Dmytro A Bozhko, Alexander JE Kreil, Halyna Yu Musiienko-Shmarova, Alexander A Serga, Anna Pomyalov, Victor S Lvov, and Burkard Hillebrands. Bogoliubov waves and distant transport of magnon condensate at room temperature. *Nature communications*, 10(1):2460, 2019.

[121] Andreas Rückriegel and Peter Kopietz. Rayleigh-jeans condensation of pumped magnons in thin-film ferromagnets. *Physical review letters*, 115(15):157203, 2015.

[122] D Kadio and YB Band. Analysis of a magnetically trapped atom clock. *Physical Review A*, 74(5):053609, 2006.

[123] Matthew PG Robbins, Niayesh Afshordi, and Robert B Mann. Bose-einstein condensates as gravitational wave detectors. *Journal of Cosmology and Astroparticle Physics*, 2019(07):032, 2019.

[124] Michael A Nielsen and Isaac L Chuang. Quantum computation and quantum information. chapter 1. *Phys. Today*, 54(2):60, 2001.

[125] Nadav Yoran and Anthony J Short. Efficient classical simulation of the approximate quantum fourier transform. *Physical Review A*, 76(4):042321, 2007.

[126] Daniel E Browne. Efficient classical simulation of the quantum fourier transform. *New Journal of Physics*, 9(5):146, 2007.

[127] Roberto E Troncoso and Álvaro S Núñez. Josephson effects in a bose–einstein condensate of magnons. *Annals of Physics*, 346:182–194, 2014.

[128] Corina Etz, Lars Bergqvist, Anders Bergman, Andrea Taroni, and Olle Eriksson. Atomistic spin dynamics and surface magnons. *Journal of Physics: Condensed Matter*, 27(24):243202, 2015.

[129] Claas Willem Abert. *Discrete Mathematical Concepts in Micromagnetic Computations*. PhD thesis, Staats-und Universitätsbibliothek Hamburg Carl von Ossietzky, 2013.

[130] Nathan Argaman and Guy Makov. Density functional theory: An introduction. *American Journal of Physics*, 68(1):69–79, 2000.

[131] Elena Yu Vedmedenko, Roland Kenji Kawakami, Denis D Sheka, Pietro Gambardella, Andrei Kirilyuk, Atsufumi Hirohata, Christian Binek, Oksana Chubykalo-Fesenko, Stefano Sanvito, Brian J Kirby, et al. The 2020 magnetism roadmap : Section 8. *Journal of Physics D: Applied Physics*, 53(45):453001, 2020.

[132] Yongbing Xu, David D Awschalom, and Junsaku Nitta. *Handbook of spintronics, Chapter 37*. Springer Publishing Company, Incorporated, 2016.

[133] Thomas L Gilbert. A phenomenological theory of damping in ferromagnetic materials. *IEEE transactions on magnetics*, 40(6):3443–3449, 2004.

[134] Arne Vansteenkiste, Jonathan Leliaert, Mykola Dvornik, Mathias Helsen, Felipe Garcia-Sanchez, and Bartel Van Waeyenberge. The design and verification of mumax3. *AIP advances*, 4(10), 2014.

[135] Massimiliano dAquino. Nonlinear magnetization dynamics in thin-films and nanoparticles. *http://wpage. unina. it/mdaquino/PhD_thesis/main/main. html*, 2004.

[136] M Lakshmanan. The fascinating world of the landau–lifshitz–gilbert equation: an overview. *Philosophical Transactions of the Royal Society A: Mathematical, Physical and Engineering Sciences*, 369(1939):1280–1300, 2011.

[137] Lukas Exl, Dieter Suess, and Thomas Schrefl. Micromagnetism. *Handbook of Magnetism and Magnetic Materials*, pages 1–44, 2020.

[138] D Kumar and AO Adeyeye. Techniques in micromagnetic simulation and analysis. *Journal of Physics D: Applied Physics*, 50(34):343001, 2017.

[139] Stefan Klingler, Philipp Pirro, Thomas Brächer, Britta Leven, Burkard Hillebrands, and Andrii V Chumak. Design of a spin-wave majority gate employing mode selection. *Applied Physics Letters*, 105(15), 2014.

[140] Qi Wang, M Kewenig, M Schneider, Roman Verba, F Kohl, B Heinz, M Geilen, M Mohseni, B Lägel, F Ciubotaru, et al. A magnonic directional coupler for integrated magnonic half-adders. *Nature Electronics*, 3(12):765–774, 2020.

[141] Michael Joseph Donahue and Donald G Porter. Oommf user's guide, version 1.0, 1999.

[142] Gunnar Selke. *Design and Development of a GPU-accelerated Micromagnetic Simulator*. PhD thesis, Staats-und Universitätsbibliothek Hamburg Carl von Ossietzky, 2013.

[143] Thomas Fischbacher, Matteo Franchin, Giuliano Bordignon, and Hans Fangohr. A systematic approach to multiphysics extensions of finite-element-based micromagnetic simulations: Nmag. *IEEE Transactions on Magnetics*, 43(6):2896–2898, 2007.

[144] R Chang, S Li, MV Lubarda, B Livshitz, and V Lomakin. Fastmag: Fast micromagnetic simulator for complex magnetic structures. *Journal of Applied Physics*, 109(7), 2011.

[145] Serban Lepadatu. Boris computational spintronicshigh performance multi-mesh magnetic and spin transport modeling software. *Journal of Applied Physics*, 128(24), 2020.

[146] Guru Venkat, D Kumar, M Franchin, O Dmytriiev, Michał Mruczkiewicz, H Fangohr, A Barman, Maciej Krawczyk, and A Prabhakar. Proposal for a standard micromagnetic problem: Spin wave dispersion in a magnonic waveguide. *IEEE Transactions on Magnetics*, 49(1):524–529, 2012.

[147] Harry Nyquist. Certain topics in telegraph transmission theory. *Transactions of the American Institute of Electrical Engineers*, 47(2):617–644, 1928.

[148] Claude E Shannon. Communication in the presence of noise. *Proceedings of the IRE*, 37(1):10–21, 1949.

[149] Stefan Klingler, Andrii V Chumak, Tim Mewes, Behrouz Khodadadi, Claudia Mewes, Carsten Dubs, Oleksii Surzhenko, Burkard Hillebrands, and Andrés Conca. Measurements of the exchange stiffness of yig films using broadband ferromagnetic resonance techniques. *Journal of Physics D: Applied Physics*, 48(1):015001, 2014.

[150] André Kapelrud. Spin pumping, spin transfer, and spin hall effects in magnetic insulator-normal metal systems. 2017.

[151] Saeedeh Mokarian Zanjani and Mehmet C Onbaşlı. Predicting new iron garnet thin films with perpendicular magnetic anisotropy. *Journal of Magnetism and Magnetic Materials*, 499:166108, 2020.

[152] Ali Ebrahimian, Anna Dyrdał, and Alireza Qaiumzadeh. Control of magnetic states and spin interactions in bilayer crcl3 with strain and electric fields: an ab initio study. *Scientific Reports*, 13(1):5336, 2023.

[153] Rf W Damon and JR Eshbach. Magnetostatic modes of a ferromagnet slab. *Journal of Physics and Chemistry of Solids*, 19(3-4):308–320, 1961.

[154] Morgan Sparks. Ferromagnetic resonance in thin films. i. theory of normal-mode frequencies. *Physical Review B*, 1(9):3831, 1970.

[155] BA Kalinikos. Excitation of propagating spin waves in ferromagnetic films. In *IEE Proceedings H (Microwaves, Optics and Antennas)*, volume 127, pages 4–10. IET, 1980.

[156] BA Kalinikos and AN Slavin. Theory of dipole-exchange spin wave spectrum for ferromagnetic films with mixed exchange boundary conditions. *Journal of Physics C: Solid State Physics*, 19(35):7013, 1986.

[157] MG Cottam and AN Slavin. Fundamentals of linear and nonlinear spin-wave processes in bulk and finite magnetic samples. In *Linear and Nonlinear Spin Waves in Magnetic Films and Superlattices*, pages 1–88. World Scientific, 1994.

[158] MJ Hurben and CE Patton. Theory of magnetostatic waves for in-plane magnetized isotropic films. *Journal of Magnetism and Magnetic Materials*, 139(3):263–291, 1995.

[159] P Landeros, Rodrigo E Arias, and DL Mills. Two magnon scattering in ultrathin ferromagnets: The case where the magnetization is out of plane. *Physical Review B*, 77(21):214405, 2008.

[160] Andreas Kreisel, Francesca Sauli, Lorenz Bartosch, and Peter Kopietz. Microscopic spin-wave theory for yttrium-iron garnet films. *The European Physical Journal B*, 71:59–68, 2009.

[161] Robert L Stamps and Helmut Schultheiss. Recent advances in topological ferroics and their dynamics preface. chapter 1, 2019.

[162] JR Eshbach and RW Damon. Surface magnetostatic modes and surface spin waves. *Physical Review*, 118(5):1208, 1960.

[163] Thomas Brächer, Philipp Pirro, and Burkard Hillebrands. Parallel pumping for magnon spintronics: Amplification and manipulation of magnon spin currents on the micron-scale. *Physics Reports*, 699:1–34, 2017.

[164] PW Anderson and H Suhl. Instability in the motion of ferromagnets at high microwave power levels. *Physical Review*, 100(6):1788, 1955.

[165] Harry Suhl. The nonlinear behavior of ferrites at high microwave signal levels. *Proceedings of the IRE*, 44(10):1270–1284, 1956.

[166] H Suhl. The theory of ferromagnetic resonance at high signal powers. *Journal of Physics and Chemistry of Solids*, 1(4):209–227, 1957.

[167] AV Chumak, GA Melkov, VE Demidov, O Dzyapko, VL Safonov, and SO Demokritov. Bose-einstein condensation of magnons under incoherent pumping. *Physical review letters*, 102(18):187205, 2009.

[168] Morteza Mohseni, Martin Kewenig, Roman Verba, Qi Wang, Michael Schneider, Björn Heinz, Felix Kohl, Carsten Dubs, Bert Lägel, Alexander A Serga, et al. Parametric generation of propagating spin waves in ultrathin yttrium iron garnet waveguides. *physica status solidi (RRL)–Rapid Research Letters*, 14(4):2000011, 2020.

[169] Björn Heinz, Morteza Mohseni, Akira Lentfert, Roman Verba, Michael Schneider, Bert Lägel, Khrystyna Levchenko, Thomas Brächer, Carsten Dubs, Andrii V Chumak, et al. Parametric generation of spin waves in nanoscaled magnonic conduits. *Physical Review B*, 105(14):144424, 2022.

[170] Viktor Hahn and Peter Kopietz. Effect of magnon decays on parametrically pumped magnons. *Physical Review B*, 103(9):094416, 2021.

[171] Viktor Hahn and Peter Kopietz. Collisionless kinetic theory for parametrically pumped magnons. *The European Physical Journal B*, 93:1–12, 2020.

[172] Roman Verba, Mario Carpentieri, Giovanni Finocchio, Vasil Tiberkevich, and Andrei Slavin. Amplification and stabilization of large-amplitude propagating spin waves by parametric pumping. *Applied Physics Letters*, 112(4), 2018.

[173] T Brächer, P Pirro, T Meyer, F Heussner, B Lägel, AA Serga, and B Hillebrands. Parallel parametric amplification of coherently excited propagating spin waves in a microscopic ni81fe19 waveguide. *Applied Physics Letters*, 104(20), 2014.

[174] Arne Brataas, Andrew D Kent, and Hideo Ohno. Current-induced torques in magnetic materials. *Nature materials*, 11(5):372–381, 2012.

[175] Michael Schneider, David Breitbach, Rostyslav O Serha, Qi Wang, Alexander A Serga, Andrei N Slavin, Vasyl S Tiberkevich, Björn Heinz, Bert Lägel, Thomas Brächer, et al. Control of the bose-einstein condensation of magnons by the spin hall effect. *Physical Review Letters*, 127(23):237203, 2021.

[176] Mikhail I Dyakonov and VI Perel. Current-induced spin orientation of electrons in semiconductors. *Physics Letters A*, 35(6):459–460, 1971.

[177] Mikhail I Dyakonov. Possibility of orienting electron spins with current. *JETP Lett. USSR*, 13:467, 1971.

[178] Luc Berger. Low-field magnetoresistance and domain drag in ferromagnets. *Journal of Applied Physics*, 49(3):2156–2161, 1978.

[179] Luc Berger. Domain drag effect in the presence of variable magnetic field or variable transport current. *Journal of Applied Physics*, 50(B3):2137–2139, 1979.

[180] John C Slonczewski. Current-driven excitation of magnetic multilayers. *Journal of Magnetism and Magnetic Materials*, 159(1-2):L1–L7, 1996.

[181] Luc Berger. Emission of spin waves by a magnetic multilayer traversed by a current. *Physical Review B*, 54(13):9353, 1996.

[182] P Monod, H Hurdequint, András Jánossy, J Obert, and J Chaumont. Giant electron spin-resonance transmission in cu ion implanted with mn. *Physical Review Letters*, 29(19):1327, 1972.

[183] RH Silsbee, A Janossy, and P Monod. Coupling between ferromagnetic and conduction-spin-resonance modes at a ferromagneticnormal-metal interface. *Physical Review B*, 19(9):4382, 1979.

[184] André Kapelrud and Arne Brataas. Spin pumping, dissipation, and direct and alternating inverse spin hall effects in magnetic-insulator/normal-metal bilayers. *Physical Review B*, 95(21):214413, 2017.

[185] Yaroslav Tserkovnyak, Arne Brataas, and Gerrit EW Bauer. Enhanced gilbert damping in thin ferromagnetic films. *Physical review letters*, 88(11):117601, 2002.

[186] Zihui Wang, Yiyan Sun, Mingzhong Wu, Vasil Tiberkevich, and Andrei Slavin. Control of spin waves in a thin film ferromagnetic insulator through interfacial spin scattering. *Physical review letters*, 107(14):146602, 2011.

[187] S.P. Rosen. Henry primakoff. *Biographical Memoirs of the National Academy of Sciences*, 66, 1995.

[188] Fuxiang Li, Wayne M Saslow, and Valery L Pokrovsky. Phase diagram for magnon condensate in yttrium iron garnet film. *Scientific reports*, 3(1):1372, 2013.

[189] Simon Streib, Nicolas Vidal-Silva, Ka Shen, and Gerrit EW Bauer. Magnon-phonon interactions in magnetic insulators. *Physical Review B*, 99(18):184442, 2019.

[190] Hannes Maier-Flaig, Stefan Klingler, Carsten Dubs, Oleksii Surzhenko, Rudolf Gross, Mathias Weiler, Hans Huebl, and Sebastian TB Goennenwein. Temperature-dependent magnetic damping of yttrium iron garnet spheres. *Physical Review B*, 95(21):214423, 2017.

[191] Sergio M Rezende, Antonio Azevedo, and Roberto L Rodríguez-Suárez. Introduction to antiferromagnetic magnons. *Journal of Applied Physics*, 126(15), 2019.

[192] AN Bogdanov and UK Rößler. Chiral symmetry breaking in magnetic thin films and multilayers. *Physical review letters*, 87(3):037203, 2001.

[193] Anne Louise Kristoffersen. Magnon condensation of magnetic insulators. Master's thesis, NTNU, 2023.

[194] XZ Yu, Yoshinori Onose, Naoya Kanazawa, Joung Hwan Park, JH Han, Yoshio Matsui, Naoto Nagaosa, and Yoshinori Tokura. Real-space observation of a two-dimensional skyrmion crystal. *Nature*, 465(7300):901–904, 2010.

[195] Johannes Hick, Francesca Sauli, Andreas Kreisel, and Peter Kopietz. Bose-einstein condensation at finite momentum and magnon condensation in thin film ferromagnets. *The European Physical Journal B*, 78:429–437, 2010.

[196] Frank J Buijnsters, Lennert JA Van Tilburg, Annalisa Fasolino, and Mikhail I Katsnelson. Two-dimensional dispersion of magnetostatic volume spin waves. *Journal of Physics: Condensed Matter*, 30(25):255803, 2018.

[197] Hartmut Zabel and Michael Farle. *Magnetic nanostructures: spin dynamics and spin transport*, volume 246. Springer, 2012.

[198] IS Tupitsyn, PCE Stamp, and AL Burin. Stability of bose-einstein condensates of hot magnons in yttrium iron garnet films. *Physical review letters*, 100(25):257202, 2008.

[199] Mona Helen Alexandra Kalthoff. *Nonequilibrium materials engineering in correlated systems via light-matter coupling*. PhD thesis, Staats-und Universitätsbibliothek Hamburg Carl von Ossietzky, 2022.

[200] G Gitgeatpong, Yang Zhao, P Piyawongwatthana, Yiming Qiu, Leland Weldon Harriger, Nicholas P Butch, TJ Sato, and K Matan. Nonreciprocal magnons and symmetry-breaking in the noncentrosymmetric antiferromagnet. *Physical review letters*, 119(4):047201, 2017.

[201] FLA Machado, PRT Ribeiro, J Holanda, RL Rodríguez-Suárez, A Azevedo, and SM Rezende. Spin-flop transition in the easy-plane antiferromagnet nickel oxide. *Physical Review B*, 95(10):104418, 2017.

Chapter 6

Papers

Paper I :

Therese Frostad, Hans Langva Skarsvåg, Alireza Qaiumzadeh, and Arne Brataas

Spin-transfer-assisted Parametric Pumping of Magnons in Yttrium Iron Garnet

Physical Review B (2022) [6]

Spin-transfer-assisted parametric pumping of magnons in yttrium iron garnet

Therese Frostad, Hans L. Skarsvåg, Alireza Qaiumzadeh, and Arne Brataas
Center for Quantum Spintronics, Department of Physics,
NTNU Norwegian University of Science and Technology, NO-7491 Trondheim, Norway

(Received 7 February 2022; accepted 30 June 2022; published 25 July 2022)

The combination of parametric pumping and spin-transfer torque is a powerful approach that enables high-level control over magnetic excitations in thin-film ferromagnets. The excitation parameters, such as pumping power and external field strength, affect the instabilities of individual magnon modes. We theoretically explore how the simultaneous effects of parametric pumping and spin transfer torque influence these magnetic instabilities in a thin-film ferromagnet. Within the Landau-Lifshitz-Gilbert framework, we perform micromagnetic simulations of magnon excitations in yttrium iron garnet by pumping, spin transfer torque, and a combination of the two. We find that consistent with experimental results, the magnitude and direction of the spin-transfer torque tune the parametric instability thresholds.

DOI: 10.1103/PhysRevB.106.024423

I. INTRODUCTION

Spin waves function as information carriers in spintronics. Magnons, the quanta of spin waves, may be created in ferromagnetic materials through numerous methods. Here, we address two common approaches for exciting the magnetization dynamics of thin-film ferromagnets.

Parametric pumping is a conventional nonlinear excitation method that uses a microwave field [1,2]. There is an applied AC magnetic field in the same direction as the external static magnetic field orienting the magnetization during parallel parametric pumping. The alternating pumping field induces oscillations in the ferromagnetic spin system. When the strength of the pumping field exceeds a certain threshold, an instability occurs that creates two magnons with opposite momenta. Energy conservation ensures that the two magnons have a lower frequency than the driving microwave field. Parametric pumping was introduced in the 1950s [3,4,6]. In 2006, parametric pumping generated Bose-Einstein condensation (BEC) of magnons in yttrium iron garnet (YIG) at room temperature [7]. This work motivated further discussions on magnon creation by pumping, thermalization processes of the created magnons, and the coherence of the emerging condensate [5,8–21]. Parametric pumping was further investigated as a tool for spin wave amplification [22,23].

Spin-transfer torque (STT) is a more recent approach to create magnons [24,25]. An external current or voltage induces a magnetization torque. One possible realization is to pass an electrical current through an adjacent metal such that the spin-Hall effect creates a spin accumulation in the metal. The spin accumulation may subsequently generate a torque on the magnetization in the neighboring ferromagnet. The STT may be employed to either inhibit or assist magnon creation because the torque has a component that acts dampinglike or antidampinglike, depending on the sign of the spin accumulation [26–30]. This control over the damping can create spin-torque oscillators. In this case, the current or voltage controls the oscillator frequency. STT can also be used to switch the magnetization configuration [31–33]. The latter feature enables concepts for magnetic random access memories. Recently, STT was utilized to create BEC in thin-film BiYIG [34].

Combining parametric pumping and STT achieves high-level control over magnon creation. It is known that STT tunes the instability thresholds of the parametric pumping mechanism [26,27,35]. Lauer *et al.* [35] merged parallel parametric pumping and STT on a thin (100 nm) YIG film. They monitored the resulting magnetization dynamics by Brillouin light scattering spectroscopy. The experiment revealed that the STT tunes the effective damping, thereby changing the threshold pumping power required to excite magnons by parametric pumping. Motivated by this experimental study, we conduct a large-scale micromagnetic simulation of a similar system. We apply both a parallel pumping field and STT. We determine the temporal evolution of the magnetization, from which we determine the stability phase diagram of spin-transfer-assisted parametric pumping. We also resolve the wave vector dependence on the nonequilibrium population of magnons.

We organize the remainder of this paper as follows. First, Sec. II introduces the theoretical framework. Therein, we present the Landau-Lifshitz-Gilbert (LLG) equation that describes the magnetization dynamics of the thin YIG film. Section III presents the setup for our micromagnetic simulations. To separate the effects of magnon excitation by parametric pumping and STT, we perform different simulations for the two phenomena. Finally, we simulate the combination of parametric pumping and STT applied to the YIG film. Section IV presents the results, and Sec. V summarizes our findings.

II. MAGNETIZATION DYNAMICS

We calculate the time evolution of the unit vector along the magnetization direction $\boldsymbol{m}(\boldsymbol{r}, t)$ within the LLG framework.

The LLG equation reads

$$\dot{\boldsymbol{m}} = -\gamma(\boldsymbol{m} \times \boldsymbol{H}_{\text{eff}}) + \alpha(\boldsymbol{m} \times \dot{\boldsymbol{m}}). \tag{1}$$

Here, $\gamma = 1.7595 \times 10^{11}\,\text{rad}\,\text{T}^{-1}\text{s}^{-1}$ is the gyromagnetic ratio, and α is the dimensionless Gilbert damping constant. The effective field $\boldsymbol{H}_{\text{eff}}$ includes contributions from the exchange field $\boldsymbol{H}_{\text{exch}}$, the external magnetic field $\boldsymbol{H}_{\text{ext}}$, and the dipole-dipole field $\boldsymbol{H}_{\text{d-d}}$. In our free energy we disregard the crystalline anisotropy since it is very small in YIG.

The exchange field arises from the Heisenberg exchange interaction between neighboring spins, and it promotes a homogeneous magnetization,

$$\boldsymbol{H}_{\text{exch}} = 2\frac{A_{\text{ex}}}{M_S}\nabla^2\boldsymbol{m}. \tag{2}$$

Here, A_{ex} is the exchange stiffness, and M_S is the saturation magnetization.

We can orient the magnetization in YIG along a desired direction by applying a sufficiently high static field of strength H_0. We define a film in the (x, y) plane and choose to apply the static field in the $\hat{\mathbf{x}}$ direction,

$$\boldsymbol{H}_{\text{ext}} = H_0\hat{\mathbf{x}}. \tag{3}$$

The external field term may include additional dynamic fields applied to the film.

The dipole-dipole field consists of the static demagnetization field and dynamic terms due to the long-range magnon-magnon interactions. In general, the dipole field at position $\boldsymbol{r}$ can be expressed in terms of contributions from the magnetization $\boldsymbol{m}(\boldsymbol{r}')$ at distance $\boldsymbol{d} = \boldsymbol{r} - \boldsymbol{r}'$ integrated over the film volume V,

$$\boldsymbol{H}_{\text{d-d}}(\boldsymbol{r}) = \frac{\mu_0}{4\pi}M_S\int_V d\boldsymbol{r}'\frac{3[\boldsymbol{m}(\boldsymbol{r}')\cdot\boldsymbol{d}]\boldsymbol{d}}{|\boldsymbol{d}|^5} - \frac{\boldsymbol{m}(\boldsymbol{r}')}{|\boldsymbol{d}|^3}. \tag{4}$$

Here, μ_0 is the permeability of free space. The dipole field can be expressed in terms of a 3×3 tensor $\hat{G}(\boldsymbol{r}, \boldsymbol{r}')$ [36,37],

$$\boldsymbol{H}_{\text{d-d}}(\boldsymbol{r}) = \mu_0 M_S\int_V d\boldsymbol{r}'\hat{G}(\boldsymbol{r}, \boldsymbol{r}')\cdot\boldsymbol{m}(\boldsymbol{r}'). \tag{5}$$

The tensor elements of $\hat{G}(\boldsymbol{r}, \boldsymbol{r}')$ are $G_{\alpha\beta} = -\frac{1}{4\pi}\frac{\partial}{\partial\alpha}\frac{\partial}{\partial\beta}\frac{1}{|\boldsymbol{d}|}$ for $\alpha, \beta = x, y, z$.

A. Spin-wave spectra

We now employ the thin-film approximation by assuming that the magnetization is uniform in the $\hat{\mathbf{z}}$ direction. Therefore, the thin film is effectively two-dimensional. In the expression for the dipole field Eq. (5), we average across the variation in the $\hat{\mathbf{z}}$ direction by integrating over the film thickness L_z. The total effective field of the LLG equation becomes a surface integral over the in-plane coordinate $\boldsymbol{\rho} = x\hat{\mathbf{x}} + y\hat{\mathbf{y}}$,

$$\begin{aligned}\boldsymbol{H}_{\text{eff}}(\boldsymbol{\rho}, t) = H_0\hat{\mathbf{x}} + 2\frac{A_{\text{ex}}}{M_S}\nabla^2_{\boldsymbol{\rho}}\boldsymbol{m}(\boldsymbol{\rho}, t)\\ + \mu_0 M_S\int_S \hat{G}(\boldsymbol{\rho}, \boldsymbol{\rho}')\boldsymbol{m}(\boldsymbol{\rho}', t)d\boldsymbol{\rho}',\end{aligned} \tag{6}$$

where the effective two-dimensional dipole tensor becomes

$$\hat{G}(\boldsymbol{\rho}, \boldsymbol{\rho}') = \frac{1}{L_z}\int_{-L_z/2}^{L_z/2}dz\int_{-L_z/2}^{L_z/2}dz'\hat{G}(\boldsymbol{r}, \boldsymbol{r}'). \tag{7}$$

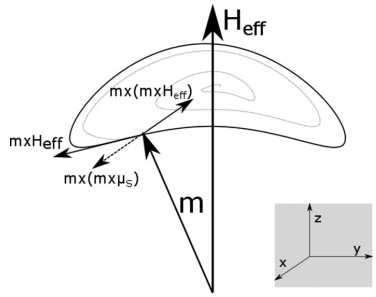

FIG. 1. The magnetization $\boldsymbol{m}$ precesses around $\boldsymbol{H}_{\text{eff}}$ due to the fieldlike torque $-\boldsymbol{m} \times \boldsymbol{H}_{\text{eff}}$. The damping $-\boldsymbol{m} \times (\boldsymbol{m} \times \boldsymbol{H}_{\text{eff}})$ can be tuned by applying an STT. The torque acts as a dampinglike or antidampinglike torque depending on the sign of the spin accumulation μ_S. The precession in the (y, z) plane is elliptical due to the dipole contributions from the finite film thickness in the $\hat{\mathbf{z}}$ direction.

We will consider the nonlinear response of the magnetization to the parallel pumping field in our numerical investigations presented below. However, relating our results to the linear response regime is also instructive.

In the linear response regime, the magnetization direction is $\boldsymbol{m}(\boldsymbol{\rho}, t) = \hat{\mathbf{x}} + \delta\boldsymbol{m}(\boldsymbol{\rho}, t)$, where the small out-of-equilibrium deviation $\delta\boldsymbol{m}(\boldsymbol{\rho}, t)$ lies in the (y, z) plane, as shown in Fig. 1. Additionally, we assume the magnetization is precessing with frequency ω; thus, $\delta\boldsymbol{m}(\boldsymbol{\rho}, t) = \delta\boldsymbol{m}(\boldsymbol{\rho})e^{i\omega t}$. We insert the effective field into the LLG Eq. (1). In the linear response regime, we retain only the first-order terms in the deviation $\delta\boldsymbol{m}(\boldsymbol{\rho}, t)$. We proceed to define the spatial Fourier transforms,

$$\boldsymbol{m}(\boldsymbol{k}) = \mathcal{F}[\boldsymbol{m}(\boldsymbol{\rho})] = \frac{1}{2\pi}\int \boldsymbol{m}(\boldsymbol{\rho})e^{-i\boldsymbol{k}\cdot\boldsymbol{\rho}}d\boldsymbol{\rho}, \tag{8}$$

$$\boldsymbol{m}(\boldsymbol{\rho}) = \int \boldsymbol{m}(\boldsymbol{k})e^{-i\boldsymbol{k}\cdot\boldsymbol{\rho}}d\boldsymbol{k}. \tag{9}$$

Here, $\boldsymbol{k} = |k|(\cos\theta_k\hat{\mathbf{x}} + \sin\theta_k\hat{\mathbf{y}})$ is the magnon wave vector. We can express the LLG equation as an eigenvalue problem, where the precession frequencies are the eigenvalues. We may then obtain the well-known dispersion relation for an extended thin film [36,38,39],

$$\begin{aligned}\omega(k, \theta_k) = \sqrt{\omega_H + \omega_M l_{\text{ex}}^2 k^2 + \omega_M(1 - f_k)\sin^2\theta_k}\\ \times\sqrt{\omega_H + \omega_M l_{\text{ex}}^2 k^2 + \omega_M f_k}.\end{aligned} \tag{10}$$

Here, we have defined $\omega_M = \gamma\mu_0 M_S$, $\omega_H = \gamma\mu_0 H_0$, and the magnetic exchange length $l_{\text{ex}} = \sqrt{2A_{\text{ex}}/\mu_0 M_S^2}$. The form factor f_k accounts for the film thickness,

$$f_k = \frac{1 - e^{-|k|L_z}}{|k|L_z}. \tag{11}$$

The spin waves traveling in the $\hat{\mathbf{x}}$ direction ($\theta_k = 0$) have the lowest energy. This lower magnon branch is shown in Fig. 2. It is symmetric in k and has a double minimum at $k = \pm k_{\text{min}}$. The exchange energy controls the spin waves at high wave vectors $k \gg l_{\text{ex}}^{-1}$, so that the dispersion is quadratic

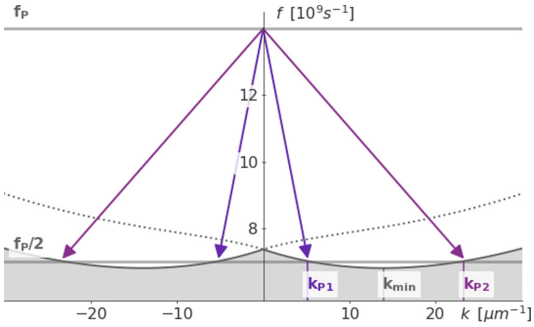

FIG. 2. The dispersion relation for spin waves traveling in the $\hat{\mathbf{x}}$ direction of a thin YIG film (k_x branch), as given by Eq. (10). Spin waves traveling in the $\hat{\mathbf{y}}$ direction have higher energies, as indicated by the dashed line (k_y branch). During parametric pumping, two magnons are created at wave vectors of opposite signs. These magnons both have frequency $\omega_p/2$. In the k_x branch, these magnons are found at $\pm k_{p1}$ and $\pm k_{p2}$. In turn, they thermalize and eventually occupy the dispersion minimum at $k_{\min}$. The parameters are from Tables I and II, with $\mu_0 H_0 = 190\,\mathrm{mT}$.

in k. On the other hand, the dipole interaction controls the spin waves at small wave vectors $k < L_z^{-1}$.

B. Magnon excitation

We proceed to examine magnon excitation by parametric pumping. In the parallel pumping geometry, the magnetization is in plane and oriented along the $\hat{\mathbf{x}}$ axis by a static field of magnitude H_0. There is an additional alternating microwave field $\boldsymbol{h}_p(t)$ parallel to the static field that functions as a magnon pump. The external field has static and oscillating contributions,

$$\boldsymbol{H}_{\mathrm{ext}} = [H_0 + h_p \sin(\omega_p t)]\hat{\mathbf{x}}. \tag{12}$$

Here, h_p is the amplitude, and ω_p is the frequency of the oscillating pumping field. When the strength of the pumping field exceeds a critical threshold, $h_p > h_p^{\mathrm{crit}}(H_0)$, the magnetization starts to precess around the $\hat{\mathbf{x}}$ axis. For a thin film, this precession is elliptical due to the dipole interactions from the finite thickness in the $\hat{\mathbf{z}}$ direction. By energy conservation, the created magnons have half the frequency of the pumping field, $\omega_{\boldsymbol{k}} = \omega_{-\boldsymbol{k}} = \omega_p/2$, and are opposite wave vectors, as illustrated in Fig. 2. This is the oscillation of the x component of the magnetic moments that couple to the magnetic pulse in the parallel pumping mechanism. Since dipolar magnons in YIG are elliptically polarized, the x component of magnetic magnons oscillates, and therefore, parallel pumping is possible. Parametric pumping mainly excites elliptical dipole-dominated low-energy magnon modes. We therefore expect that magnons are pumped in the k_x branch at points $k_x = \pm k_{p1}$, as illustrated in Fig. 2. Following this reasoning, the most efficient pumping occurs when $k_{p1} = k_{p2} = 0$ at ferromagnetic resonance (FMR) conditions since the ellipticity is highest in that situation. For a fixed pumping frequency ω_p, the external magnetic field strength H_{FMR} corresponding to the resonance frequency ω_{FMR} is approximated by the *Kittel formula* [40], as expected from Eq. (10) in the limit $k \to 0$,

$$\omega_{\mathrm{FMR}} = \omega_p/2 = \gamma\sqrt{H_{\mathrm{FMR}}(H_{\mathrm{FMR}} + \mu_0 M_S)}. \tag{13}$$

Next, we consider how the STT affects the magnetization dynamics. In thick films, the effective volume of surface modes is smaller than that of volume modes. Therefore, exciting surface modes by STT is easier than exciting bulk modes by STT [41,42]. However, we consider a thin film without any surface anisotropy, where the magnetization is uniform along the thickness direction. Surface modes are thus less important in this case, and we will not discuss them further.

The STT typically arises from a spin accumulation in an adjacent normal metal. We assume that a charge current in the adjacent metal layer (e.g., Pt) produces the spin accumulation polarized along the $\hat{\mathbf{x}}$ axis. The resulting torque on the YIG interface is expressed in terms of the spin-mixing conductance per area $g_\perp\,[1/\Omega\mathrm{m}^2]$ and spin accumulation density $\boldsymbol{\mu}_S = \mu_S\hat{\mathbf{x}}$,

$$\dot{\boldsymbol{m}} = -\gamma(\boldsymbol{m}\times\boldsymbol{H}_{\mathrm{eff}}) + \alpha(\boldsymbol{m}\times\dot{\boldsymbol{m}}) - \frac{\gamma\hbar}{2e^2 L_z M_S} g_\perp \boldsymbol{m}\times(\boldsymbol{m}\times\boldsymbol{\mu}_S). \tag{14}$$

Here, e is the elementary charge, and $\hbar$ is the reduced Planck constant. In our geometry, a positive (negative) spin accumulation results in a dampinglike (antidampinglike) STT. We proceed to find an expression for the critical spin accumulation μ_S^{crit} at which the damping is overpowered. As before, the effective field in Eq. (6) includes the static field, exchange interaction, and dipole interactions. Inserting the effective field into Eq. (14), the imaginary part of the eigenfrequencies determines the critical spin accumulation required to excite magnons with a specific wave vector,

$$\mu_S^{\mathrm{crit}}(k,\theta_k) = -\frac{2L_z e^2 \alpha M_S}{\hbar g_\perp \gamma}\left\{\omega_H + \omega_M l_{\mathrm{ex}}^2 k^2 + \frac{1}{2}\omega_M[f_k + (1-f_k)\sin^2\theta_k]\right\}. \tag{15}$$

Equation (15) can be minimized to yield the first magnon wave vector to be excited by STT. This wave vector denoted by $\boldsymbol{k}_{\mathrm{STT}}$ is in the k_x branch ($\theta_k = 0$), as illustrated in Fig. 3.

TABLE I. Material parameters of YIG.

Parameter	Symbol	Value in SI
Saturation magnetization [35]	$\mu_0 M_S$	173 mT
Exchange stiffness [44]	A_{ex}	$3.65\times10^{-12}\,\mathrm{J\,m^{-1}}$
Gilbert damping parameter	α	0.01

TABLE II. System parameters.

Parameter	Symbol	Value in SI
YIG film thickness	L_z	100 nm
YIG film lateral dimensions	$L_{x,y}$	5 μm
Lateral number of cells	$n_{x,y}$	2^9
Lateral cell size	$l_{x,y}$	∼10 nm
Microwave pumping frequency	$\omega_{\mathrm{p}} = 2\pi f_p$	$2\pi \times 14$ GHz

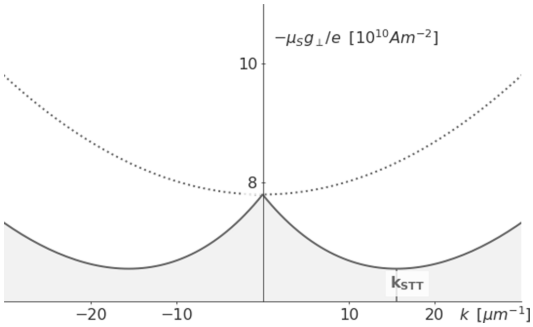

FIG. 3. The critical spin accumulation $-\mu_S^{\text{crit}} g_\perp/e$ for exciting spin waves traveling in the $\hat{\mathbf{x}}$ direction of a thin YIG film (k_x branch), as given by Eq. (15). Spin waves traveling in the $\hat{\mathbf{y}}$ direction require a higher spin accumulation, as indicated by the dashed line (k_y branch). The parameters are from Tables I and II, with $\mu_0 H_0 = 100\,\text{mT}$. For these parameters, we find that the first magnons are excited at $\theta_k = 0$, $|\boldsymbol{k}_{\text{STT}}| \approx 15.5\,\mu\text{m}^{-1}$ for the critical spin accumulation $\mu_S^{\text{crit}}(\boldsymbol{k}_{\text{STT}}) g_\perp/e \approx -6.55 \times 10^{10}\ \text{Am}^{-2}$.

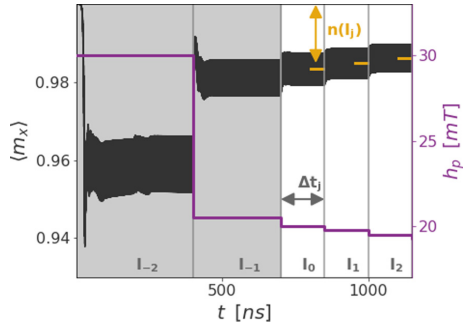

FIG. 4. The temporal evolution of the spatial average of the magnetization $\langle m_x \rangle(t)$. At $t = 0$, the magnetization randomly deviates from the uniform state. The shaded areas show the initialization intervals I_{-2} and I_{-1}. During these intervals, the pumping is strong and creates an initial state. Thereafter, the pumping power h_p decreases in intervals I_j (purple). Within each interval, we compute the temporal average of the magnetization (orange) resulting in the magnon density $\eta(H_0, h_p)$. The presented data are an excerpt from the simulations at $\mu_0 H_0 = 190\,\text{mT}$.

We note that the threshold spin accumulation in Eq. (15) is linear in the external field strength.

III. NUMERICAL APPROACH

We consider the magnetization dynamics in a thin film of YIG. First, we define a square film with lateral side lengths $L_{x,y}$ in the (x, y) plane. The film thickness $L_z = 100\,\text{nm}$ is much smaller than the lateral side lengths. We use the thin-film approximation in which there is no magnetization variation in the $\hat{\mathbf{z}}$ direction. Laterally, we divide the film into $N = n_{x,y}^2$ cells, each of size $l_{x,y}^2 \times L_z$. The unit vector in the magnetization direction of each cell is $\boldsymbol{m}(\boldsymbol{\rho}_i, t)$. We find the time evolution of each magnetization vector by solving the LLG equation at successive time intervals.

The simulations provide full information on the local magnetization within each cell of the film. This information allows the definition of a relative magnon density η in terms of the longitudinal component of the average magnetization,

$$\eta = 1 - \langle \boldsymbol{m}_x \rangle, \tag{16}$$

where $\langle \boldsymbol{m}_x \rangle = \sum_{i=1}^{i=N} \boldsymbol{m}(\boldsymbol{\rho}_i, t)/N$. We can find the magnon distribution $\zeta(k_x, k_y)$ as a function of the wave vector evaluating the Fourier transform of the transverse components of the magnetization,

$$\zeta(k_x, k_y) = |\mathcal{F}[m_y(\boldsymbol{\rho}, t)]|^2 + |\mathcal{F}[m_z(\boldsymbol{\rho}, t)]|^2. \tag{17}$$

Here, $\mathcal{F}[\cdot]$ denotes a discrete Fourier transform defined similar to the continuous transform in Eq. (8).

Our simulations include magnon excitation by parallel pumping, the STT, and the combination of the two. To this end, we use the open-source GPU-accelerated software MUMAX3 [43]. The simulations start from an initial magnetization state $\boldsymbol{m}(\boldsymbol{\rho}_i, t = 0)$, which must deviate from the uniform state for the magnetization dynamics to start. We apply the pumping fields and/or the STT over the entire surface of the film, and we investigate the resulting magnon density as a function of the bias field H_0, the pumping field amplitude h_p, and the spin accumulation μ_S. Section IV provides more details on the initialization and parameter variation of each simulation. Although the lateral size of the film is much larger than the film thickness, we expect some finite-size effects. The material parameters for YIG are listed in Table I. The damping coefficient $\alpha = 10^{-2}$ is set higher than, e.g., Ref. [35] ($\alpha \sim 10^{-4}$), such that the magnetization may reach steady state at acceptable running times. We detail the typical numerical parameters of the simulations in Table II.

IV. NUMERICAL RESULTS

We discuss the numerical results of three scenarios: (i) excitations performed exclusively by parallel pumping, (ii) excitations performed exclusively by STT, and (iii) excitations resulting from the combination of pumping and STT.

A. Magnon excitation by parallel parametric pumping

We first present simulations of magnon excitation by parallel parametric pumping. The number of created magnons is a measure of the efficiency of the pumping process. The simulations determine the relative magnon density as a function of the external field strength H_0 and pumping power h_p. In doing so, the simulations provide the critical threshold strength $h_p^{\text{crit}}(H_0)$ required to excite magnons. The threshold excitation strength may show hysteretic behavior depending on whether we increase or decrease H_0 [45,46]. For each fixed value of H_0, we run simulations in which h_p is decreased in steps for each time interval of length Δt, as illustrated in Fig. 4.

Each simulation starts from a chosen initial magnetization state. A noisy input state is created by randomly pulling each magnetization vector slightly away from its uniform state. This contributes to the initial magnon density, as observed at

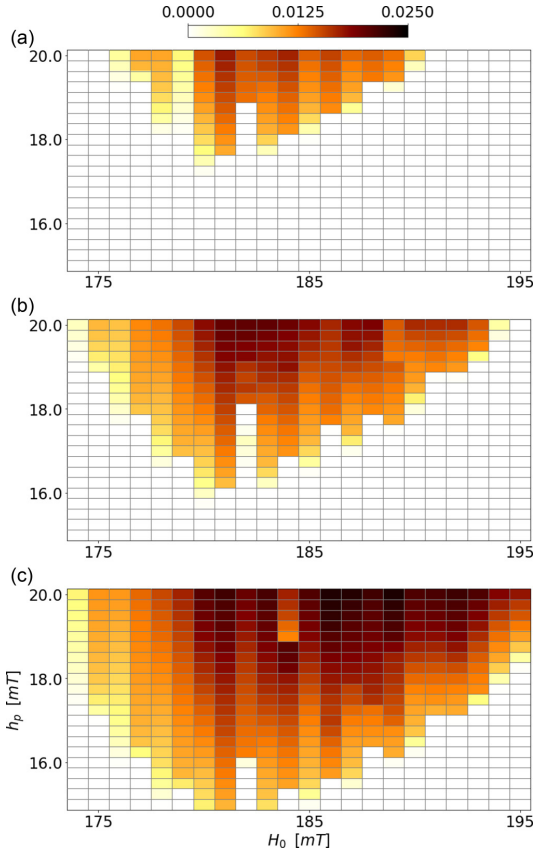

FIG. 5. The relative magnon density $\eta(H_0, h_p)$ during the parametric pumping of a thin YIG film. H_0 and h_p are the strengths of the external magnetic field and pumping field. The simulation series for each fixed H_0 (similar to Fig. 4) represents one column, where each pixel represents the relative magnon density $\eta(I_j)$. In (a) and (c), an STT due to the weak spin accumulation μ_S is applied. (a) Dampinglike STT, $\mu_S g_\perp/e = +1 \times 10^{10}$ Am^{-2}. (b) No STT, $\mu_S = 0$. (c) Antidampinglike STT, $\mu_S g_\perp/e = -1 \times 10^{10}$ Am^{-2}.

$t = 0$ in Fig. 4. We proceed to strongly pump the system for two intervals I_{-2} and I_{-1}. The gray shading in Fig. 4 shows these initialization intervals, which are not included in the extracted results in Fig. 5. After the initialization, we pump the systems in intervals I_j ($j = 0, 1, 2, \ldots$) while decreasing the pumping strength for each interval.

Figure 4 shows how the magnetization reaches a steady state when the pumping is decreased. In the steady state, the magnetization precession is elliptical. The spatial average of the magnetization $\langle \boldsymbol{m}_x \rangle(t)$ determines the relative density of the magnons, as in Eq. (16). We compute a time-averaged value $\eta(I_j)$ for the magnon density within a time window of 50 ns at the end of each interval, as illustrated in Fig. 4. The resulting magnon density represents one data point in Fig. 5(b).

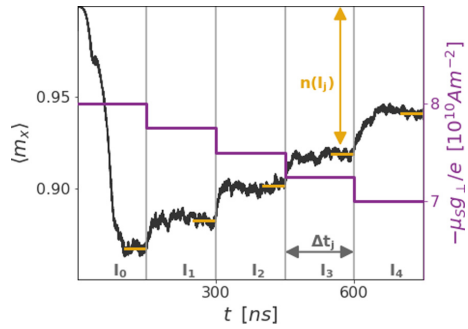

FIG. 6. The temporal evolution of the spatial average of the magnetization $\langle m_x \rangle(t)$ during excitation by STT. The simulations start from a magnetization state with random deviations from the uniform state. Magnons are created by the application of a large spin accumulation that results in an antidamping STT. The spin accumulation decreases in intervals I_j (purple). We compute the temporal average of the magnetization (orange) resulting in the magnon density $\eta(H_0, \mu_S)$. The presented data are an excerpt from the simulations at $\mu_0 H_0 = 100$ mT.

The threshold parametric pumping power $h_p^{\text{crit}}(H_0)$ to excite magnons is occasionally referred to as a *butterfly curve* [17,46,47]. The minimum of the threshold curve lies near the external field corresponding to resonance conditions H_{FMR}, which can be approximated by the Kittel formula in Eq. (13). Inserting the values of M_S and $\omega_{\text{FMR}} = \omega_p/2$ from Table II results in $H_{\text{FMR}} \approx 178$ mT. Note that the Kittel formula is valid for extended thin films, where $L_z/L_{x,y} \to 0$. In contrast, $L_z/L_{x,y} \approx 0.02$ in the simulated film (see Table II). This causes a small deviation between the simulated FMR frequency and the Kittel formula. Furthermore, because the lateral lengths of the simulated films are finite, the magnon energy levels are discrete. Looking at Fig. 5(b), we find that the discrete energy levels result in spikes, where it is difficult to excite magnons. The threshold curve can be compared to experimental results by Lauer *et al.* [35].

B. Magnon excitation by STT

We now proceed to discuss how STT generates magnons. The number of magnons created by STT is a function of the spin accumulation μ_S and the external field strength H_0. The STT effectively controls the damping. The sign of the spin accumulation determines whether the torque acts as a dampinglike or antidampinglike torque.

We use a range of applied bias field strengths to investigate the threshold spin accumulation for exciting magnons by STT. We decrease the strength of the spin accumulation in intervals for each H_0 series, as illustrated in Fig. 6. The initial magnetization at $t = 0$ is set to randomly deviate from the uniform state. An applied spin accumulation ($\mu_S g_\perp/e = -8 \times 10^{10}$ Am^{-2}) causes a strong STT well above the excitation threshold. The torque is present at the entire surface of the film. Next, we gradually decrease the strength of the torque at intervals I_j of duration Δt_j. The magnetization dynamics is chaotic, and occasionally, the system does not easily find a steady state at high current strengths, as shown in Fig. 6. The

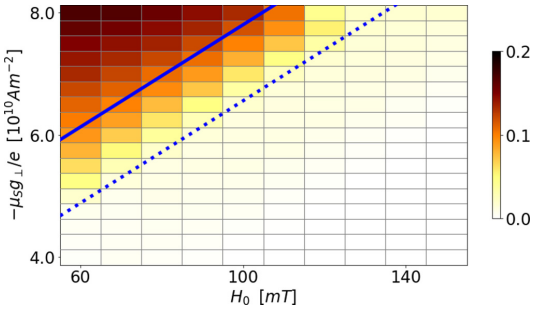

FIG. 7. The relative magnon density $\eta(H_0, \mu_S)$ during STT excitation of a YIG film as a function of the external magnetic field and spin accumulation. The simulation series for each fixed H_0 as in Fig. 6 represents one column, where each pixel represents the relative magnon density $\eta(I_j)$. The dashed blue line is the critical spin accumulation $\mu_S^{\text{crit}}(\boldsymbol{k}_{\text{STT}})$ required to excite magnons, as in Eq. (15). For comparison, the solid blue line shows $\mu_S^{\text{crit}}(k = 0)$.

magnon densities $\eta(H_0, \mu_S)$ calculated for the time windows are shown in Fig. 7.

We now consider the spin accumulation found by analytical approximations. The threshold spin accumulation for exciting magnons at wave vector $\boldsymbol{k}$ is given in Eq. (15). For the chosen parameters in Tables I and II, we find that $\mu_S^{\text{crit}}(\boldsymbol{k})$ reaches its minimum when $\theta_{k_{\text{STT}}} = 0$, $|\boldsymbol{k}_{\text{STT}}| \approx 15.5\,\mu\text{m}^{-1}$.

C. Parallel parametric pumping and weak STT

The STT is dissipative and effectively changes the Gilbert damping parameter. We therefore expect that the STT changes the threshold of parametric pumping. We investigate this expectation by applying a weak STT ($\mu_S g_\perp/e = \pm 1 \times 10^{10}$ Am^{-1}2) while performing parametric pumping on the YIG film. The procedure of initialization and interval pumping is similar to that in Sec. IV A.

The torque is applied at the entire surface of the film at all times, including during the initialization intervals I_{-2} and I_{-1}. In our sign convention, a positive (negative) spin accumulation results in a dampinglike (antidampinglike) torque. Figure 5(a) shows the effect of applying a dampinglike torque. The magnon instability threshold moves to higher pumping powers since the torque results in a higher effective damping. Figure 5(c) shows the results of an antidamping torque, which moves the threshold to lower pumping powers required to excite magnons. Note that in the high magnon density limit, which is the case in the presence of an antidampinglike torque, the magnetization dynamics is highly nonlinear.

D. Excited magnon modes

Parametric pumping favors the excitation of spin waves with elliptical precession. The dipole interaction dominates the dispersion in the long-wavelength limit when the spins precess with an elliptical character. In contrast, the exchange-dominated spin waves with a shorter wavelength have a circular precession. As illustrated in Fig. 2, we expect to mainly pump magnons at relatively long wavelengths,

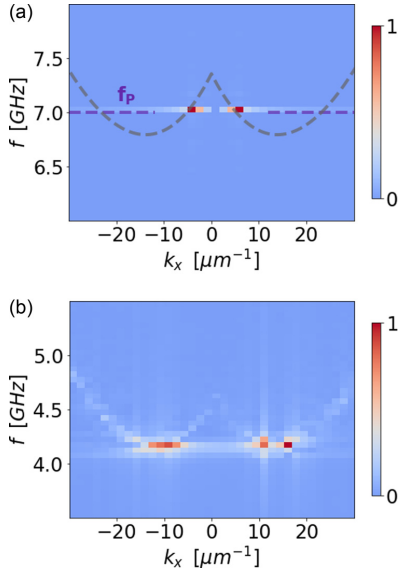

FIG. 8. The relative distributions of the magnons as a function of frequency and wave vector k_x, ($k_y = 0$). Magnons are excited in the YIG film during (a) only parametric pumping, $\mu_0 H_0 = 190$ mT, $\mu_0 h_p = 18$ mT, and (b) only STT, $\mu_0 H_0 = 100$ mT, $\mu_S g_\perp/e = -6.5 \times 10^{10}$ Am^{-2}. We show the square root of the magnon distribution, $\sqrt{\zeta(k_x, k_y)}$, from Eq. (17), where we disregard edge effects by taking the Fourier transform over the film middle (64 cell edges). The data are normalized with respect to the maximum intensity. In (a), the analytical energy dispersion from Eq. (10) is illustrated by a gray dashed line, while the pumping frequency is drawn with a purple dashed line.

$k = k_{p1}$. To further investigate this aspect, we perform a Fourier transform of the magnetization during parametric pumping and present the results in Fig. 8(a). Our numerical results confirm that the pumped magnons center around $k = k_{p1}$. Keeping the pumping frequency fixed, k_{p1} can be moved to higher (lower) values if we increase (decrease) the strength of the bias field.

In general, the STT excites spin waves at a wide range of frequencies and wave vector numbers [48]. For weak currents, the STT is expected to predominantly excite magnons at k_{STT}, the magnon wave vector that minimizes the spin accumulation given in Eq. (15). Starting from the lowest spin accumulation needed to excite magnons by STT, k_{STT} is the wave vector of the first magnons that we expect to excite. k_{STT} does not change with the bias field strength, but it depends on the film thickness. From Fig. 8(b), we find that we also excite magnons at neighboring energies. We find that the parametric pumping mainly creates dipole-dominated magnons at $k_x = k_{p1} \leqslant k_{\text{min}}$. The exchange-dominated magnons at $k_x \geqslant k_{\text{min}}$ are more easily excited by using the STT.

V. CONCLUSIONS

We have theoretically investigated the density of magnons excited by parametric pumping, STT, and a combination of the

two. The excitation processes in a thin YIG film are studied by performing micromagnetic simulations. Spin waves traveling parallel to the bias field direction (k_x branch) have lower energy than perpendicular spin waves. During parametric pumping, magnons of elliptic precession are predominantly excited at low wave vector numbers ($k = k_{p1}$) in the k_x branch. For STT, we expect the first magnons to be excited at $k = k_{\mathrm{STT}}$ before being distributed around the energy minimum of the k_x branch.

We found the critical pumping amplitude or spin accumulation for exciting magnons. The presence of a dampinglike or antidampinglike STT increases or decreases the threshold power for parametric pumping, depending on the sign of the STT. Our computed results are consistent with the measurements in recent experiments [35].

ACKNOWLEDGMENTS

The research leading to these results has received funding from the Research Council of Norway through its Centres of Excellence funding scheme, Project No. 262633, "QuSpin." The simulation work was supported by computational resources from the NTNU Idun infrastructure [49]. We thank A. A. Serga and A. Kapelrud for helpful and stimulating discussions. A.Q. was supported by the Norwegian Financial Mechanism 2014-2021 under the Polish–Norwegian Research Project NCN GRIEG "2Dtronics" No. 2019/34/H/ST3/00515.

[1] F. R. Morgenthaler, Survey of ferromagnetic resonance in small ferrimagnetic ellipsoids, J. Appl. Phys. **31**, S95 (1960).

[2] E. Schlömann, J. Green, and U. Milano, Recent developments in ferromagnetic resonance at high power levels, J. Appl. Phys. **31**, S386 (1960).

[3] P. Anderson and H. Suhl, Instability in the motion of ferromagnets at high microwave power levels, Phys. Rev. **100**, 1788 (1955).

[4] H. Suhl, The nonlinear behavior of ferrites at high microwave signal levels, Proc. IRE **44**, 1270 (1956).

[5] S. Demokritov, V. Demidov, O. Dzyapko, G. Melkov, and A. Slavin, Quantum coherence due to Bose-Einstein condensation of parametrically driven magnons, New J. Phys. **10**, 045029 (2008).

[6] H. Suhl, The theory of ferromagnetic resonance at high signal powers, J. Phys. Chem. Solids **1**, 209 (1957).

[7] S. Demokritov, V. Demidov, O. Dzyapko, G. Melkov, A. Serga, B. Hillebrands, and A. Slavin, Bose–Einstein condensation of quasi-equilibrium magnons at room temperature under pumping, Nature (London) **443**, 430 (2006).

[8] V. E. Demidov, O. Dzyapko, S. O. Demokritov, G. A. Melkov, and A. N. Slavin, Observation of Spontaneous Coherence in Bose-Einstein Condensate of Magnons, Phys. Rev. Lett. **100**, 047205 (2008).

[9] I. S. Tupitsyn, P. C. E. Stamp, and A. L. Burin, Stability of Bose-Einstein Condensates of Hot Magnons in Yttrium Iron Garnet Films, Phys. Rev. Lett. **100**, 257202 (2008).

[10] S. M. Rezende, Theory of coherence in Bose-Einstein condensation phenomena in a microwave-driven interacting magnon gas, Phys. Rev. B **79**, 174411 (2009).

[11] S. M. Rezende, Theory of microwave superradiance from a Bose-Einstein condensate of magnons, Phys. Rev. B **79**, 060410(R) (2009).

[12] P. Nowik-Boltyk, O. Dzyapko, V. Demidov, N. Berloff, and S. Demokritov, Spatially non-uniform ground state and quantized vortices in a two-component Bose-Einstein condensate of magnons, Sci. Rep. **2**, 482 (2012).

[13] A. A. Serga, V. S. Tiberkevich, C. W. Sandweg, V. I. Vasyuchka, D. A. Bozhko, A. V. Chumak, T. Neumann, B. Obry, G. A. Melkov, A. N. Slavin, and B. Hillebrands, Bose–Einstein condensation in an ultra-hot gas of pumped magnons, Nat. Commun. **5**, 3452 (2014).

[14] P. Clausen, D. A. Bozhko, V. I. Vasyuchka, B. Hillebrands, G. A. Melkov, and A. A. Serga, Stimulated thermalization of a parametrically driven magnon gas as a prerequisite for Bose-Einstein magnon condensation, Phys. Rev. B **91**, 220402(R) (2015).

[15] O. Dzyapko, P. Nowik-Boltyk, B. Koene, V. E. Demidov, J. Jersch, A. Kirilyuk, T. Rasing, and S. O. Demokritov, High-resolution magneto-optical Kerr-effect spectroscopy of magnon Bose–Einstein condensate, IEEE Magn. Lett. **7**, 3501805 (2016).

[16] V. Hahn and P. Kopietz, Collisionless kinetic theory for parametrically pumped magnons, Eur. Phys. J. B **93**, 132 (2020).

[17] M. Mohseni, M. Kewenig, R. Verba, Q. Wang, M. Schneider, B. Heinz, F. Kohl, C. Dubs, B. Lägel, A. A. Serga, B. Hillebrands, A. V. Chumak, and P. Pirro, Parametric generation of propagating spin waves in ultrathin yttrium iron garnet waveguides, Phys. Status Solidi RRL **14**, 2000011 (2020).

[18] H. Hayashi and K. Ando, Spin Pumping Driven by Magnon Polarons, Phys. Rev. Lett. **121**, 237202 (2018).

[19] B. Heinz, M. Mohseni, A. Lentfert, R. Verba, M. Schneider, B. Lägel, K. Levchenko, T. Brächer, C. Dubs, A. V. Chumak, and P. Pirro, Parametric generation of spin waves in nanoscaled magnonic conduits, Phys. Rev. B **105**, 144424 (2022).

[20] T. B. Noack, V. I. Vasyuchka, D. A. Bozhko, B. Heinz, P. Frey, D. V. Slobodianiuk, O. V. Prokopenko, G. A. Melkov, P. Kopietz, B. Hillebrands, and A. A. Serga, Enhancement of the spin pumping effect by magnon confluence process in YIG/Pt bilayers, Phys. Status Solidi B **256**, 1900121 (2019).

[21] V. Hahn and P. Kopietz, Effect of magnon decays on parametrically pumped magnons, Phys. Rev. B **103**, 094416 (2021).

[22] R. Verba, M. Carpentieri, G. Finocchio, V. Tiberkevich, and A. Slavin, Amplification and stabilization of large-amplitude propagating spin waves by parametric pumping, Appl. Phys. Lett. **112**, 042402 (2018).

[23] T. Brächer, P. Pirro, T. Meyer, F. Heussner, B. Lägel, A. Serga, and B. Hillebrands, Parallel parametric amplification of coherently excited propagating spin waves in a microscopic $Ni_{81}Fe_{19}$ waveguide, Appl. Phys. Lett. **104**, 202408 (2014).

[24] D. C. Ralph and M. D. Stiles, Spin transfer torques, J. Magn. Magn. Mater. **320**, 1190 (2008).

[25] A. Brataas, A. D. Kent, and H. Ohno, Current-induced torques in magnetic materials, Nat. Mater. **11**, 372 (2012).

[26] S. Urazhdin, V. Tiberkevich, and A. Slavin, Parametric Excitation of a Magnetic Nanocontact by a Microwave Field, Phys. Rev. Lett. **105**, 237204 (2010).

[27] E. R. J. Edwards, H. Ulrichs, V. E. Demidov, S. O. Demokritov, and S. Urazhdin, Parametric excitation of magnetization oscillations controlled by pure spin current, Phys. Rev. B **86**, 134420 (2012).

[28] A. Hamadeh, O. d'Allivy Kelly, C. Hahn, H. Meley, R. Bernard, A. H. Molpeceres, V. V. Naletov, M. Viret, A. Anane, V. Cros, S. O. Demokritov, J. L. Prieto, M. Muñoz, G. de Loubens, and O. Klein, Full Control of the Spin-Wave Damping in a Magnetic Insulator Using Spin-Orbit Torque, Phys. Rev. Lett. **113**, 197203 (2014).

[29] Y. Tserkovnyak, A. Brataas, and G. E. W. Bauer, Enhanced Gilbert Damping in Thin Ferromagnetic Films, Phys. Rev. Lett. **88**, 117601 (2002).

[30] Z. Wang, Y. Sun, M. Wu, V. Tiberkevich, and A. Slavin, Control of Spin Waves in a Thin Film Ferromagnetic Insulator through Interfacial Spin Scattering, Phys. Rev. Lett. **107**, 146602 (2011).

[31] J. C. Slonczewski, Current-driven excitation of magnetic multilayers, J. Magn. Magn. Mater. **159**, L1 (1996).

[32] E. Myers, D. Ralph, J. Katine, R. Louie, and R. Buhrman, Current-induced switching of domains in magnetic multilayer devices, Science **285**, 867 (1999).

[33] J. A. Katine, F. J. Albert, R. A. Buhrman, E. B. Myers, and D. C. Ralph, Current-Driven Magnetization Reversal and Spin-Wave Excitations in Co/Cu/Co Pillars, Phys. Rev. Lett. **84**, 3149 (2000).

[34] B. Divinskiy, H. Merbouche, V. E. Demidov, K. O. Nikolaev, L. Soumah, D. Gouéré, R. Lebrun, V. Cros, J. B. Youssef, P. Bortolotti, A. Anane, and S. O. Demokritov, Evidence for spin current driven Bose-Einstein condensation of magnons, Nat. Commun. **12**, 6541 (2021).

[35] V. Lauer, D. A. Bozhko, T. Brächer, P. Pirro, V. I. Vasyuchka, A. A. Serga, M. B. Jungfleisch, M. Agrawal, Yu. V. Kobljanskyj, G. A. Melkov, C. Dubs, B. Hillebrands, and A. V. Chumak, Spin-transfer torque based damping control of parametrically excited spin waves in a magnetic insulator, Appl. Phys. Lett. **108**, 012402 (2016).

[36] B. Kalinikos and A. Slavin, Theory of dipole-exchange spin wave spectrum for ferromagnetic films with mixed exchange boundary conditions, J. Phys. C **19**, 7013 (1986).

[37] B. Kalinikos, Spectrum and linear excitation of spin waves in ferromagnetic films, Sov. Phys. J. **24**, 718 (1981).

[38] A. Kreisel, F. Sauli, L. Bartosch, and P. Kopietz, Microscopic spin-wave theory for yttrium-iron garnet films, Eur. Phys. J. B **71**, 59 (2009).

[39] A. Rückriegel and P. Kopietz, Rayleigh-Jeans Condensation of Pumped Magnons in Thin-Film Ferromagnets, Phys. Rev. Lett. **115**, 157203 (2015).

[40] C. Kittel, On the theory of ferromagnetic resonance absorption, Phys. Rev. **73**, 155 (1948).

[41] J. Xiao and G. E. Bauer, Spin-Wave Excitation in Magnetic Insulators by Spin-Transfer Torque, Phys. Rev. Lett. **108**, 217204 (2012).

[42] A. Kapelrud and A. Brataas, Spin Pumping and Enhanced Gilbert Damping in Thin Magnetic Insulator Films, Phys. Rev. Lett. **111**, 097602 (2013).

[43] A. Vansteenkiste, J. Leliaert, M. Dvornik, M. Helsen, F. Garcia-Sanchez, and B. Van Waeyenberge, The design and verification of MuMax3, AIP Adv. **4**, 107133 (2014).

[44] S. Klingler, A. V. Chumak, T. Mewes, B. Khodadadi, C. Mewes, C. Dubs, O. Surzhenko, B. Hillebrands, and A. Conca, Measurements of the exchange stiffness of YIG films using broadband ferromagnetic resonance techniques, J. Phys. D **48**, 015001 (2015).

[45] Y.-J. Chen, H. K. Lee, R. Verba, J. A. Katine, I. Barsukov, V. Tiberkevich, J. Q. Xiao, A. N. Slavin, and I. N. Krivorotov, Parametric resonance of magnetization excited by electric field, Nano Lett. **17**, 572 (2017).

[46] F. Guo, L. M. Belova, and R. D. McMichael, Parametric pumping of precession modes in ferromagnetic nanodisks, Phys. Rev. B **89**, 104422 (2014).

[47] C. E. Patton and W. Jantz, Anomalous subsidiary absorption in single-crystal YIG and evaluation of spin-wave linewidth, J. Appl. Phys. **50**, 7082 (1979).

[48] V. E. Demidov, S. Urazhdin, E. R. J. Edwards, M. D. Stiles, R. D. McMichael, and S. O. Demokritov, Control of Magnetic Fluctuations by Spin Current, Phys. Rev. Lett. **107**, 107204 (2011).

[49] M. Själander, M. Jahre, G. Tufte, and N. Reissmann, EPIC: An energy-efficient, high-performance GPGPU computing research infrastructure, arXiv:1912.05848.

Paper II :

Therese Frostad, Philipp Pirro, Alexander A. Serga, Burkard Hillebrands, Arne Brataas, and Alireza Qaiumzadeh

Anisotropy-assisted Magnon Condensation in Ferromagnetic Thin Films

arXiv preprint arXiv:2309.05982 (2023) [🗎]

Anisotropy-assisted magnon condensation in ferromagnetic thin films

Therese Frostad,[1] Philipp Pirro,[2] Alexander A. Serga,[2]
Burkard Hillebrands,[2] Arne Brataas,[1] and Alireza Qaiumzadeh[1]

[1] *Center for Quantum Sprintronics, Department of Physics, Norwegian University of Science and Technology, NO-7491 Trondheim, Norway*
[2] *Dapartment of Physics and Research Center OPTIMAS, Rhainland-Pfälzische Technische Universität Kaiserslautern-Landau, 67663 Kaiserslautern, Germany*

We theoretically demonstrate that adding an easy-axis magnetic anisotropy facilitates magnon condensation in thin yttrium iron garnet (YIG) films. Dipolar interactions in a quasi-equilibrium state stabilize room-temperature magnon condensation in YIG. Even though the out-of-plane easy-axis anisotropy generally competes with the dipolar interactions, we show that adding such magnetic anisotropy may assist the generation of the magnon condensation electrically, via the spin transfer torque mechanism. We use analytical calculations and micromagnetic simulations to illustrate this effect. Our results may explain the recent experiment on Bi-doped YIG and open a new pathway toward application of current-driven magnon condensation in quantum spintronics.

Introduction—. Magnon condensation with nonzero momentum at room temperature [1] is a fascinating phenomenon first observed in 2006. The condensed magnons were observed at the two degenerate magnon band minima of yttrium iron garnet (YIG), and easy-plane ferrimagnetic insulator with very low magnetic dissipation [2, 3], as the spontaneous formation of a quasi-equilibrium and coherent magnetization dynamics in the momentum space [4]. To generate condensate magnons, magnon must be pumped into the system by an incoherent stimulus such as parametric pumping [1, 5–14] and/or spin-transfer torque [15–19]. The system may thermalize above a critical magnon density to form a quasi-equilibrium magnon condensation state at the bottom of magnon bands. The study of magnon condensation is not only interesting from an academic point of view, but it is also of great importance in various areas of quantum technology and applied spintronics [11, 20–22].

At high magnon densities, the relevant regime for the magnon condensation state and nonlinear magnon-magnon interactions becomes important. A (meta)stable and steady quasi-equilibrium magnon condensation requires an effective repulsive interaction between magnon quasiparticles. It was shown that in a system mainly influenced by exchange interaction, magnons are attractive, but dipolar interactions in YIG may change the sign of nonlinear magnon interactions and thus are crucial for the creation of a (meta)stable condensate magnon state [8–10, 23–29].

Recently, it was shown that the thermalization time of magnon condensation is reduced in confined nanoscopic systems [30]. It was also demonstrated that the lateral confinement in YIG enhances the dipolar interaction along the propagation direction and causes a deeper band depth, i.e., the difference between ferromagnetic resonance (FMR) and magnon band minima. Increasing the magnon condensation lifetime was attributed to this enhancement of the band depth [30].

In another recent achievement in magnon condensation experiments, Divinsky et al. [31] found evidence of condensation of magnons by spin-transfer torque mechanism. They introduced a small perpendicular magnetocrystalline anisotropy (PMA) through bismuth doping in the thin film of YIG, while the magnetic ground state still resides within the plane. This discovery opens a new route toward electronic control of magnon condensation.

However, the interplay between the dipolar interactions, which was previously shown to be essential for the stability and thermalization of magnon condensation, and the counteracting out-of-plane easy-axis magnetic anisotropy, is so far uncharted. This article studies the nonlinear magnon interactions by analyzing the mechanism behind the anisotropy-assisted formation of the magnon condensate. We present simulations within the Landau-Lifshitz-Gilbert framework [32–34] that support analytical calculations.

Model—. We consider a thin ferromagnetic film in the $y-z$ plane to model YIG. The magnetic moments are directed along the z direction by an external magnetic field of strength H_0. The magnetic potential energy of the film contains contributions from the isotropic exchange interaction $\mathcal{H}_{\rm ex}$, Zeeman interaction $\mathcal{H}_{\rm Z}$, dipolar interaction $\mathcal{H}_{\rm dip}$, and additionally a PMA energy $\mathcal{H}_{\rm an}$ in the x direction, normal to the film plane. YIG has a weak in-plane easy-axis that can be neglected compared to the other energy scales in the system. The total spin Hamiltonian of the system reads,

$$\mathcal{H} = \mathcal{H}_{\rm ex} + \mathcal{H}_{\rm Z} + \mathcal{H}_{\rm dip} + \mathcal{H}_{\rm an}. \tag{1}$$

The PMA energy is given by,

$$\mathcal{H}_{\rm an} = -K_{\rm an} \sum_j (\boldsymbol{S}_j \cdot \hat{x})^2, \tag{2}$$

where $K_{\rm an} > 0$ is the easy-axis energy, $\hbar \boldsymbol{S}_j$ is the vector of spin operator at site j, with $\hbar$ is the reduced Planck constant. Details of the Hamiltonian can be found in the Supplemental Material (SM) [35].

The Holstein-Primakoff spin-boson transformation [36] allows us to express the spin Hamiltonian in terms of the

magnon creation and annihilation operators. The amplitude of the effective spin per unit cell in YIG at room temperature is large $\hbar S \approx 14.3\hbar$, [27, 37, 38], and thus we can expand the spin Hamiltonian in the inverse powers of the spin S. Up to the lowest order in nonlinear terms, the magnon Hamiltonian $\mathcal{H}$ of a YIG thin film can be expressed as the sum of two components: $\mathcal{H}_2$ and $\mathcal{H}_4$. The former represents a noninteracting magnon gas comprising quadratic magnon operators. The latter, on the other hand, constitutes nonlinear magnon interactions characterized by quartic magnon operators; see the SM for details [35]. Note that three-magnon interactions are forbidden in our geometry by the conservation laws [39]

Magnon dispersion of YIG with a finite PMA—. The magnon dispersion in YIG is well known and has been studied extensively in both experimental and theoretical works [2, 40, 41]. Magnons travelling in the direction of the external magnetic field have the lowest energy. These so-called backward volume magnetostatic (BVM) magnons have a dispersion with a double degenerate minimum at finite wavevectors $q_z = \pm Q$. When pumping magnons into the thin film, the magnons may thermalize and eventually form a condensate state in these two degenerate minima with opposite wavevectors.

The noninteracting magnon Hamiltonian and the dispersion of BVM magnons, along the z direction, in the presence of a finite PMA reads,

$$\mathcal{H}_2 = \sum q_z \hbar\omega_{q_z} \hat{c}^\dagger_{q_z} \hat{c}_{q_z}, \tag{3a}$$

$$\hbar\omega_{q_z} = \sqrt{A^2_{q_z} - B^2_{q_z}}, \tag{3b}$$

where $\hat{c}^\dagger_{q_z}(\hat{c}_{q_z})$ are the magnon creation (annihilation) operators, and

$$A_{q_z} = D_{\rm ex} q_z^2 + \gamma(H_0 + 2\pi M_S f_q) - K_{\rm an} S, \tag{4a}$$

$$B_{q_z} = 2\pi M_S f_q - K_{\rm an} S. \tag{4b}$$

Here, $D_{\rm ex}$ is the exchange stiffness, $M_S = \gamma\hbar S/a^3$ is the saturation magnetization, with $\gamma = 1.2 \times 10^{-5}\,\mathrm{eV\,Oe^{-1}}$ is the gyromagnetic ratio, and $a = 12.376$Å is the lattice constant of YIG. The form factor $f_q = (1 - e^{-|q_z|L_x})/(|q_z|L_x)$ stems from dipolar interactions in a thin magnetic film with thickness L_x [42, 43].

Fig. 1 shows the effect of PMA on the magnon dispersion of YIG. PMA decreases both the ferromagnetic resonance (FMR), and the magnon band gap at the Γ point $\omega_{q_z=0}$, in addition to a greater decrease in the magnon band gap at the band minima $\omega_{q_z=\pm Q}$. Therefore the band depth $\Delta\omega = \omega_{q_z=0} - \omega_{q_z=\pm Q}$ is increased. The position of the band minima at $q_z = \pm Q$ is also shifted to larger momenta. In addition, the curvature of the minima increases as a function of the anisotropy strength. Above a critical PMA, $K^{c_2}_{\rm an}$, the magnetic ground state is destabilized and the in-plane magnetic state becomes out-of-plane. We are interested in the regime in which the magnetic ground state remains in-plane, and thus the effective saturation magnetization is positive $M_{\rm eff} = M_S - 2K_{\rm an}/(\mu_0 M_S) > 0$

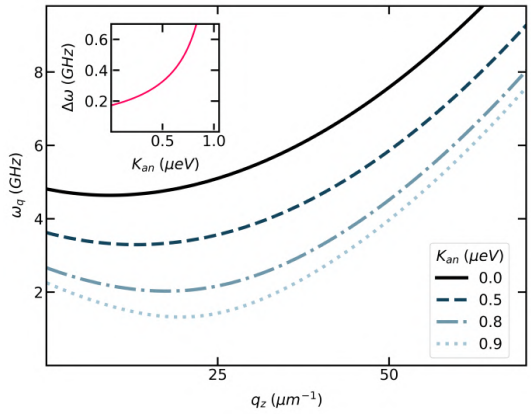

FIG. 1. The dispersion of noninteracting BVM magnons in a YIG thin film for various PMA strengths. The inset shows the depth of the band minima as a function of the PMA strength. We set $L_x = 50\,\mathrm{nm}$ and $H_0 = 1\,\mathrm{kOe}$

The effect of PMA on magnon dispersion resembles the effect of confinement in the magnon spectra of YIG. In Ref. 30, it was shown that transverse confinement in a YIG thin film leads to an increase of the FMR frequency, the band depth, as well as shifting the band minima to higher momenta while the magnon band gap at the band minima is also increased. It was shown that this change of the spectrum in confined systems increases the magnon condensate lifetime. Therefore, we expect, in a similar way, PMA increases the magnon condensate lifetime and assists the generation of magnon condensation.

Nonlinear magnon interactions in the presence of PMA—. Magnons are considered quasiparticles that exhibit weak interactions in the low-density regime, but their intensity of nonlinear interactions increases as their density increases. Repulsive interactions are essential for thermalizing injected nonequilibrium magnons and creating a metastable magnon condensation at a steady and quasi-equilibrium state. Since the discovery of magnon condensation, there has been a long debate over the origin of magnon thermalization [8, 9, 26–28, 44].

The nonlinear interaction of condensate magnons at the two degenerate minima, $q_z = \pm Q$, consists of intra- and inter-band contributions, $\mathcal{H}_4 = \mathcal{H}_4^{\rm intra} + \mathcal{H}_4^{\rm inter}$, where

$$\mathcal{H}_4^{\rm intra} = A(\hat{c}^\dagger_Q \hat{c}^\dagger_Q \hat{c}_Q \hat{c}_Q + \hat{c}^\dagger_{-Q} \hat{c}^\dagger_{-Q} \hat{c}_{-Q} \hat{c}_{-Q}), \tag{5a}$$

$$\mathcal{H}_4^{\rm inter} = 2B(\hat{c}^\dagger_Q \hat{c}^\dagger_{-Q} \hat{c}_Q \hat{c}_{-Q}) + C(\hat{c}^\dagger_Q \hat{c}_{-Q} \hat{c}_Q \hat{c}_{-Q} \hat{c}^\dagger_{-Q} \hat{c}_{-Q} \hat{c}_Q + \text{h.c.}) + D(\hat{c}^\dagger_Q \hat{c}^\dagger_Q \hat{c}^\dagger_{-Q} \hat{c}^\dagger_{-Q} + \text{h.c.}). \tag{5b}$$

The interaction amplitudes are given by,

$$A = -\frac{\gamma\pi M_S}{SN}\left[(\alpha_1+\alpha_3)f_Q - 2\alpha_2(1-f_{2Q})\right] - \frac{D_{\rm ex}Q^2}{2SN}(\alpha_1-4\alpha_2) + \frac{K_{\rm an}}{2N}(\alpha_1+\alpha_3), \quad (6a)$$

$$B = \frac{\gamma 2\pi M_S}{SN}\left[(\alpha_1-\alpha_2)(1-f_{2Q}) - (\alpha_1-\alpha_3)f_Q\right] + \frac{D_{\rm ex}Q^2}{2SN}(\alpha_1-2\alpha_2) + \frac{K_{\rm an}}{N}(\alpha_1+\alpha_3), \quad (6b)$$

$$C = \frac{\gamma\pi M_S}{2SN}\left[(3\alpha_1+3\alpha_2+4\alpha_3)f_Q - \frac{8}{3}\alpha_3(1-f_{2Q})\right] + \frac{D_{\rm ex}Q^2}{3SN}\alpha_3 + \frac{K_{\rm an}}{4N}(3\alpha_1+3\alpha_2+4\alpha_3), \quad (6c)$$

$$D = \frac{\gamma\pi M_S}{2SN}\left[(3\alpha_1+3\alpha_2+4\alpha_3)f_Q - 2\alpha_2(1-f_{2Q})\right] + \frac{D_{\rm ex}Q^2}{2SN}\alpha_2 + \frac{K_{\rm an}}{2N}(3\alpha_2+\alpha_3). \quad (6d)$$

Here, N is the total number of spin sites. The dimensionless parameters α_1, α_2, and α_3 are related to the Bogoliubov transformation coefficients, listed in the SM [35].

An off-diagonal long-rage order characterizes the condensation state. The condensate state is a macroscopic occupation of the ground state and can be represented by a classical complex field. Therefore, to analyze the stability of the magnon condensate state, we perform the Madelung's transform $\hat{c}_{\pm Q} \to \sqrt{N_{\pm Q}}e^{i\phi_{\pm Q}}$, in which the macroscopic condensate magnon state is described with a coherent phase $\phi_{\pm Q}$ and a population number $N_{\pm Q}$ [27, 28]. The total number of condensed magnons is $N_c = N_{+Q} + N_{-Q}$, while the distribution difference is $\delta = N_{+Q} - N_{-Q}$. We also define the total phase as $\Phi = \phi_{+Q} + \phi_{-Q}$.

Finally, the macroscopic four-magnon interaction energy of condensed magnons is expressed as ,

$$\mathcal{V}_4(\delta,\Phi) = \frac{N_c^2}{2}\Big[A + B + 2C\cos\Phi\sqrt{1-\frac{\delta^2}{N_c^2}} + D\cos 2\Phi - \big(B - A + D\cos 2\Phi\big)\frac{\delta^2}{N_c^2}\Big]. \quad (7)$$

Without PMA, this expression is reduced to the one derived in [45].

Now, we can look at the total interaction energy and interaction amplitudes in more detail. Figure 2 shows the effective interaction potential as a function of the PMA. In a critical PMA strength, $K_{\rm an}^{c_1}$, the sign of the interaction changes from repulsive to attractive. This critical anisotropy is well below the critical magnetic anisotropy strength $K_{\rm an}^{c_2}$ that destabilizes the inplane magnetic ground state.

The necessary condition to reach a steady-state quasi-equilibrium magnon condensation is the presence of repulsive interactions between magnons; thus, in the following, we consider a PMA strength below the critical anisotropy $K_{\rm an} < K_{\rm an}^{c_1}$. I this regime, the intraband interaction is attractive, and thus interband contributions are important.

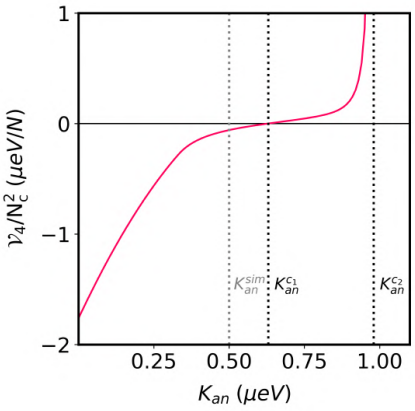

FIG. 2. The total nonlinear magnon interaction energy, Eq. (7), as a function of the PMA strength. N and N_c are the total number of spins and condensate magnons, respectively. $K_{\rm an}^{c_1}$ represents the critical value of the PMA at which the sign of nonlinear interactions is changed. On the other hand, $K_{\rm an}^{c_2}$ corresponds to the critical value of PMA at which the in-plane magnetic ground state becomes unstable. We set $L_x = 50\,\text{nm}$ and $H_0 = 1\,\text{kOe}$. $K_{\rm an}^{sim} = 0.5\,\mu\text{eV}$ denotes the PMA used in our micromagnetic simulations.

TABLE I: The material parameters used in the micromagnetic simulations.

Parameter	Symbol	Value
Saturation magnetization	$4\pi M_S$	1.75 kOe
Effective spin	S	14.3
Exchange stiffness	$D_{\rm ex}$	$0.64\times10^{-20}\,\text{eV m}^2$
Gilbert damping parameter	α	1×10^{-3}

The interacting potential energy, Eq. (7), has five extrema at,

$$\delta_1 = 0, \Phi = 0; \quad (8a)$$

$$\delta_2 = 0, \Phi = \pi; \quad (8b)$$

$$\delta_3 = 0, \Phi = \cos^{-1}(-\frac{C}{D}); \quad (8c)$$

$$\delta_4 = N_c\big[1 - (\frac{C}{B-A+D})^2\big]^{\frac{1}{2}}, \Phi = 0; \quad (8d)$$

$$\delta_5 = \delta_4, \Phi = \pi. \quad (8e)$$

Whether these extrema represent minima of the interacting potential energy relies on the system thickness L_x and the strength of the applied magnetic field H_0.

Phase diagram for magnon condensate—. Now, we explore the stability of the magnon condensate as a function of the thickness of the film L_x and the strength of the external magnetic field H_0, using the typical YIG parameters, see Table I.

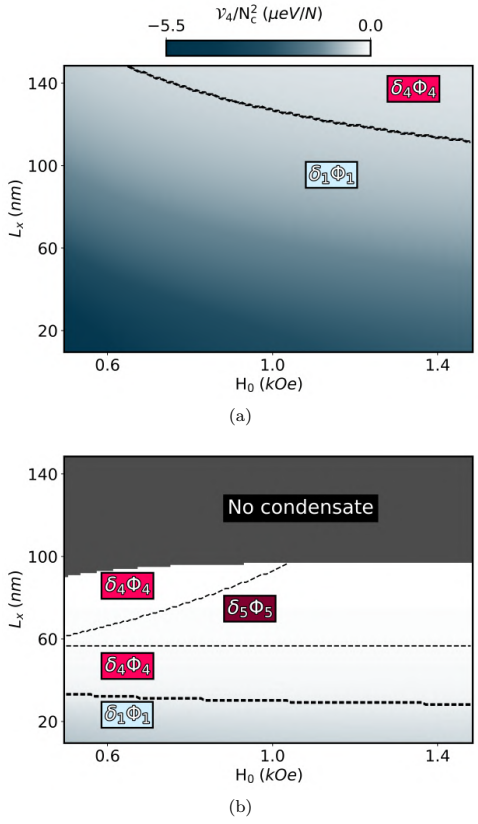

FIG. 3. The phase diagram pf the condensate magnon in the absence (a) and presence (b) of PMA. We plot the magnon interaction energy $\mathcal{V}_4/N_c^2$, Eq. (7), as a function of the film thickness L_x and external magnetic field strength H_0. The dashed black lines indicate the boundaries between the different condensate phases, Eq. (8). We set $K_{an} = 0.5\,\mu$eV in (b).

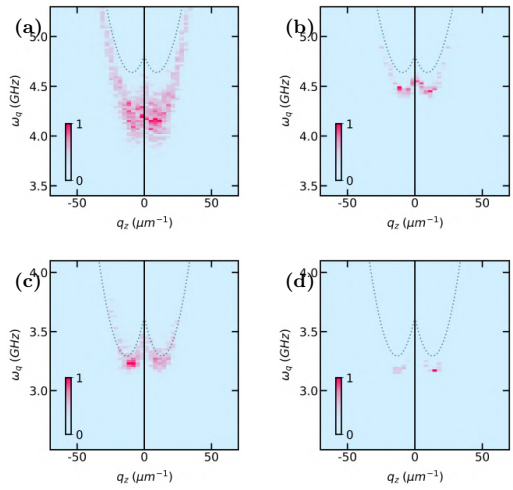

FIG. 4. Magnon distribution from micromagnetic simulations of a 50 nm thick YIG film at an external magnetic field strength $H_0 = 1$ kOe. In the absence of the PMA, $K_{\rm an} = 0$: (a) and (b) show magnon distributions of initial nonequilibrium excited magnons and final quasi-equilibrium magnon condensate steady state, respectively. In the presence of the PMA, $K_{\rm an} = 0.5\,\mu$eV : (c) and (d) show magnon distributions of initial nonequilibrium excited magnons and final quasi-equilibrium magnon condensate steady state, respectively. The dotted line indicates the analytical dispersion relation of noninteracting magnons, Eq. 3b. Because of nonlinear magnon interactions, there is a spectrum shift in the simulated magnon dispersion compared to the noninteracting result. Although the duration of magnon pumping by spin-transfer torque is the same in the absence or presence of the PMA, the critical torque amplitude is lower in the presence of PMA.

First, we present the phase diagram for magnon condensation in YIG, in the absence of PMA, in Fig. 3a. The thinnest films are expected to have a symmetric distribution of magnon condensation between the two minima. This phase diagram is in agreement with previous studies [27, 45].

Next, we add a PMA, with strength $K_{\rm an} = 0.5\,\mu$eV, and plot the phase diagram of the magnon condensate in Fig. 3b for different thicknesses. For the selected material parameters, PMA tends to push the magnon condensate towards a more asymmetric population distribution between the two magnon band minima. Since both minima are degenerate thus there is an oscillation of magnon condensate between these two minima. The asymmetry of condensate magnon populations agrees with our previous analysis of interaction amplitudes. Within out parameters for thickness and PMA strength, the intraband interaction A is attractive, while the interband interactions are still repulsive.

This phase diagram shows that in the presence of a PMA, condensate magnon can still be a metastable state. In addition, as we discussed earlier, a PMA increases the band depth and reduces the curvature of noninteracting magnon dispersion, see Fig. 1, which leads to an enhancement of the condensate magnon lifetime. Thus, we expect that introducing a small PMA into a thin film of YIG facilitates the magnon condensation process.

Micromagnetic simulation of magnon condensate—. To validate our theoretical predictions and demonstrate the facilitation of condensate formation by including a PMA, we conducted a series of micromagnetic simulations using the LLG framework [46]. We simulate a ferromagnetic system where the magnons are excited by a spin-transfer torque. We perform calculations at zero temperature; thus, the system has no thermal magnons. Nonequilibrium magnons in the magnetic thin film are

excited by a spin-transfer torque mechanism through injection of a spin current on the entire sample surface [31]. The sign of the spin torque and its amplitude should be chosen so that the injected magnon population reaches the condensation critical density, we refer to the SM for simulation details [35]. With the spin-transfer torque mechanism, we expect nonequilibrium magnons with different wavevectors and frequencies to be excited. A fraction of these magnons will eventually be thermalized via repulsive nonlinear magnon-magnon interactions and form a steady and quasi-equilibrium state of condensate magnons at the bottom of magnon band dispersion, see Fig. 4.

The numerical simulations confirm the supportive role of PMA in the condensation process. First, there is a reduction in the threshold of spin transfer torque necessary to inject the critical magnon density into the system enabling the system to attain said critical magnon density even at lower torque amplitudes. Second, final condensate magnons in the presence of the PMA are more localized around the band minima than in the case where PMA is absent. Simulations also indicate that PMA shifts the population of condensate magnons from a symmetric distribution between two band minima to an asymmetric distribution, Fig. 4. This is in agreement with the analytical phase diagram in Fig. 3b.

Summary and concluding remarks—. The thermalization of nonequilibrium-magnons and the stability of the condensate require a repulsive sign for effective magnon-magnon interactions. This typically requires the presence of strong dipolar interactions. The presence of PMA is expected to counteract dipolar interactions. We show that even at intermediate strengths of the PMA field, the magnon interactions are still repulsive, and the magnon condensate can be created as a metastable state. We note that the anisotropy increases the band depth and curvature of the magnon dispersion. These adjustments to the spectra shape are expected to benefit the condensate formation. From the calculations of effective magnon-magnon interactions at the band minima, we present a classification diagram predicting whether the relative number of condensate magnons in the two degenerate minima might be symmetric. The presence of PMA strength, in a certain range, will tend to push the condensate toward a more uneven population distribution between two degenerate band minima. Micromagnetic simulations, within the LLG framework, confirms our analytical results and analyses.

ACKNOWLEDGEMENTS

The authors thank Anne Louise Kristoffersen for helpful discussions. We acknowledge financial support from the Research Council of Norway through its Centers of Excellence funding scheme, project number 262633, "QuSpin". A. Q. was supported by the Norwegian Financial Mechanism Project No. 2019/34/H/ST/00515, "2Dtronics".

[1] S. O. Demokritov, V. E. Demidov, O. Dzyapko, G. A. Melkov, A. A. Serga, B. Hillebrands, and A. N. Slavin, Bose–Einstein condensation of quasi-equilibrium magnons at room temperature under pumping, Nature **443**, 430 (2006).

[2] V. Cherepanov, I. Kolokolov, and V. L'vov, The saga of YIG: Spectra, thermodynamics, interaction and relaxation of magnons in a complex magnet, Phys. Rep. **229**, 81 (1993).

[3] M. Onbasli, A. Kehlberger, D. H. Kim, G. Jakob, M. Kläui, A. V. Chumak, B. Hillebrands, and C. A. Ross, Pulsed laser deposition of epitaxial yttrium iron garnet films with low Gilbert damping and bulk-like magnetization, APL Mater. **2**, 106102 (2014).

[4] S. Demokritov, Comment on "Bose–Einstein Condensation and Spin Superfluidity of Magnons in a Perpendicularly Magnetized Yttrium Iron Garnet Film", JETP Lett. **115**, 691 (2022).

[5] P. Anderson and H. Suhl, Instability in the motion of ferromagnets at high microwave power levels, Phys. Rev. **100**, 1788 (1955).

[6] H. Suhl, The non-linear behaviour of ferrites at high signal level, Proceedings of the IRE **44**, 1270 (1956).

[7] V. Demidov, O. Dzyapko, M. Buchmeier, T. Stockhoff, G. Schmitz, G. Melkov, and S. Demokritov, Magnon kinetics and Bose-Einstein condensation studied in phase space, Phys. Rev. Lett. **101**, 257201 (2008).

[8] S. M. Rezende, Theory of coherence in Bose-Einstein condensation phenomena in a microwave-driven interacting magnon gas, Phys. Rev. B **79**, 174411 (2009).

[9] P. Nowik-Boltyk, O. Dzyapko, V. Demidov, N. Berloff, and S. Demokritov, Spatially non-uniform ground state and quantized vortices in a two-component Bose-Einstein condensate of magnons, Sci. Rep. **2**, 482 (2012).

[10] A. A. Serga, V. S. Tiberkevich, C. W. Sandweg, V. I. Vasyuchka, D. A. Bozhko, A. V. Chumak, T. Neumann, B. Obry, G. A. Melkov, A. N. Slavin, *et al.*, Bose–Einstein condensation in an ultra-hot gas of pumped magnons, Nat. Commun. **5**, 3452 (2014).

[11] D. A. Bozhko, A. A. Serga, P. Clausen, V. I. Vasyuchka, F. Heussner, G. A. Melkov, A. Pomyalov, V. S. L'vov, and B. Hillebrands, Supercurrent in a room-temperature Bose–Einstein magnon condensate, Nat. Phys. **12**, 1057 (2016).

[12] C. Sun, T. Nattermann, and V. L. Pokrovsky, Unconventional superfluidity in yttrium iron garnet films, Phys. Rev. Lett. **116**, 257205 (2016).

[13] O. Dzyapko, P. Nowik-Boltyk, B. Koene, V. E. Demidov, J. Jersch, A. Kirilyuk, T. Rasing, and S. O. Demokritov, High-resolution magneto-optical Kerr-effect spectroscopy of magnon Bose–Einstein condensate, IEEE Magn. Lett. **7**, 1 (2016).

[14] I. Borisenko, B. Divinskiy, V. Demidov, G. Li, T. Nattermann, V. Pokrovsky, and S. Demokritov, Direct evidence of spatial stability of Bose-Einstein condensate of magnons, Nat. Commun. **11**, 1691 (2020).

[15] V. E. Demidov, S. Urazhdin, E. Edwards, M. D. Stiles, R. D. McMichael, and S. O. Demokritov, Control of magnetic fluctuations by spin current, Phys. Rev. Lett. **107**, 107204 (2011).

[16] V. Demidov, S. Urazhdin, G. De Loubens, O. Klein, V. Cros, A. Anane, and S. Demokritov, Magnetization oscillations and waves driven by pure spin currents, Phys. Rep. **673**, 1 (2017).

[17] S. A. Bender, R. A. Duine, and Y. Tserkovnyak, Electronic pumping of quasiequilibrium Bose-Einstein-condensed magnons, Phys. Rev. Lett. **108**, 246601 (2012).

[18] S. A. Bender, R. A. Duine, A. Brataas, and Y. Tserkovnyak, Dynamic phase diagram of dc-pumped magnon condensates, Phy. Rev. B **90**, 094409 (2014).

[19] Y. Tserkovnyak, S. A. Bender, R. A. Duine, and B. Flebus, Bose-Einstein condensation of magnons pumped by the bulk spin Seebeck effect, Phys. Rev. B **93**, 100402 (2016).

[20] S. Andrianov and S. Moiseev, Magnon qubit and quantum computing on magnon Bose-Einstein condensates, Phys. Rev. A **90**, 042303 (2014).

[21] M. Mohseni, V. I. Vasyuchka, V. S. L'vov, A. A. Serga, and B. Hillebrands, Classical analog of qubit logic based on a magnon Bose–Einstein condensate, Commun. Phys. **5**, 196 (2022).

[22] Y. M. Bunkov, A. N. Kuzmichev, T. R. Safin, P. M. Vetoshko, V. I. Belotelov, and M. S. Tagirov, Quantum paradigm of the foldover magnetic resonance, Sci. Rep. **11**, 7673 (2021).

[23] S. Demokritov, V. Demidov, O. Dzyapko, G. Melkov, and A. Slavin, Quantum coherence due to Bose–Einstein condensation of parametrically driven magnons, New J. Phys. **10**, 045029 (2008).

[24] V. Demidov, O. Dzyapko, S. Demokritov, G. Melkov, and A. Slavin, Observation of spontaneous coherence in Bose-Einstein condensate of magnons, Phys. Rev. Lett. **100**, 047205 (2008).

[25] S. M. Rezende, Theory of microwave superradiance from a Bose-Einstein condensate of magnons, Phys. Rev. B **79**, 060410 (2009).

[26] I. Tupitsyn, P. Stamp, and A. Burin, Stability of bose-einstein condensates of hot magnons in yttrium iron garnet films, Phys. Rev. Lett. **100**, 257202 (2008).

[27] F. Li, W. M. Saslow, and V. L. Pokrovsky, Phase diagram for magnon condensate in yttrium iron garnet film, Sci. Rep. **3**, 1372 (2013).

[28] H. Salman, N. G. Berloff, and S. O. Demokritov, Microscopic theory of Bose-Einstein condensation of magnons at room temperature, in *Universal Themes of Bose-Einstein Condensation*, edited by N. P. Proukakis, D. W. Snoke, and P. B. Littlewood (Cambridge University Press, 2017) Chap. 25, p. 493.

[29] J. Hick, F. Sauli, A. Kreisel, and P. Kopietz, Bose-Einstein condensation at finite momentum and magnon condensation in thin film ferromagnets, Eur. Phys. J. B **78**, 429 (2010).

[30] M. Mohseni, A. Qaiumzadeh, A. A. Serga, A. Brataas, B. Hillebrands, and P. Pirro, Bose–Einstein condensation of nonequilibrium magnons in confined systems, New J. Phys. **22**, 083080 (2020).

[31] B. Divinskiy, H. Merbouche, V. E. Demidov, K. Nikolaev, L. Soumah, D. Gouéré, R. Lebrun, V. Cros, J. B. Youssef, P. Bortolotti, A. Anane, and D. S. O., Evidence for spin current driven Bose-Einstein condensation of magnons, Nat. Commun. **12**, 6541 (2021).

[32] M. Lakshmanan, The fascinating world of the Landau–Lifshitz–Gilbert equation: an overview, Philos. Trans. R. Soc. A **369**, 1280 (2011).

[33] L. Landau and E. Lifshitz, 3 - On the theory of the dispersion of magnetic permeability in ferromagnetic bodies, in *Perspectives in Theoretical Physics*, edited by L. P. Pitaevski (Pergamon, Amsterdam, 1992) pp. 51–65.

[34] T. L. Gilbert, A phenomenological theory of damping in ferromagnetic materials, IEEE Trans. Magn. **40**, 3443 (2004).

[35] See supplementary material for more details on the magnon hamiltonian and simulation.

[36] T. Holstein and H. Primakoff, Field dependence of the intrinsic domain magnetization of a ferromagnet, Phys. Rev. **58**, 1098 (1940).

[37] S. Streib, N. Vidal-Silva, K. Shen, and G. E. Bauer, Magnon-phonon interactions in magnetic insulators, Phys. Rev. B **99**, 184442 (2019).

[38] H. Maier-Flaig, S. Klingler, C. Dubs, O. Surzhenko, R. Gross, M. Weiler, H. Huebl, and S. T. Goennenwein, Temperature-dependent magnetic damping of yttrium iron garnet spheres, Phys. Rev. B **95**, 214423 (2017).

[39] A. Boardman and S. Nikitov, Three-and four-magnon decay of nonlinear surface magnetostatic waves in thin ferromagnetic films, Phys. Rev. B **38**, 11444 (1988).

[40] A. J. Princep, R. A. Ewings, S. Ward, S. Tóth, C. Dubs, D. Prabhakaran, and A. T. Boothroyd, The full magnon spectrum of yttrium iron garnet, npj Quantum Mater. **2**, 63 (2017).

[41] Serga, AA and Chumak, AV and Hillebrands, B, Yig magnonics, J. Phys. D: Appl. Phys. **43**, 264002 (2010).

[42] F. J. Buijnsters, L. J. Van Tilburg, A. Fasolino, and M. I. Katsnelson, Two-dimensional dispersion of magnetostatic volume spin waves, J. Phys. Condens. Matter. **30**, 255803 (2018).

[43] H. Zabel and M. Farle, *Magnetic nanostructures: spin dynamics and spin transport*, Vol. 246 (Springer, 2012).

[44] V. Demidov, O. Dzyapko, S. Demokritov, G. Melkov, and A. Slavin, Thermalization of a parametrically driven magnon gas leading to Bose-Einstein condensation, Phys. Rev. Lett. **99**, 037205 (2007).

[45] C. Sun, T. Nattermann, and V. L. Pokrovsky, Bose–Einstein condensation and superfluidity of magnons in yttrium iron garnet films, J. Phys. D: Appl. Phys. **50**, 143002 (2017).

[46] A. Vansteenkiste, J. Leliaert, M. Dvornik, M. Helsen, F. Garcia-Sanchez, and B. Van Waeyenberge, The design and verification of MuMax3, AIP Adv. **4**, 107133 (2014).

[47] A. Kreisel, F. Sauli, L. Bartosch, and P. Kopietz, Microscopic spin-wave theory for yttrium-iron garnet films, Eur. Phys. J. B **71**, 59 (2009).

[48] T. Frostad, H. L. Skarsvåg, A. Qaiumzadeh, and A. Brataas, Spin-transfer-assisted parametric pumping of magnons in yttrium iron garnet, Phys. Rev. B **106**, 024423 (2022).

SUPPLEMENTAL MATERIAL

1. Diagonalization of Magnon Hamiltonian

The total spin Hamiltonian of a thin film, in the $y-z$ plane with a small perpendicular anisotropy along the $\hat{\mathbf{x}}$ direction reads,

$$\mathcal{H} = \mathcal{H}_{\rm ex} + \mathcal{H}_{\rm Z} + \mathcal{H}_{\rm dip} + \mathcal{H}_{\rm an}. \tag{9}$$

The exchange energy between neighboring spins reads

$$\mathcal{H}_{\rm ex} = -\frac{1}{2} J_{\rm ex} \sum_{i,j} \boldsymbol{S}_i \cdot \boldsymbol{S}_j, \tag{10}$$

where $J_{\rm ex} > 0$ is the ferromagnetic exchange constant. The Zeeman energy due to an inplane external magnetic field of strength H_0 along the $\hat{\mathbf{z}}$-direction reads,

$$\mathcal{H}_{\rm Z} = -g\mu_B H_0 \sum_j \boldsymbol{S}_j^z, \tag{11}$$

where μ_B is the Bohr magneton and g is the the effective Landé g-factor. The dipolar field is expressed as [47],

$$\mathcal{H}_{\rm dip} = -\frac{1}{2} \sum_{i,j} \sum_{\alpha,\beta} D_{i,j}^{\alpha,\beta} S_i^\alpha S_j^\beta, \tag{12a}$$

$$D_{i,j}^{\alpha,\beta} = (g\mu_B)^2 (1-\delta_{i,j}) \frac{\partial^2}{\partial r_{ij}^\alpha \partial r_{ij}^\beta} \frac{1}{|\boldsymbol{r}_{ij}|}, \tag{12b}$$

where α, β denote the spatial components x, y and z; and $\boldsymbol{r}_{ij}$ is the distance vector between the spin sites i and j. Finally, the PMA anisotropy is given by,

$$\mathcal{H}_{\rm an} = -K_{\rm an} \sum_j (\boldsymbol{S}_j \cdot \hat{x})^2. \tag{13}$$

The Holstein-Primakoff transformation allows us to express the spin operators in terms of bosonic creation and annihilation operators $\hat{a}^\dagger$ and $\hat{a}$ respectively. Using the large-S approximation, we have, $S^+ \approx \hbar\sqrt{2S}(\hat{a} - \hat{a}^\dagger\hat{a}\hat{a}/(4S))$, $S^- \approx \hbar\sqrt{2S}(\hat{a}^\dagger - \hat{a}^\dagger\hat{a}^\dagger\hat{a}/(4S))$, and $S^z = \hbar(S - \hat{a}^\dagger\hat{a})$.

The corresponding noniteracting boson Hamiltonian in the Fourier space reads,

$$\mathcal{H}_2 = \sum_{\boldsymbol{q}} A_{\boldsymbol{q}} \hat{a}_{\boldsymbol{q}}^\dagger \hat{a}_{\boldsymbol{q}} + \frac{1}{2} B_{\boldsymbol{q}} \hat{a}_{\boldsymbol{q}} \hat{a}_{-\boldsymbol{q}} + \frac{1}{2} B_{\boldsymbol{q}}^* \hat{a}_{\boldsymbol{q}}^\dagger \hat{a}_{-\boldsymbol{q}}^\dagger, \tag{14}$$

where $\hat{a}_j^\dagger = \frac{1}{N}\sum_{\boldsymbol{q}} e^{i\boldsymbol{k}\cdot\boldsymbol{r}_j} \hat{a}_{\boldsymbol{q}}^\dagger$ and $A_{\boldsymbol{q}}$ ($B_{\boldsymbol{q}}$) is presented in Eq. (4b). We utilize the Bogoliubov transformation to diagonalize this bosonic Hamiltonian and find the corresponding noninteracting magnon Hamiltonian,

$\hat{a}_{\boldsymbol{q}} = u_{\boldsymbol{q}}\hat{c}_{\boldsymbol{q}} + v_{\boldsymbol{q}}\hat{c}_{-\boldsymbol{q}}^\dagger$ $\hat{a}_{\boldsymbol{q}}^\dagger = u_{\boldsymbol{q}}^\dagger\hat{c}_{\boldsymbol{q}} + v_{\boldsymbol{q}}\hat{c}_{-\boldsymbol{q}}$. Here, $u_{\boldsymbol{q}} = u_{-\boldsymbol{q}}$ and $v_{\boldsymbol{q}} = v_{-\boldsymbol{q}}$ are the Bogoliubov coefficients, $u_{\boldsymbol{q}} = \big((A_{\boldsymbol{q}} + 2\hbar\omega_{\boldsymbol{q}})/(2\hbar\omega_{\boldsymbol{q}})\big)^{1/2}$, $v_{\boldsymbol{q}} = \mathrm{sgn}(B_{\boldsymbol{q}})\big(B_{\boldsymbol{q}} - 2\hbar\omega_{\boldsymbol{q}})/(2\hbar\omega_{\boldsymbol{q}})\big)^{1/2}$

TABLE II: Simulation parameters

Parameter	Value
Excitation time, first interval	100 ns
Excitation time, second interval	200 ns
Excitation strength, first interval	-1.2×10^{10} A m^{-2}
Excitation strength, second interval ($K_{\rm an} = 0$)	-0.35×10^{10} A m^{-2}
Excitation strength, second interval ($K_{\rm an} = 0.5\,\mu$eV)	-0.2×10^{10} A m^{-2}

It can be shown that the off-diagonal terms ($\alpha \neq \beta$) of the dipolar interaction vanish in the uniform mode approximation for a thin film of infinite lateral lengths [29, 47]. In this case, the dipolar interaction contains no three-magnon operator terms. We omit any renormalization correction to the noninteracting magnon Hamiltonian, as they are of the order of $1/S$ and small. We define the following parameters in the 4-magnon interaction amplitudes, introduced in Eq. (6) [27, 28].

$$\alpha_1 = u_{\boldsymbol{Q}}^4 + v_{\boldsymbol{Q}}^4 + 4u_{\boldsymbol{Q}}^2 v_{\boldsymbol{Q}}^2, \tag{15a}$$

$$\alpha_2 = 2u_{\boldsymbol{Q}}^2 v_{\boldsymbol{Q}}^2, \tag{15b}$$

$$\alpha_3 = 3u_{\boldsymbol{Q}} v_{\boldsymbol{Q}} (u_{\boldsymbol{Q}}^2 + v_{\boldsymbol{Q}}^2). \tag{15c}$$

2. Micromagnetic Simulations

We perform simulations of magnon creation by spin-transfer torque with and without out-of-plane anisotropy. We define an initial state in which the spins, on average, point along the $\hat{\mathbf{z}}$-direction. We introduce a random noise in the spin direction to mimic the thermal noise as the initial condition of our simulation. Next, we excite magnons in the ferromagnetic thin film by applying a spin torque to the entire film surface. The film is discretized in the lateral directions and uniform in the $\hat{\mathbf{x}}$ direction. The lateral dimensions of the ilm are large compared to the film thickness. In this way, the film is effectively a 2D spin system. The LLG equation is solved for each successive time step, using the open-source software mumax3 [46]. We refer to Ref. 48 for examples that illustrate the simulation of magnon creation via STT.

The spin accumulation determines the strength of the spin torque, see Ref. [48]. We start the simulations by exciting magnons with a strong spin torque (interval I_1), before lowering the torque strength to keep the magnetization dynamics in a semi-stable state where the total number of magnons does not change dramatically over time (interval I_2). In this semistable state, the two magnon populations may interact with each other, and the density of magnons in both minima may oscillate in time. However, the total number of magnons remains relatively unchanged. The current strength and time duration of the two intervals are listed in Table II. The magnetization data in Fig. 4 is from the last 50 ns of the intervals.

The magnon density in the film is proportional to the

longitudinal component of the average magnetization, $\eta = 1 - \langle m_z \rangle$ [48].

The torque strength, or spin accumulation due to the injected current, determines the number of magnons created. The anisotropy lowers the spin-wave spectra, meaning that one can use a weaker torque for the stronger anisotropy. In Fig. 4 we choose the torque strength so that $\eta \approx 0.01$.

The deviation of spin from the ground-state direction is proportional to the magnon density. The magnon distribution ξ can be found by performing a Fourier transform of the transverse magnetization components, $\xi(q_y, q_z) = |\mathcal{F}[m_x(y,z)]|^2 + |\mathcal{F}[m_y(y,z)]|^2$ [48].

To reduce the consequences of the finite-size effect in our results, we analyze the magnetization data in the middle region of the film, $y, z \in [L/8, 7L/8]$, where L is the lateral dimension of the square film.

Paper III :

Anne Louise Kristoffersen, Therese Frostad, Roberto E. Troncoso, Arne Brataas and Alireza Qaiumzadeh

Phase Diagram for Magnon Condensate in Antiferromagnetic Insulators

Preprint (2023) [9]

Phase Diagram for Magnon Condensate in Antiferromagnetic Insulators

Anne Louise Kristoffersen[1], Therese Frostad[1], Roberto E. Troncoso[2], Arne Brataas[1], and Alireza Qaiumzadeh[1]
[1]*Center for Quantum Spintronics, Department of Physics, Norwegian University of Science and Technology, NO-7491 Trondheim, Norway and*
[2]*School of Engineering and Sciences, Universidad Adolfo Ibáñez, Santiago, Chile*
(Dated: December 12, 2023)

We analyze the stability of magnon condensation in uniaxial and biaxial antiferromagnetic insulators. We implement both Hosltein-Primakoff and Dyson-Maleev bosonization methods. We show that the interparticle interactions between two types of quasiparticles in antiferromagnetic materials with two sublattices, i.e., α and β magnons, enable magnon condensation as a metastable state. This is different from magnon condensation in ferromagnetic yttrium iron garnet.

I. INTRODUCTION

Bose-Einstein condensation (BEC) is a fascinating phenomenon in quantum physics that occurs at temperatures close to absolute zero, where a collection of particles, typically bosons, undergo a phase transition into a state of matter with unique quantum properties [1]. When the temperature decreases, the thermal wavelength of the particles increases, leading to a macroscopic occupation of the lowest quantum state. This results in the particles behaving collectively as a single quantum entity characterized by a coherent wave function. While BEC was initially observed in dilute atomic gases, researchers have extended the concept to quasiparticles, excitations, or collective modes in condensed matter systems. Exploring BEC in quasiparticles, such as exciton-polaritons or magnons, opens up new avenues for studying quantum phenomena in diverse physical systems, from superfluidity to novel states of matter with potential applications in quantum technologies.

There are some similarities and differences between the BEC of particles and quasiparticles. BEC of magnons was observed in Yttrium Iron Garnet (YIG) in 2006 [2] at room temperature, where non-equilibrium magnons were excited under microwave parallel pumping. Later on the stabilization of magnon condensates has been under scrutiny in ferromagnetic (FM) systems [3–9] under parametric parallel pumping, as well as electrically injection of magnons via spin-transfer torque mechanism.

Although there are many studies on non-equilibrium magnon injection and magnon BEC in FM systems, there are very few studies on magnon pumping [10] and magnon BEC in antiferromagnetic (AFM) systems [11, 12]. BECs of AFM magnons have not yet been observed experimentally. With recent advancements in AFM spintronics [13], we deem it opportune to delve into a more comprehensive exploration of this phenomenon. This manuscript is dedicated to the detailed stability analysis of magnon condensates within uniaxial and biaxial AFMs.

II. MODEL HAMILTONIANS AND PHASE DIAGRAMS

A. Uniaxial AFM: HP formalism

The direct exchange interaction between spins at all lattice sites i and all nearest neighbors at lattice sites j are modeled by $H_{\rm ex} = -J\sum_{\langle i,j\rangle}\vec{S}_i\cdot\vec{S}_j$, where J>0. The total number of nearest neighbors is denoted by z. We assume on-site, easy-axis anisotropy $H_{\rm ani} = -K_z\sum_i (S_i^z)^2$. Magnetic field along the $\hat{\mathbf{z}}$-direction, $\mathbf{h} = h\hat{\mathbf{z}}$ contributes by $H_{\rm Zee} = -\mu\sum_i hS_i^z$. The Hamiltonian for the DMI between spins $\vec{S}_i$, $\vec{S}_j$ is $H_{\rm DMI} = \sum_{i,j}\mathbf{D}_{ij}\cdot(\vec{S}_i\times\vec{S}_j)$, where $\mathbf{D}_{ij} = -\mathbf{D}_{ji}$ is the DM vector. We also assume i and j to be the nearest neighbors for the DMI. We will assume that the DM-vector is parallel to the $\hat{\mathbf{z}}$-axis, $\mathbf{D}_{ij} = D\nu_{ij}\hat{\mathbf{z}}$.

The total Hamiltonian for the uniaxial AFM is

$$H = H_{\rm ex} + H_{\rm ani} + H_{\rm Zee} + H_{\rm DMI}. \tag{1}$$

We now introduce raising and lowering operators, $S_i^+ = S_i^x + iS_i^y$ and $S_i^- = S_i^x - iS_i^y$, respectively. We perform a Holstein-Primakoff transformation for these operators, keeping fourth-order expansion terms. For sublattice A, we denote these a and denote b for sublattice B. The quantization axis is along the $\hat{\mathbf{z}}$-axis, giving $S_i^z = S - a_i^\dagger a_i$ and $S_j^z = -S + b_j^\dagger b_j$. For sublattice A, the transformation is

$$\begin{aligned} S_i^+ &= \sqrt{2S}\,\sqrt{1 - a_i^\dagger a_i/2S}\,a_i \approx \sqrt{2S}\,(1 - a_i^\dagger a_i/4S)\,a_i, \\ S_i^- &= \sqrt{2S}\,a_i^\dagger\,\sqrt{1 - a_i^\dagger a_i/2S} \approx \sqrt{2S}\,a_i^\dagger\,(1 - a_i^\dagger a_i/4S). \end{aligned} \tag{2}$$

For sublattice B, the transformation is

$$\begin{aligned} S_j^+ &= \sqrt{2S}\,b_j^\dagger\,\sqrt{1 - b_j^\dagger b_j/2S} \approx \sqrt{2S}\,b_j^\dagger\,(1 - b_j^\dagger b_j/4S), \\ S_j^- &= \sqrt{2S}\sqrt{1 - b_j^\dagger b_j/2S}\,b_j \approx \sqrt{2S}\,(1 - b_j^\dagger b_j/4S)\,b_j. \end{aligned} \tag{3}$$

Inserting an inverse Fourier transformation, $a_i = (N/2)^{-1/2}\sum_{\mathbf{k}} a_{\mathbf{k}}\,e^{-i\mathbf{k}\cdot r_i}$ and $a_i^\dagger = (N/2)^{-1/2}\sum_{\mathbf{k}} a_{\mathbf{k}}^\dagger\,e^{i\mathbf{k}\cdot r_i}$,

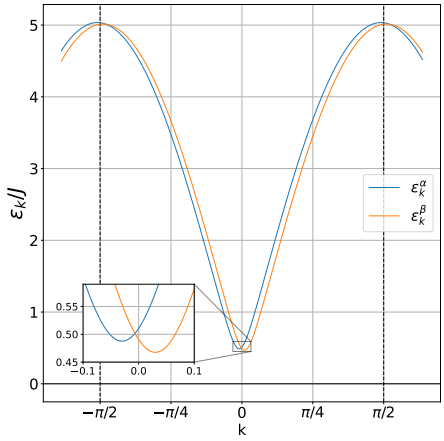

FIG. 1: Dispersion relations for α- and β-magnons with parameters $D/J = 0.03$, $K_z/J = 0.05$ and $H/J = 0.01$. The dashed, vertical lines mark the boundaries of the first Brillouin zone.

the total Hamiltonian of second order in the new basis is

$$H^2 = SJ\sum_{\mathbf{k}} z[a^\dagger_{\mathbf{k}}a_{\mathbf{k}} + b^\dagger_{\mathbf{k}}b_{\mathbf{k}}] + 2SJ[a_{\mathbf{k}}b_{-\mathbf{k}} + a^\dagger_{\mathbf{k}}b^\dagger_{-\mathbf{k}}]\cos(k) + 2SK_z\sum_{\mathbf{k}}[a^\dagger_{\mathbf{k}}a_{\mathbf{k}} + b^\dagger_{\mathbf{k}}b_{\mathbf{k}}] - \mu h\sum_{\mathbf{k}}[b^\dagger_{\mathbf{k}}b_{\mathbf{k}} - a^\dagger_{\mathbf{k}}a_{\mathbf{k}}] - D4S\sum_{\mathbf{k}}[a^\dagger_{\mathbf{k}}b^\dagger_{-\mathbf{k}} + a_{\mathbf{k}}b_{-\mathbf{k}}]\sin(k). \quad (4)$$

By writing the Hamiltonian in Eq. (4) in matrix form, we see that the matrix elements form a 4x4 block diagonal matrix. The two blocks are identical when $\mathbf{k} \to -\mathbf{k}$. Performing a Bogoliubov transformation on the independent blocks allows us to rewrite Eq. (4) as

$$H^{2,\mathrm{I}} = \sum_{\mathbf{k}}\left[\varepsilon^\alpha_{\mathbf{k}}\alpha^\dagger_{\mathbf{k}}\alpha_{\mathbf{k}} + \varepsilon^\beta_{\mathbf{k}}\beta_{-\mathbf{k}}\beta^\dagger_{-\mathbf{k}}\right], \quad (5)$$

where $\alpha_{\mathbf{k}}$ and $\beta_{\mathbf{k}}$ are long-ranged right-handed and left-handed magnons. They are defined by $\alpha_{\mathbf{k}} = u_{\mathbf{k}}a_{\mathbf{k}} + v_{\mathbf{k}}b^\dagger_{-\mathbf{k}}$ and $\beta_{\mathbf{k}} = v_{-\mathbf{k}}a^\dagger_{-\mathbf{k}} + u_{-\mathbf{k}}b_{\mathbf{k}}$. For simplicity, we define $\omega_E = 2SJ$, $\omega_D = 2DS$, $\omega_A = SK_z$ and $\omega_H = \frac{1}{2}\mu h$. The dispersion relations are $\varepsilon^\alpha_{\mathbf{k}} = \left[(\omega_E+\omega_A)^2 - (\omega_E\cos(k) - \omega_D\sin(k))^2\right]^{1/2} + \omega_H$ for $\alpha_{\mathbf{k}}$ magnons and $\varepsilon^\beta_{\mathbf{k}} = \left[(\omega_E+\omega_A)^2 - (\omega_E\cos(k) + \omega_D\sin(k))^2\right]^{1/2} - \omega_H$ for $\beta_{\mathbf{k}}$ magnons. In Figure 1 we have plotted $\varepsilon^\alpha_{\mathbf{k}}$ and $\varepsilon^\beta_{\mathbf{k}}$.

Define $f_2(k) = J\cos(k)$ and $f_3(k) = D\sin(k)$. The interaction Hamiltonian with fourth order terms, is

$$H^4 = -\sum_{\mathbf{k},\mathbf{q},\mathbf{q}'}\frac{f_2(k)}{(N/2)}[a_{\mathbf{k}}b^\dagger_{\mathbf{k}+\mathbf{q}+\mathbf{q}'}b_{\mathbf{q}}b_{\mathbf{q}'} + a^\dagger_{\mathbf{k}+\mathbf{q}+\mathbf{q}'}a_{\mathbf{q}}a_{\mathbf{q}'}b_{\mathbf{k}} + \mathrm{h.c.} + 4a^\dagger_{\mathbf{q}-\mathbf{k}}a_{\mathbf{q}}b^\dagger_{\mathbf{q}'+\mathbf{k}}b_{\mathbf{q}'}] - \frac{K_z}{(N/2)}\sum_{\mathbf{k}\mathbf{q}\mathbf{q}'}\left[a^\dagger_{\mathbf{q}-\mathbf{k}}a_{\mathbf{q}}a^\dagger_{\mathbf{q}'+\mathbf{k}}a_{\mathbf{q}'} + b^\dagger_{\mathbf{q}-\mathbf{k}}b_{\mathbf{q}}b^\dagger_{\mathbf{q}'+\mathbf{k}}b_{\mathbf{q}'}\right] + \sum_{\mathbf{k}\mathbf{q}\mathbf{q}'}\frac{f_3(k)}{(N/2)}\Big[a^\dagger_{\mathbf{k}}b^\dagger_{\mathbf{q}}b^\dagger_{\mathbf{q}'}b_{\mathbf{k}+\mathbf{q}+\mathbf{q}'} + a_{\mathbf{k}}b^\dagger_{\mathbf{k}+\mathbf{q}+\mathbf{q}'}b_{\mathbf{q}}b_{\mathbf{q}'} - a^\dagger_{\mathbf{q}}a^\dagger_{\mathbf{q}'}a_{\mathbf{q}+\mathbf{q}'+\mathbf{k}}b^\dagger_{\mathbf{k}} - a^\dagger_{\mathbf{q}+\mathbf{q}'+\mathbf{k}}a_{\mathbf{q}}a_{\mathbf{q}'}b_{\mathbf{k}}\Big]. \quad (6)$$

Before executing the next step, to insert the Bogoliubov transformation into Eq. (6), we reduced the triple k-sum. The only magnons that are candidates for BEC are those around the minima, namely $\alpha^{(\dagger)}_{k=-Q}$ and $\beta^{(\dagger)}_{k=Q}$. Therefore, we reduce the sum to consider only combinations that give $\alpha^{(\dagger)}_{-\mathbf{Q}}$ and $\beta^{(\dagger)}_{k=+\mathbf{Q}}$.

We utilise the Bogoliubov transformation, and write $a_{\mathbf{k}}$ and $b_{\mathbf{k}}$ in terms of $\alpha_{\mathbf{k}}$ and $\beta_{\mathbf{k}}$ in Eq. (6). For simplicity, we first define coefficients $A = (2/N)\left[-f_2(Q) - f_3(Q)\right]\left[\alpha^1_Q + \alpha^2_Q\right] - 4J\left[\alpha^3_Q\right] - K_z\left[2\alpha^3_Q\right]$, $B = (2/N)\left[-f_2(Q) - f_3(Q)\right]\left[2\alpha^3_Q\right] - 4J\left[(1/2)\alpha^2_Q\right] - K_z\left[\alpha^2_Q\right]$, $C = (2/N)\left[-f_2(Q) - f_3(Q)\right]\left[2\alpha^3_Q\right] - 4J\left[(1/2)\alpha^2_Q\right] - K_z\left[\alpha^1_Q - 2\alpha^2_Q\right]$ and $D = (2/N)\left[-f_2(Q) - f_3(Q)\right]\left[8\alpha^3_Q\right] - 4J\left[\alpha^1_Q - \alpha^2_Q\right] - K_z\left[4\alpha^2_Q\right]$. In coefficients A, B, C and D we have defined three coefficients, which are functions of the Bogoliubov parameters, $\alpha^1_Q = u^4_{-Q} + v^4_{-Q} + 4u^2_{-Q}v^2_{-Q}$, $\alpha^2_Q = 2u^2_{-Q}v^2_{-Q}$ and $\alpha^3_Q = -u_{-Q}v_{-Q}(u^2_{-Q} + v^2_{-Q})$. Note the superscript, which differentiates from the notation for R/H-handed magnons $\alpha_{\mathbf{k}}$. The final interaction Hamiltonian in the diagonal basis is

$$\begin{aligned} H_Q &= H_{\mathrm{intra}} + H_{\mathrm{inter}}, \\ H_{\mathrm{inter}} &= C\left[\alpha_{-\mathbf{Q}}\alpha_{-\mathbf{Q}}\alpha^\dagger_{-\mathbf{Q}}\alpha^\dagger_{-\mathbf{Q}} + \beta^\dagger_{\mathbf{Q}}\beta^\dagger_{\mathbf{Q}}\beta_{\mathbf{Q}}\beta_{\mathbf{Q}}\right] \\ H_{\mathrm{intra}} &= A\left[\alpha_{-\mathbf{Q}}\beta^\dagger_{\mathbf{Q}}\beta_{\mathbf{Q}}\beta_{\mathbf{Q}} + \beta^\dagger_{\mathbf{Q}}\alpha_{-\mathbf{Q}}\alpha^\dagger_{-\mathbf{Q}}\alpha^\dagger_{-\mathbf{Q}} + \alpha_{-\mathbf{Q}}\alpha_{-\mathbf{Q}}\beta_{\mathbf{Q}}\alpha^\dagger_{-\mathbf{Q}} + \beta^\dagger_{\mathbf{Q}}\beta^\dagger_{\mathbf{Q}}\beta_{\mathbf{Q}}\alpha^\dagger_{-\mathbf{Q}}\right] \\ &\quad + B\left[\alpha_{-\mathbf{Q}}\alpha_{-\mathbf{Q}}\beta_{\mathbf{Q}}\beta_{\mathbf{Q}} + \beta^\dagger_{\mathbf{Q}}\beta^\dagger_{\mathbf{Q}}\alpha^\dagger_{-\mathbf{Q}}\alpha^\dagger_{-\mathbf{Q}}\right] \\ &\quad + D\alpha_{-\mathbf{Q}}\beta^\dagger_{\mathbf{Q}}\beta_{\mathbf{Q}}\alpha^\dagger_{-\mathbf{Q}}. \end{aligned} \quad (7)$$

In Eq. (7) we defined two Hamiltonians H_{intra} and H_{inter} for, respectively, intravalley scattering and intervalley scattering between the two condensates.

We want to analyze the potential between the magnons. Performing a Madelung transformation allows us to do that. We substitute $\langle\alpha_{-\mathbf{Q}}\rangle = \sqrt{N_\alpha}\,\mathrm{e}^{i\phi^\alpha}$ and $\langle\beta_{\mathbf{Q}}\rangle = \sqrt{N_\beta}\,\mathrm{e}^{i\phi^\beta}$ in Eq. (7). $N_{\alpha/\beta}$ is the total number of magnons in the α/β-populated condensates. The total number of magnons in the condensates $N_c = N_\alpha + N_\beta$, the total phase $\Phi = \phi_\alpha + \phi_\beta$ and the difference in population $\delta = N_\alpha - N_\beta$. We have now obtained the interaction

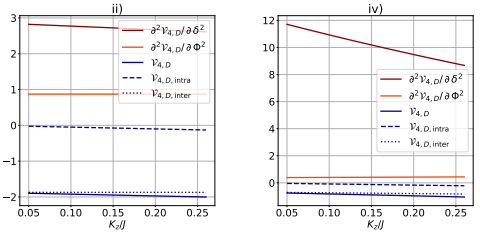

(a) (b)

FIG. 2: The value of the interaction strength $\mathcal{V}_4$ and its second derivatives, $\partial^2\mathcal{V}_4/\partial\delta^2$ and $\partial^2\mathcal{V}_4/\partial\Phi^2$ for a specific value of D/J are shown in a for extremum point ii) and b for extremum point iv). We also included $\mathcal{V}_{\text{intra}}$ and $\mathcal{V}_{\text{inter}}$ in the figures.

potentials

$$\begin{aligned}\mathcal{V}_4 &= \mathcal{V}_{\text{intra}} + \mathcal{V}_{\text{inter}}\\ \mathcal{V}_{\text{intra}} &= \frac{N_c^2}{2}C\left[1+(\delta/N_c)^2\right]\\ \mathcal{V}_{\text{inter}} &= \frac{N_c^2}{2}\Big[\frac{D}{2}-(\frac{D}{2}+B\,\cos(2\Phi))(\delta/N_c)^2\\ &\quad + B\,\cos(2\Phi)+2A\sqrt{1-(\delta/N_c)^2}\,\cos(\Phi)\Big].\end{aligned} \tag{8}$$

The total number of magnons N_c, can be held constant. To find the minima of $\mathcal{V}_4$, we find the extrema with respect to δ and Φ. We find four valid extrema

$$\begin{aligned}&\text{i) } (\delta/N_c)^2 = 0, \Phi = 0\\ &\text{ii) } (\delta/N_c)^2 = 0, \Phi = \pi\\ &\text{iii) } (\delta/N_c)^2 = 1-\left[\frac{A\,\cos(\Phi)}{C-D/2-B\,\cos(2\Phi)}\right]^2, \Phi = 0\\ &\text{iv) } (\delta/N_c)^2 = 1-\left[\frac{A\,\cos(\Phi)}{C-D/2-B\,\cos(2\Phi)}\right]^2, \Phi = \pi.\end{aligned} \tag{9}$$

Inspecting the phase diagrams for $\partial^2\mathcal{V}_4/\partial\delta^2$, $\partial^2\mathcal{V}_4/\partial\Phi^2$ and $(\partial^2\mathcal{V}_4/\partial\delta^2)\,(\partial^2\mathcal{V}_4/\partial\Phi^2) - (\partial^2\mathcal{V}_4/\partial\delta\partial\Phi)^2$, we find that both extremum point ii) and iv) allows for condensation. We thus have degenerate condensates. In Fig. 2a, for extremum point ii) and 2b, for extremum point iv), we have plotted the value of $\mathcal{V}_4$, $\partial^2\mathcal{V}_4/\partial\delta^2$, $\partial^2\mathcal{V}_4/\partial\Phi^2$ as a function of K_z/J for a specific value of D/J. We also plotted the values for $\mathcal{V}_{\text{intra}}$ and $\mathcal{V}_{\text{inter}}$. We observe that the value of $\mathcal{V}_4$ is dominated by $\mathcal{V}_{\text{inter}}$.

B. Uniaxial AFM with DMI : Dyson-Maleev

The spin operators on sublattice A are,

$$S_i^+ = \hbar\sqrt{2S}(\hat{a}_i - \hat{a}_i^\dagger\hat{a}_i\hat{a}_i/(2S)) \tag{10}$$
$$S_i^- = \hbar\sqrt{2S}\hat{a}_i^\dagger \tag{11}$$
$$S_i^z = \hbar(S-\hat{a}_i^\dagger\hat{a}_i) \tag{12}$$

The spin operators on sublattice B are,

$$S_j^+ = \hbar\sqrt{2S}(\hat{b}_i^\dagger - \hat{b}_i^\dagger\hat{b}_i\hat{b}_i/(2S)) \tag{13}$$
$$S_j^- = \hbar\sqrt{2S}\hat{b}_i \tag{14}$$
$$S_j^z = -\hbar(S-\hat{b}_i^\dagger\hat{b}_i) \tag{15}$$

We follow the same procedure as in the Holstein-Primakoff framework earlier. The Dyson-Maleev transformation gives the same results for the two-magnon Hamiltonian. When analyzing the four-magnon Hamiltonian, we find the same prefactors for B,C, and D. However, there is some difference in the A-prefactor. We define a new four-magnon operator for the A-terms,

$$\begin{aligned}\mathcal{H}_4^A =& A_{1,2}(\hat{\alpha}_{-Q}\hat{\beta}_Q^\dagger\hat{\beta}_Q\hat{\beta}_Q + \hat{\beta}_Q^\dagger\hat{\alpha}_{-Q}\hat{\alpha}_{-Q}^\dagger\hat{\alpha}_{-Q}^\dagger)\\ &+ A_{3,4}(\hat{\alpha}_{-Q}\hat{\alpha}_{-Q}\hat{\beta}_Q\hat{\alpha}_{-Q}^\dagger + \hat{\beta}_Q^\dagger\hat{\beta}_Q^\dagger\hat{\beta}_Q\hat{\alpha}_{-Q}^\dagger)\end{aligned} \tag{16}$$

We define the difference Δ_A relative to the prefactor A found in the Holstein-Primakoff framework so that $A_{1,2} = A + \Delta_A$ and $A_{3,4} = A - \Delta_A$.

After the Madelung transform, we obtain the following interaction term,

$$\mathcal{H}_4^A = \frac{N_c^2}{2}\sqrt{1-(\frac{\delta}{N_c})^2}(2A\cos(\Phi) + 2i\frac{\delta}{N_c}\sin(\Phi)\Delta_A) \tag{17}$$

In the Holstein-Primakoff transformation, $\Delta_A = 0$ and the interaction is fully real. However, in the Dyson Maleev bosonization, we find that $\Delta_A = -\frac{2}{N}(3\alpha_2 - \alpha_1)(f_2(Q)+f_3(Q))$. We note that the real part of Eq. (17) is similar for the Holstein-Primakoff and Dyson-Maleev transformation.

C. Biaxial AFM without DMI: Holstein-Primakoff

We consider a similar Hamiltonian as the uniaxial system, but this time without the DMI interaction. We add an additional out-of-plane hard-axis anisotropy in the x-direction,

$$H_{Ax} = K_{Ax}(\sum_A (S_A^x)^2 + \sum_B (S_B^x)^2) \tag{18}$$

$K_{Ax} > 0$ is the anisotropy strength. The system is similar to the one studied in Ref. [14]. For materials suchas NiO we assume that $J_{ex} > K_{Ax} > K_{Az}$ [14, 15].

The spin wave spectra have a minimum at $k = 0$, and we will only consider the magnon population in the lowest energy state. The magnon energies in the minima from Ref. [14] are given by,

$$\omega^2_{\alpha,\beta} = \frac{1}{4}(\omega_E + \omega_{Ax} + 2\omega_{Az})^2 + \omega_H - \frac{1}{4}(\omega^2_{Ax} + \omega^2_E) \pm \frac{1}{2}\sqrt{4\omega_H((\omega_E + \omega_{Ax} + 2\omega_{Az})^2 - \omega^2_E) + \omega^2_E\omega^2_{Ax}} \tag{19}$$

Here, β-magnons have the lowest energy. We have defined $\omega_{Ax} = SK_{Ax}$. We see that the degeneracy is broken even if $\omega_H = 0$, sue to the presence of the out-of-plane hard-axis anisotropy.

We proceed to investigate the four-magnon interactions. We use the following Bogoliubov transformation,

$$\hat{a} = u_\alpha\hat{\alpha} - v_\beta\hat{\beta}^\dagger \tag{20}$$

$$\hat{b}^\dagger = -v_\alpha\hat{\alpha} + u_\beta\hat{\beta}^\dagger \tag{21}$$

We use the approximated Bogoliubov parameters from Ref. [14] evaluated at $k = 0$

$$u_{\alpha,\beta} = \sqrt{\frac{(\omega_E + \omega_{Ax} + 2\omega_{Az})^2 + \omega_{\alpha,\beta}}{2\omega_{\alpha,\beta}(\omega_H = 0)}} \tag{22}$$

$$v_{\alpha,\beta} = \sqrt{\frac{(\omega_E + \omega_{Ax} + 2\omega_{Az})^2 - \omega_{\alpha,\beta}}{2\omega_{\alpha,\beta}(\omega_H = 0)}} \tag{23}$$

We are interested in analyzing the interactions of the magnon population of lowest energy, which means that we will only analyze the β-magnon interactions. There are only a few four-magnon combinations involving the β-population only,

$$\mathcal{H}^\beta_4 = C_2(\hat{\beta}\hat{\beta}\hat{\beta}^\dagger\hat{\beta}^\dagger) + G_{5,8}(\hat{\beta}\hat{\beta}\hat{\beta}\hat{\beta} + h.c.) + G_{6,7}(\hat{\beta}\hat{\beta}\hat{\beta}\hat{\beta}^\dagger + h.c.) \tag{24}$$

We perform the Madelung transformation,

$$\langle\beta\rangle \to \sqrt{N_\beta}e^{i\phi_\beta} \tag{25}$$

Here N_β is the number of magnons of the population, and ϕ_β is their phase. We obtain the general expression for the magnon-interaction of the β-population,

$$\mathcal{H}^\beta_4/N^2_\beta = C_2 + 2G_{6,7}cos(2\phi_\beta) + 2G_{5,8}cos(4\phi_\beta) \tag{26}$$

We find the following prefactors,

$$C_2N = -8J(u^2_\beta v^2_\beta) + 4J(u_\beta v_\beta(u^2_\beta + v^2_\beta)) - \frac{1}{2}K_{Az}(u^4_\beta + v^4_\beta) \tag{27}$$

$$- 16K_{Ax}(u^4_\beta + v^4_\beta) \tag{28}$$

$$G_{6,7}N = -8K_{Ax}(u^4_\beta + v^4_\beta) \tag{29}$$

$$G_{5,8}N = 0 \tag{30}$$

The possible critical points of Eq. (26) are,

$$\phi^\beta_1 = \frac{1}{2}\cos^{-1}(\frac{C_2}{2G_{6,7}}) \tag{31}$$

$$\phi^\beta_2 = n\pi\frac{1}{2}\cos^{-1}(\frac{C_2}{2G_{6,7}}) \tag{32}$$

Since we assumed that the exchange energy is much stronger than the out-of-plane anisotropy strength, $\frac{C_2}{2G_{6,7}} > 1$, and the angle ϕ_β is ill-defined. Then there are no valid critical points of Eq. (26).

III. DISCUSSION AND CONCLUDING REMARKS

We show that even in the absence of dipolar interactions, which play a crucial role in the stability of FM magnon BEC, it is possible to have a metastable magnon BEC in AFM systems. The underlying mechanism of stability is the interaction between two types of AFM magnons. We showed that even though it is possible to inject magnons into biaxial AFM systems by parallel pumping [10], since magnon degeneracy has been broken in these systems and thus the interaction between two magnon modes becomes weaker then it is harder to stabilize an AFM magnon BEC state. On the other hand, in uniaxial AFM cases, since the two low-energy magnon bands are degenerate, the intermode interactions can be strong enough to stabilize magnon BEC. In the latter case, it is possible to inject magnons into the system electrically [11]. We propose by choosing a uniaxial AFM material $\alpha - Cu_2V_2O_7$, we can test our theory. Without an external magnetic field, this system has two magnon bands minima with the same energy at $\pm Q$ because of DMI [16]. By applying a magnetic field, this degeneracy will be lifted. If we create a magnon BEC in the absence of a magnetic field electrically, we can destroy it by applying a magnetic field.

ACKNOWLEDGMENT

This project has been supported by the Norwegian Financial Mechanism Project No. 2019/34/H/ST3/00515, "2Dtronics"; and partially by the Research Council of Norway through its Centers of Excellence funding scheme, Project No. 262633, "QuSpin".

[1] I. Georgescu, 25 years of bec, Nat. Rev. Phys. **2**, 396 (2020).

[2] S. O. Demokritov, V. E. Demidov, O. Dzyapko, G. A. Melkov, A. A. Serga, B. Hillebrands, and A. N. Slavin, Bose–einstein condensation of quasi-equilibrium magnons at room temperature under pumping, Nature **443**, 430–433 (2006).

[3] R. E. Troncoso and S. Núñez, Dynamics and spontaneous coherence of magnons in ferromagnetic thin films, Journal of Physics: Condensed Matter **24**, 036006 (2011).

[4] F. Li, W. M. Saslow, and V. L. Pokrovsky, Phase diagram for magnon condensate in yttrium iron garnet film, Scientific Reports **3**, 10.1038/srep01372 (2013).

[5] R. E. Troncoso and S. Núñez, Josephson effects in a bose–einstein condensate of magnons, Annals of Physics **346**, 182–194 (2014).

[6] P. O. Sukhachov, S. Banerjee, and A. V. Balatsky, Bose-einstein condensate of dirac magnons: Pumping and collective modes, Phys. Rev. Res. **3**, 013002 (2021).

[7] T. Frostad, P. Pirro, A. A. Serga, B. Hillebrands, A. Brataas, and A. Qaiumzadeh, Anisotropy-assisted magnon condensation in ferromagnetic thin films (2023), arXiv:2309.05982 [cond-mat.mes-hall].

[8] T. Frostad, H. L. Skarsvåg, A. Qaiumzadeh, and A. Brataas, Spin-transfer-assisted parametric pumping of magnons in yttrium iron garnet, Phys. Rev. B **106**, 024423 (2022).

[9] M. Mohseni, A. Qaiumzadeh, A. A. Serga, A. Brataas, B. Hillebrands, and P. Pirro, Bose–einstein condensation of nonequilibrium magnons in confined systems, New Journal of Physics **22**, 083080 (2020).

[10] H. Yamazaki, Parallel pumping of spin-waves in an orthorhombic antiferromagnet, J. Phys. Soc. Jpn. **32**, 1227 (1972).

[11] E. L. Fjærbu, N. Rohling, and A. Brataas, Electrically driven bose-einstein condensation of magnons in antiferromagnets, Phys. Rev. B **95**, 144408 (2017).

[12] N. Arakawa, Controlling stability of bose-einstein condensation of interacting magnons in an antiferromagnet by an external magnetic field, Phys. Rev. B **99**, 014405 (2019).

[13] V. Baltz, A. Manchon, M. Tsoi, T. Moriyama, T. Ono, and Y. Tserkovnyak, Antiferromagnetic spintronics, Rev. Mod. Phys. **90**, 015005 (2018).

[14] F. Machado, P. Ribeiro, J. Holanda, R. Rodríguez-Suárez, A. Azevedo, and S. Rezende, Spin-flop transition in the easy-plane antiferromagnet nickel oxide, Physical Review B **95**, 104418 (2017).

[15] S. M. Rezende, A. Azevedo, and R. L. Rodríguez-Suárez, Introduction to antiferromagnetic magnons, Journal of Applied Physics **126** (2019).

[16] G. Gitgeatpong, Y. Zhao, P. Piyawongwatthana, Y. Qiu, L. W. Harriger, N. P. Butch, T. J. Sato, and K. Matan, Nonreciprocal magnons and symmetry-breaking in the noncentrosymmetric antiferromagnet, Phys. Rev. Lett. **119**, 047201 (2017).

ISBN 978-82-326-7726-9 (printed ver.)
ISBN 978-82-326-7725-2 (electronic ver.)
ISSN 1503-8181 (printed ver.)
ISSN 2703-8084 (online ver.)

NTNU

Norwegian University of
Science and Technology